β-parvin Mediates Adhesion Receptor Cross-Talk During *Xenopus laevis* Gastrulation

by

Catherine Studholme

A thesis
presented to the University of Waterloo
in fulfillment of the
thesis requirement for the degree of
Doctor of Philosophy
in
Biology

Waterloo, Ontario, Canada, 2013

AUTHOR'S DECLARATION

I hereby declare that I am the sole author of this thesis. This is a true copy of the thesis, including any required final revisions, as accepted by my examiners.

I understand that my thesis may be made electronically available to the public.

Abstract

Modulation of cell adhesion is essential to the cell rearrangements that characterize *Xenopus* gastrulation. The spatial and temporal regulation of cell movement requires a highly coordinated cross-talk between cadherin and integrin adhesion receptors. While the adhesive properties and morphogenetic movements are well described, the molecular mechanisms controlling these behaviors remain unknown. However, experimental evidence indicates that the signals regulating cell adhesion originate from within the cell. β-parvin is an integrin associated scaffolding protein consisting of two calponin homology (CH) domains. I have examined the role that β-parvin plays in the modulation of cell adhesion during the tissue movements that define gastrulation in *Xenopus*. *Xenopus* β-parvin is highly conserved being ~95% similar to mammalian orthologs. β-parvin is expressed in the blastocoel roof and dorsal marginal zone of the embryo during gastrulation suggesting a potential role in morphogenesis. Over-expression of full-length β-parvin has no effect on embryogenesis, however, over-expression of either CH domain causes a failure in gastrulation. When over-expressed the CH1 domain causes a failure in fibronectin (FN) matrix assembly, epiboly and convergent extension *in vivo*. CH1 domain over-expression also inhibits tissue separation (TS) and Brachet's cleft formation in post-involution mesoderm. The CH1 domain of β-parvin localizes to sites of cell-cell adhesion, and down-regulates C-cadherin adhesion through activation of Rac1 and independent of receptor expression. Significantly, the CH1 domain can rescue convergent extension downstream of integrin *ex vivo* suggesting a role for β-parvin in the integrin mediated control of cell intercalation. Over-expression of the CH2

domain also inhibits morphogenesis in a similar fashion as CH1. However, the CH2 domain localizes to sites of integrin adhesion and inhibits integrin function resulting in a loss of FN assembly. The CH2 domain binds ILK and inhibits integrin function. When over-expressed the CH2 domain promotes TS in the pre-involution mesoderm through the activation of Rho. While the CH1 domain inhibits TS through Rac and the CH2 domain promotes TS through Rho, full-length β-parvin over-expression has no embryonic phenotype and its signaling properties appear to be intermediate between expression of either isolated CH domain. At the dorsal lip full-length β-parvin shuttles between integrin in the pre-involution mesoderm and cell-cell adhesion sites in the post-involution mesoderm indicating it plays significant roles in the previously characterized integrin-cadherin cross talk. My research has defined novel roles for β-parvin as a key player in the regulation of integrin-cadherin cross-talk during tissue morphogenesis.

Acknowledgements

Thank you to everyone who has supported me through my graduate career, especially my husband Ryan Studholme and our family and friends.

Table of Contents

List of Figures

List of Tables

List of Abbreviations

ANK	Ankyrin
ATCC	American Type Culture Collection
BCR	Blastocoel Roof
BS	Bluescript
BSA	Bovine Serum Albumin
CCBD	Central Cell Binding Domain
CE	Convergent Extension
CH	Calponin Homology
DIG	Digoxygenin
DMZ	Dorsal Marginal Zone
DTT	Dithiothreitol
ECM	Extracellular Matrix
EDTA	Ethylenediaminetetraacetic Acid
EF1-α	Elongation Factor 1-α
EST	Expressed Sequence Tag
ESB	Embryo Solubilization Buffer
EtOH	Ethanol
FA	Focal Adhesion
FBS	Fetal Bovine Serum
FN	Fibronectin
Fz7	Frizzled 7
GEF	Guanine Nucleotide Exchange Factor
GFP	Green Fluorescent Protein
Grb-4	Growth Factor Receptor-Bound Protein-4
HCG	Human Chorionic Gonadotropin
HEPES	Hyroxyethylpiperazineethanesulfonic Acid
HRP	Horseradish Peroxidase

ILK	Integrin-linked Kinase
IPP	ILK-PINCH-parvin
L-15	Leibovitz-15 Media
LB	Luria Bertani Medium
LiCl	Lithium Chloride
LIM	Lin-11, Isl-1, Mec-3
MBS	Modified Barth's Saline
MBT	Midblastula Transition
MEMFA	MOPS, EGTA, $MgSO_4$, formaldehyde
MLC	Myosin Light Chain
MO	Morpholino
MSS	Modified Stearn's Solution
PAK	p21-Activated Kinase
PAPC	Paraxial Protocadherin
PBD	p21-Binding Domain
PBS	Phosphate Buffered Saline
PBST	Phosphate Buffered Saline with 0.1% Tween20
PCR	Polymerase Chain Reaction
PH	Pleckstrin Homology
PHSRN/synergy	Proline-Histidine-Serine-Arginine-Asparagine
PINCH	Particularly Interesting New Cysteine-Histidine rich protein
PIX	p21-Activated Serine-Threonine Kinase-Interacting Exchange Factor
PMSF	Phenylmethylsulfonyl Fluoride
RBD	Rhotekin-Binding Domain
RFP	Red Fluorescent Protein
RGD	Arginine-Glycine-Aspartic Acid
RT-PCR	Reverse Transcription-PCR
SDS	Sodium Dodecyl Sulfate
SDS-PAGE	Sodium Dodecyl Sulfate-Polyacrylamide Gel Electrophoresis

TAE	Tris-Acetate EDTA
TBS	Tris Buffered Saline
TBST	Tris Buffered Saline with 0.1% Tween20
TCA	Thrichloroacetic Acid
TS	Tissue Separation

Chapter 1
Introduction

1.1 *Xenopus* Gastrulation

Among metazoans gastrulation is a highly conserved stage of development that establishes the triploblastic architecture of the embryo. Due to the well characterized cell and tissue movements, *Xenopus laevis* embryos are a widely used model to study the molecular processes that regulate gastrulation. Upon fertilization the future dorsal side of the embryo is established opposite to the site of sperm entry through cortical rotation. Fertilization is followed by a series of rapid cell divisions independent of cell growth, creating a blastula composed of 4000 cells surrounding a fluid filled cavity known as the blastocoel. The tissue in the animal pole positioned above the blastocoel is the animal cap, and contains presumptive ectodermal cells (Figure 1.1, blue cells). Presumptive endoderm is located at the vegetal pole (Figure 1.1, yellow cells), while the presumptive mesoderm is located in the marginal zone (Figure 1.1, orange cells). The midblastula transition (MBT), the onset of zygotic transcription, begins five hours post fertilization at the twelfth cleavage. Gastrulation is initiated at the fifteenth cell cycle on the future dorsal side of the embryo before spreading laterally and ventrally. Formation of pigmented bottle cells is the first visible sign of gastrulation (Figure 1.1; Hardin and Keller, 1988). Concomitantly, vegetal rotation of superficial endoderm from the vegetal cell mass and mesoderm from the marginal zone move to the interior of the embryo (Winklbauer and Schurfeld, 1999). The combined movements of vegetal rotation and bottle cell formation define the dorsal blastopore lip, and the initiation of

mesoderm involution. The endodermal rotation initially leads to a passive rotation in the marginal zone, resulting in the mesendoderm rolling over the blastopore lip to the interior of the embryo (Figure 1.1; Winklbauer and Schurfeld, 1999; Ibrahim and Winklbauer, 2001). This is followed by active involution of the dorsal marginal zone (DMZ) mesoderm around the blastopore lip, a process driven by epiboly and convergent extension (CE) in the blastocoel roof (BCR). Inside the embryo, involution brings the mesendoderm into contact with ectoderm lining the blastocoel. The mesendoderm remains separate from the ectoderm as it translocates across the BCR towards the animal pole. A stable interface called Brachet's cleft develops between the pre-involution and post-involution mesoderm at the blastopore lip (Figure 1.1; Wacker et al., 2000). In the later stages of gastrulation, epiboly in the BCR as well as CE in the marginal zone continue to drive superficial mesoderm to involute around the blastopore lip into the interior of the embryo. As involution progresses laterally and ventrally, a ring-like blastopore forms on the vegetal surface of the embryo. Epiboly eventually expands the ectoderm to completely cover the embryo and close the blastopore. On the inside of the embryo, CE in the post-involution mesoderm extends the anterior-posterior axis and helps drive the anterior mesendoderm across the BCR.

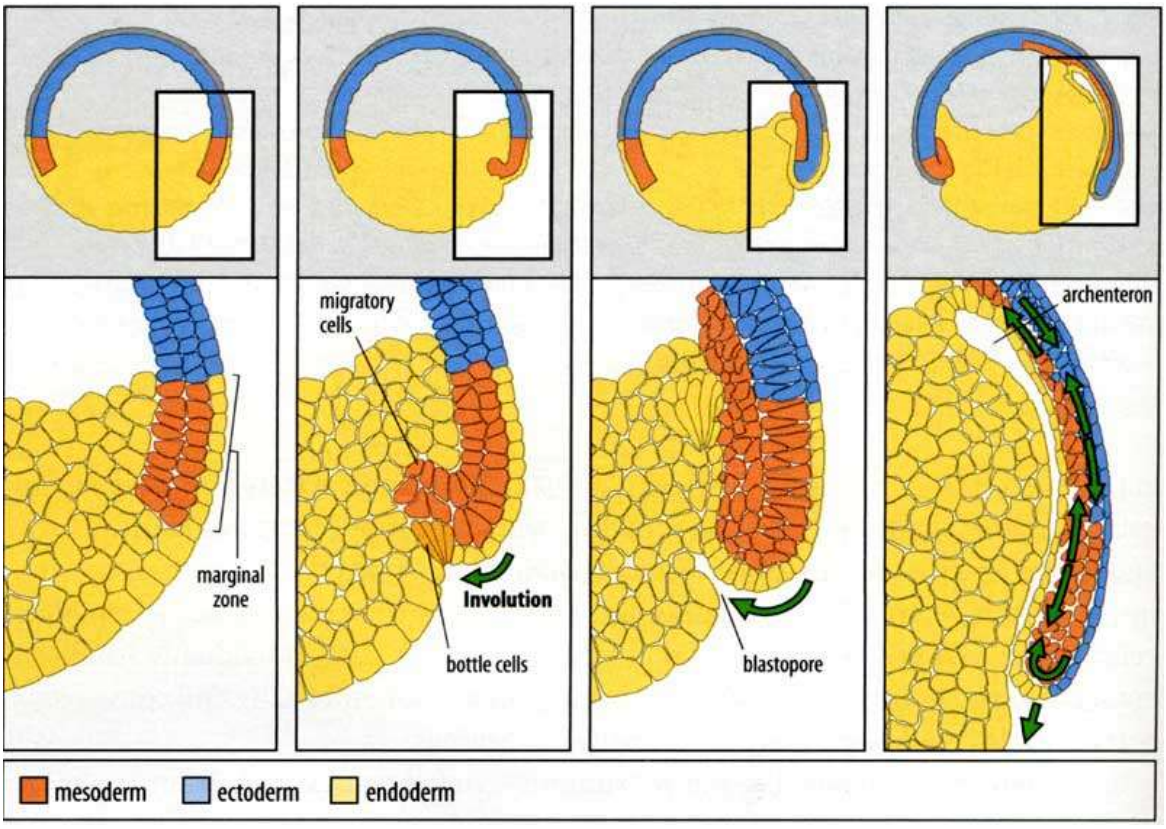

Figure 1.1 Morphogenetic movements of *Xenopus* gastrulation. First panel: last blastula stage embryo prior to gastrulation. Second panel: early gastrula stage embryo displays the onset of involution. Third panel: as gastrulation proceeds the post-involution mesoderm contacts the pre-involution mesoderm and BCR. Fourth panel: involution around the blastopore lip continues, and CE is occurring in both pre- and post-involution mesoderm (green double arrows) coincident with epiboly (green arrow in blue tissue). *Adapted from Wolpert and Tickle, 2011.*

1.1.1 Epiboly is a Driving Force for Blastopore Closure During Gastrulation

During *Xenopus* gastrulation radial intercalation of deep BCR cells results in thinning and spreading of the tissue, eventually encompassing the embryo in a two-cell thick sheet of ectoderm (Figure 1.2; Keller, 1980; Marsden and DeSimone, 2001). These cell movements collectively known as epiboly begin in the animal cap prior to the onset of gastrulation and progresses ventrally towards the marginal zone (Keller, 1978). Prior to gastrulation the BCR at the animal pole is three to four cell layers thick, and the marginal zones of the BCR are five to six cell layers thick. The superficial cells do not participate in the intercalation movements and become thinner and more expansive as deep cells intercalate (Figure 1.2; Keller, 1980). Experimental perturbation of the cell intercalations that occur during epiboly result in a delay or failure in blastopore closure indicating that epiboly is essential for proper gastrulation (Marsden and DeSimone, 2001; Rozario et al., 2009).

1.1.2 Convergent Extension Elongates the Anterior-Posterior Axis

Excision of the BCR roof from the embryo does not completely inhibit tissue involution and axis extension (Keller and Jansa, 1992), indicating that CE of mesodermal tissues in the DMZ also helps drive involution and results in narrowing and lengthening of the anterior-posterior axis (Figure 1.2). Prior to gastrulation, mesodermal cells in the DMZ exhibit multipolar protrusive activity (Keller et al., 2000). At the onset of gastrulation, DMZ mesodermal cells acquire a bipolar morphology with mediolateral protrusions aligned perpendicular to the anterior-posterior axis (Keller et al., 2000; Shih and Keller, 1992). The

cells then use these protrusions to crawl past each other in a mediolateral direction towards the midline, resulting in narrowing and lengthening of the tissue (Keller et al., 2000). CE occurs in both non-involuting and involuting dorsal marginal zone tissues; however, the majority of elongation occurs in the post-involution mesoderm (Figure 1.2).

Epiboly and CE are concurrent and in the embryo are interdependent morphogenetic movements. Evidence that epiboly and CE are distinct morphogenetic events comes from experiments involving DMZ explants cultured *ex vivo* (Keller et al., 1992). These explants dissociate the interdependence of morphogenetic movements and undergo CE, but not epiboly (Keller et al., 1992). CE movements are also observed *ex vivo* in mesoderm induced animal cap tissue (Symes and Smith, 1987), providing us with a simple model for morphogenesis.

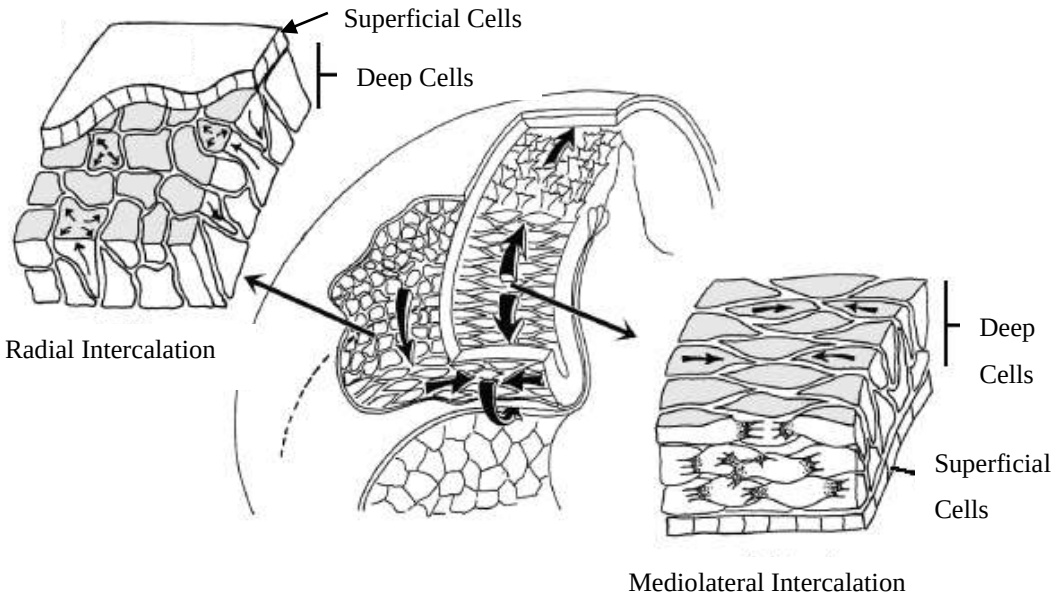

Figure 1.2 Radial and mediolateral cell intercalation. Radial intercalation occurs in deep cells of the BCR and DMZ, where several layers intercalate to thin the tissue creating a larger surface area. Mediolateral cell intercalation occurs in deep mesodermal and neural cells on the dorsal side, where cells intercalate along the mediolateral axis to form a longer thinner tissue. *Adapted from Keller et al., 2003*.

1.1.3 Tissue Separation Behavior is Required for Normal Gastrulation

Tissue separation (TS) behavior is acquired during gastrulation, and is necessary for boundary formation between post-involution mesendoderm and the BCR (Wacker et al., 2000). The physical separation of pre- and post-involution mesoderm at the dorsal lip is known as Brachet's cleft. The anterior portion of Brachet's cleft develops during vegetal rotation, while the posterior portion extends as mesoderm involutes around the dorsal blastopore lip (Figure 1.3; Winklbauer and Schurfeld, 1999). As marginal zone mesoderm involutes around the dorsal blastopore lip and comes into contact with the pre-involution

mesoderm at Brachet's cleft, the post-involution tissue acquires a change in cell behavior that prevents it from reintegrating into the pre-involution mesoderm, a process known as tissue separation (TS; Wacker et al., 2000). Inhibition of TS abolishes the development of the posterior portion of Brachet's cleft, resulting in CE defects and a failure in gastrulation (Medina et al., 2004; Koster et al., 2010).

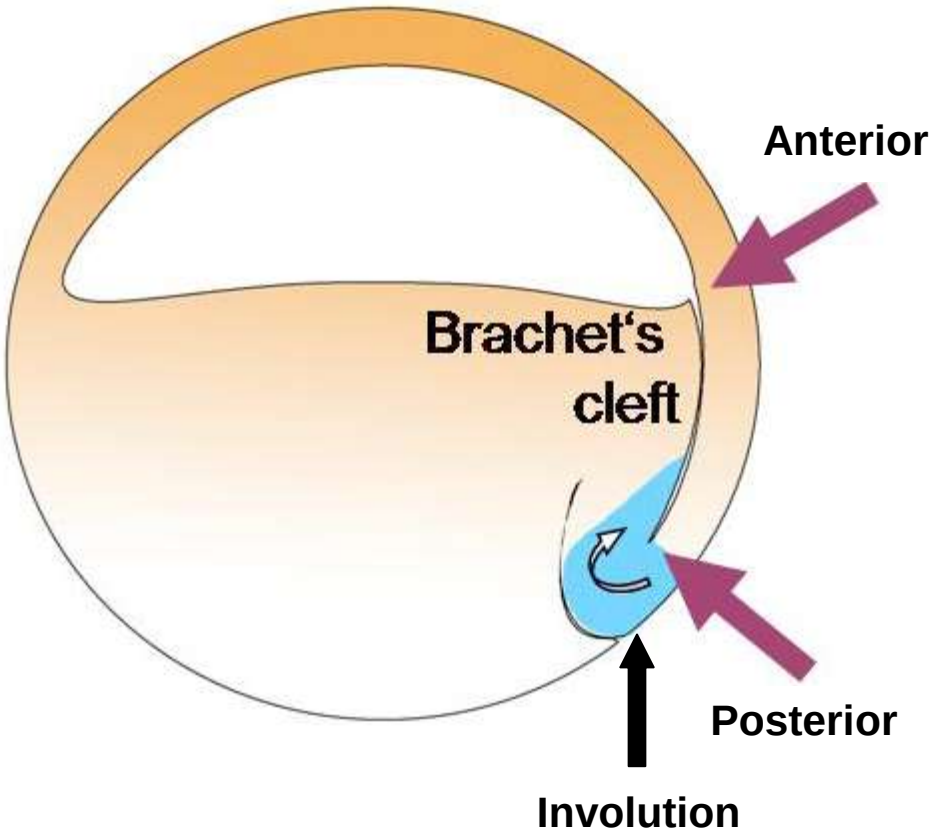

Figure 1.3 Brachet's cleft develops during gastrulation in *Xenopus* embryos. Tissue separation is acquired during gastrulation, and the space between pre- and post-involution tissue *in vivo* is called Brachet's cleft. The anterior portion of Brachet's cleft is formed by the leading edge of the mesendodermal cell mass, while the posterior portion develops during mesoderm involution (purple arrows). Mesoderm is depicted in blue, with directional involution depicted by the white arrow. *Adapted from Koster et al., 2010.*

1.2 Regulation of Cell Behaviors During Gastrulation

Cell and tissue rearrangements required to drive morphogenetic movements during *Xenopus* gastrulation are dependent upon modulation of integrin and cadherin cell adhesion receptors (Marsden and DeSimone, 2001; 2003; Davidson et al., 2002, 2006; Dzamba et al., 2009; Brieher and Gumbiner, 1994). During *Xenopus* gastrulation one integrin receptor, integrin α5β1, is required for regulation of cell-extracellular matrix (ECM) adhesion (Joos et al., 1995; Gwantka et al., 1994), while C-cadherin regulates cell-cell adhesion in deep BCR cells undergoing morphogenetic movements. The superficial cells of the ectoderm express E-cadherin, but do not actively participate in morphogenetic rearrangements (Kuhl and Wedlich, 1996).

Integrins are transmembrane heterodimers that consist of one α and one β subunit, and are able to mediate interactions between proteins found on the cell surface, or in the extracellular space, such as ECM proteins. Upon ligation integrin receptors can transmit signals across the cell membrane and into the cell through the cytoplasmic domain, a process known as 'outside-in' signaling (Hynes, 2002). This leads to the clustering of protein complexes at integrin tails that mediate interactions with the actin cytoskeleton (Hynes, 2002). Signals can also be sent from inside cells altering the structure of the extracellular domain of integrin subunits, and this is referred to as 'inside-out' signaling (Hynes, 2002). Therefore, integrins are capable of mediating bi-directional signaling between the ECM and the actin cytoskeleton.

C-cadherin is a classical cadherin, which are calcium dependent transmembrane proteins that mediate homophilic (*trans*) binding. Cadherins undergo parallel dimer (*cis*) formation in the cell membrane, which induces cytoplasmic protein clustering at the cytoplasmic tails. Catenins are the core proteins that interact with the cytoplasmic cadherin domain, and these can mediate interactions with the actin cytoskeleton. Cadherins are also capable of mediating inside-out signaling (Gumbiner, 2005), as cadherin adhesion can be modulated independent of surface expression (Tsuiji et al., 2007).

1.2.1 Cadherin Mediated Cell Behavior

Fibronectin (FN) matrix assembly on the free surface of the blastocoel roof is dependent upon C-cadherin mediated adhesion during *Xenopus* gastrulation (Winklbauer, 1998; Dzamba et al., 2009). At the onset of gastrulation BCR cells are rounded, however, as gastrulation proceeds the cells become polygonal, indicating an increase in cell-cell adhesion and intracellular tension (Dzamba et al., 2009). The initial step in FN matrix assembly occurs when integrin α5β1 receptors bind FN dimers at cell-cell boundaries in the BCR at the onset of gastrulation. As gastrulation proceeds, C-cadherin adhesion increases (Reintsch and Hausen, 2001) resulting in assembly of the cortical actin cytoskeleton, and myosin light chain phosphorylation results in cytoskeletal contraction, generating tension along the surface of the BCR (Dzamba et al., 2009). Tension is transmitted to integrin α5β1 via anchoring to the actin cytoskeleton, which enables active translocation of these complexes from sites of cell-cell adhesion centripetally along the free surface of cells in the BCR

(Davidson et al., 2008). The increased BCR tension and integrin translocation promotes unfolding of integrin associated FN dimers, exposing cryptic sites and promoting self-assembly of a FN matrix. Regulation of C-cadherin adhesion is required for FN matrix assembly as expression of a dominant negative C-cadherin leads to a decrease in tissue tension and cells retain a round morphology, and precocious FN matrix assembly occurs upon over-expression of cadherin (Dzamba et al., 2009).

Cells undergoing CE movements exhibit a decrease in C-cadherin mediated adhesion (Zhong et al., 1999; Lee and Gumbiner, 1995). The requirement for modulation of C-cadherin adhesion during CE has been demonstrated experimentally using a C-cadherin activating antibody (Zhong et al., 1999) dominant negative C-cadherin construct, and over-expression of C-cadherin (Lee and Gumbiner, 1995). Both C-cadherin over-expression and addition of the C-cadherin activating antibody result in upregulation of C-cadherin mediated adhesion and consequently CE and gastrulation fail (Zhong et al., 1999; Lee and Gumbiner, 1995). A similar phenotype was observed in embryos expressing a dominant negative C-cadherin construct (Lee and Gumbiner, 1995), suggesting that balanced regulation of C-cadherin mediated cell-cell adhesion at the blastopore lip is a requirement for tissue involution and axial extension.

Inhibition of a normal decrease in C-cadherin mediated adhesion in post-involution tissue via over-expression of C-cadherin results in an inhibition of TS (Wacker et al., 2000). This indicates that decreased C-cadherin adhesion in post-involution tissue is essential for TS (Wacker et al., 2000). Some insights into the regulation of C-cadherin adhesion in the marginal zone have recently been published, suggesting paraxial protocadherin (PAPC)

expression in the DMZ decreases C-cadherin adhesion (Medina et al., 2004; Kraft et al., 2012). PAPC inhibits the lateral clustering of C-cadherin and β-catenin as well as *cis* dimerization (Kraft et al., 2012). PAPC expression is localized to the involuting tissue, and surface expression is dependent upon both Wnt-11 and Fz7 (Kraft et al., 2012). Inhibition of Fz7 resulted in PAPC degradation, and inhibition of Wnt-11 resulted in internalization of PAPC (Kraft et al., 2012). Inhibition of PAPC surface expression results in an inhibition of the posterior part of Brachet's cleft, TS, and CE (Medina et al., 2004). Thus, Fz7 and Wnt-11 expression in the DMZ leads to PAPC stabilization and localization to the cell surface resulting in decreased C-cadherin mediated cell-cell adhesion necessary for TS and CE movements (Medina et al., 2004; Kraft et al., 2012).

1.2.2 Integrin Mediated Behavior

Morphogenetic movements in the BCR require intact integrin α5β1 signaling (Marsden and DeSimone, 2001; Rozario et al., 2009). During gastrulation a dense FN matrix is assembled along the free surfaces of the ectodermal cells lining the BCR (described in 1.2.1). Inhibition of integrin α5β1-FN ligation or FN matrix assembly via FN function blocking antibodies, a dominant negative integrin construct (Marsden and DeSimone, 2001), or a 70kDa FN construct that inhibits matrix assembly (Rozario et al., 2009) result in inhibition of cell polarity in the BCR, that is required for radial intercalation during epiboly. Rozario et al. (2009) demonstrated that not only is integrin α5β1-FN ligation required for epiboly and gastrulation, but FN matrix outside-in signaling through integrin α5β1 is also required. When

FN matrix assembly was perturbed via 70kDa FN fragment expression, BCR cells became rounded indicative of a decrease in tissue tension (Rozario et al., 2009). Tissue tension in the BCR may impinge upon cell polarity via mechanical coupling of the ECM to the cytoskeleton, as a decrease in tissue tension results in BCR thickening and inhibition of epiboly (Rozario et al., 2009).

Interestingly, integrin α5β1-FN ligation is necessary for cell intercalation movements in the DMZ that drive convergent extension; however, fibrillar FN is not (Rozario et al., 2009). Fibrillar FN may not be necessary for CE in the DMZ as integrin α5β1 adhesive behavior changes upon mesoderm involution (Ramos and DeSimone, 1996). Integrin α5β1 receptors in pre-involution mesoderm bind to the Arg-Gly-Asp (RGD) site of FN, and this binding results in a state of static adhesion (Ramos and DeSimone, 1996). Both post-involution as well as *in vitro* induced mesoderm exhibit a change in integrin α5β1 adhesive behavior such that integrin α5β1 binds to both the RGD and synergy sites of FN located within the central cell binding domain (CCBD; Ramos and DeSimone, 1996). This change in adhesive behavior results in a change from static adhesion to motile as cells undergo migration (Ramos and DeSimone, 1996). Since the anterior mesendoderm migrates along the BCR, and the posterior mesoderm undergoes CE movements, neither tissue is stably attached to a FN matrix through integrins. This suggests that FN may act as a spatial cue for regulation of post-involution tissue morphogenesis.

1.3 Regulation of Integrin Adhesion

Cell-ECM adhesion is mediated via ligation of the extracellular domain of integrins with a ligand. Upon ligation multiprotein cytoplasmic complexes are recruited to integrin tails (Hynes, 2002). In tissue culture cells these complexes are known as focal adhesions (FA), which can contain over 180 different molecules with over 700 predicted protein-protein interactions (Zaidel-Bar and Geiger, 2010). These diverse complexes result in a wide variety of signaling networks involved in regulation of cell shape, migration, proliferation, differentiation, survival, polarity, and morphogenesis.

Xenopus morphogenesis requires integrin α5β1 ligation to the ECM protein FN. One complex that has been shown to bind to β1 and β3 integrin tails *in vitro* (Hannigan et al., 1996) is the ILK (integrin-linked kinase), PINCH (particularly interesting cysteine-histidine rich protein), parvin complex. This complex forms in the cytosol and is recruited to sites of integrin β1 or β3 tails upon integrin ligation, where it is involved in regulating integrin mediated changes in cell shape, adhesion, and migration (Zhang et al., 2002b, 2004; Yamaji et al., 2001; Wickstrom et al., 2010). Depletion of ILK, PINCH, or parvin in invertebrates *in vivo* results in cell-ECM adhesion defects and consequently embryonic lethality (Wickstrom et al., 2010; Fukuda et al., 2003; Zervas et al., 2001; Vakaloglou et al., 2012). In *Drosophila melanogaster* (*Drosophila*) triple mutants of the ILK-PINCH-parvin (IPP) complex have identical phenotype to single deletions of ILK, PINCH, or parvin, suggesting that IPP complex formation is necessary for normal cell-ECM adhesion during embryogenesis (Vakaloglou et al., 2012).

1.3.1 ILK

ILK contains five tandem ankyrin (ANK) domains, followed by a pleckstrin homology domain (PH) and a kinase-like domain (Figure 1.4; Legate et al., 2006). The N-terminal ANK domain mediates interaction with PINCH, while the kinase domain mediates interactions with parvin and β1 and β3 integrin tails (Figure 1.4; Hannigan et al., 1996; Tu et al., 2001; Legate et al., 2006). Recent evidence from *Drosophila* suggests that the recruitment of ILK and other members of the IPP complex are regulated in a tissue specific manner (Vakaloglou et al., 2012). In wing epithelium, recruitment and stabilization of ILK and the other members of the IPP complex are interdependent on the abundance of all three members (Vakaloglou et al., 2012); similar to what is observed in mammalian tissue culture cells (Zhang et al., 2002b). However, at muscle attachment sites ILK stability is not dependent on PINCH or parvin abundance, although ILK is necessary for the recruitment of both PINCH and parvin, as well as the actin cytoskeleton to sites of integrin-ECM ligation (Vakaloglou et al., 2012). ILK depletion results in loss of localization of both PINCH and parvin, however, depletion of either PINCH or parvin does not inhibit ILK localization (Zervas et al., 2011; Vakaloglou et al., 2012). This suggests that unlike the situation in tissue culture cells (Zhang et al., 2002b) several distinct mechanisms are involved in regulating ILK localization and recruitment *in vivo*.

Knock down of ILK expression in *Xenopus laevis* embryos using morpholinos results in inhibition of blastopore closure and CE defects (Yasunaga et al., 2005). Similar defects are observed in embryos where integrin-ECM binding is inhibited via expression of dominant

negative integrin constructs (Marsden and DeSimone, 2001, 2003), function blocking antibodies (Marsden and DeSimone, 2001, 2003), or morpholinos to FN (Marsden and DeSimone, 2003; Davidson et al., 2006). The common defects seen between embryos lacking integrin and ILK suggests ILK may be downstream of or involved in regulating cell-ECM adhesion during *Xenopus* gastrulation.

1.3.2 PINCH

PINCH is a member of the LIM (Lin-11, Isl-1, Mec-3) family of proteins, and consists of five tandem LIM domains (Figure 1.4). Invertebrate genomes contain one PINCH gene, while two PINCH genes are encoded in mammalian genomes (Legate et al., 2006). Mammalian PINCH-1 and PINCH-2 have 82% amino acid sequence homology (Kovalevich et al., 2011). PINCH-1 and PINCH-2 are co-expressed in a variety of mammalian cells including human mesangial cells, mouse C2C12 myoblasts, and human IMR-90 lung fibroblasts, where PINCH-2 negatively regulates expression of PINCH-1 (Zhang et al., 2002a). PINCH-1 and PINCH-2 bind to ILK in a mutually exclusive manner and have antagonistic affects on cell-ECM adhesion, spreading, and migration (Zhang et al., 2002a). Inhibition of PINCH-ILK interaction inhibits PINCH localization to FAs, suggesting PINCH-ILK interaction is necessary for recruitment of PINCH to sites of integrin adhesion (Zhang et al., 2002a).

Outside of ILK binding, PINCH can also bind to Grb4 (Growth factor receptor-bound protein-4) via the LIM4 domain (Tu et al., 1998). Grb4 has been shown to interact with the

cytoplasmic domain of B ephrins (Cowan and Henkemeyer, 2001). Ephrins are ligands to the Eph receptor tyrosine kinases and interaction of Ephs with ephrins occurs at the interface of opposing tissues, promoting bidirectional signaling. Eph-ephrin signaling is required for cell-repulsion during tissue separation in *Xenopus* gastrulae (Park et al., 2011; Rohani et al., 2011).

Since there is one PINCH ortholog present in invertebrate genomes, this suggests there is an ancestral form of PINCH regulation. *Drosophila* PINCH null mutants display a similar phenotype to ILK and parvin mutants at muscle attachment sites (described in section 1.3.1; Clark et al., 2003; Vakaloglou et al., 2012; Zervas et al., 2011). However, ILK localization occurs independently of PINCH expression while parvin localization was slightly reduced suggesting PINCH has a minor role on the regulation of parvin *in vivo* (Clark et al., 2003; Vakaloglou et al., 2012; Zervas et al., 2011).

The *Xenopus* genome contains one PINCH ortholog, similar to invertebrates (Pilli, 2012; Legate et al., 2006). During *Xenopus* gastrulation PINCH appears to function independent of ILK, as PINCH and ILK do not co-immunoprecipitate (Pilli, 2012). Consistent with this, inhibiting potential PINCH-ILK interactions via a LIM1 domain mutation construct does not reduce PINCH localization to sites of integrin adhesion (Pilli, 2012). This indicates that PINCH localization to sites of integrin adhesion occurs independent of the IPP complex, suggesting that members of the IPP complex may have unique roles in *Xenopus* gastrulae. In contrast to the role PINCH plays in regulation of cell-ECM adhesion during invertebrate embryogenesis, PINCH inhibits epiboly, FN matrix assembly, and blastopore closure (Pilli, 2012). These phenotypes are similar to those

observed in embryos lacking integrin function (Marsden and DeSimone, 2001; Rozario et al., 2009), however, when dissociated cells were plated onto FN substrates, no change in integrin mediated adhesion was observed when the PINCH LIM1 domain was deleted (Pilli et al., 2012). The phenotypes observed in *Xenopus* upon PINCH over-expression could also be caused by decreased cadherin adhesion and tissue tension (Dzamba et al., 2009), however, no change in C-cadherin mediated adhesion was observed, (Pilli, 2012), indicating that PINCH may regulate cell adhesion via an integrin cadherin independent mechanism.

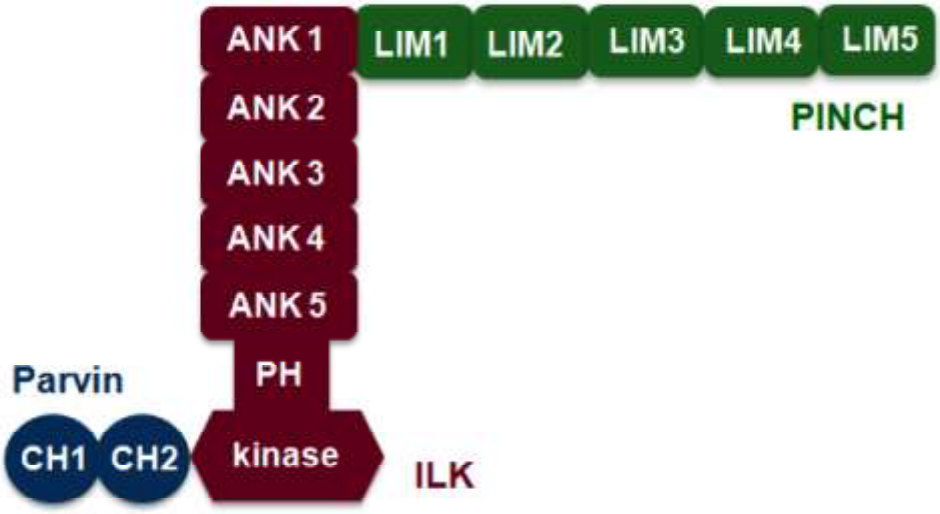

Figure 1.4 The IPP complex. The IPP complex is composed of three proteins. The central protein integrin-linked kinase is composed of 5 N-terminal ankyrin (ANK) repeats followed by one pleckstrin homology domain and a C-terminal kinase-like domain. The N-terminal ANK domain binds to the N-terminal Lin11, Isl-1, Mec-3 (LIM) domain of particularly interesting new cysteine-histidine rich protein which is composed of five LIM domains. The C-terminal kinase-like domain mediates interaction with the second calponin homology (CH) domain of parvin (CH2), which is composed of two CH domains. *Figure adapted from Legate et al., 2006.*

1.3.4 Parvin Regulates Cell-ECM Adhesion

The parvins are a family of scaffolding proteins. In mammals there are three family members α-, β-, and γ-parvin (Sepulveda and Wu, 2006). Both α- and β-parvin are ubiquitously expressed whereas γ-parvin expression is limited to the hematopoeitc system (Sepulveda and Wu, 2006), and will not be discussed further. Parvins consists of two calponin homology (CH) domains separated by a 60 amino acid linker (Sepulveda and Wu, 2006). Parvins have no intrinsic catalytic capability, and they act to assemble signaling scaffolds.

In mammalian cultured cells the CH2 domain of α- and β-parvin interact with the kinase domain of ILK in a mutually exclusive manner (Figure 1.4; Tu et al., 2001; Yamaji et al., 2001; Zhang et al., 2004). Neither α- or β-parvin CH2 deletion constructs are able to localize to sites of integrin adhesion, suggesting interaction with ILK is required for parvin localization (Yamaji et al., 2001; Tu et al., 2001; Olski et al., 2001). Both α- and β-parvin CH1 deletion constructs retain the ability to bind ILK and localize to FAs, however, cells display a rounded morphology with decreased cell-ECM adhesion, spreading, and migration (Nikolopoulos and Turner, 2000, 2002; Olski et al., 2001; Tu et al., 2001; Yamaji et al., 2001). This suggests that the CH2 domain of parvin is necessary for recruitment to sites of integrin adhesion, and the CH1 domain is necessary for signaling downstream of cell-ECM adhesion.

The CH1 domain of β-parvin is able to interact with α- and β-PIX (p21-activated serine-threonine kinase-interacting exchange factor), which are Rho guanine nucleotide exchange factors (GEF; Rosenberger et al., 2003; Mishima et al., 2004; Matsuda et al.,

2008). Activation of the small Rho GTPases results in changes in the actin cytoskeleton resulting in increased filopodia (Cdc42), lamellipodia (Rac1), or stress fiber formation (RhoA) in tissue culture cells (Hall, 1998). Over-expression of full-length or the CH1 domain of β-parvin in C2C12 myoblast cells (Matsuda et al., 2008) or Madin-Darby canine kidney cells (Mishima et al., 2004) led to an increase in lamellipodia formation and cell migration, mediated by the activation of Rac1 through α- (Mishima et al., 2004) or β-PIX (Matsuda et al., 2008). Inhibition of the GEF activity of α-PIX abrogated the effects of CH1 domain over-expression, indicating α-PIX activates Rac1 activity downstream of β-parvin signaling (Mishima et al., 2004). Full-length β-parvin has been shown to both interact and localize with ILK, α-PIX, and β-PIX at the tips of lamellipodia in C2C12 cells (Matsuda et al., 2008), suggesting a possible link between integrin ligation and actin cytoskeleton assembly.

Many of the tissue rearrangements that occur during *Xenopus* gastrulation are dependent upon integrin signaling. While the movements during gastrulation have been well characterized the signaling pathways downstream of integrin have yet to be elucidated. β-parvin has been shown to be involved in integrin signaling downstream of FN ligation (Yamaji et al., 2001; Rosenberger et al., 2003). As *Xenopus* gastrulation requires integrin-FN ligation, *Xenopus* embryos provide a powerful *in vivo* model for elucidating the role of β-parvin during cell adhesion, migration, and intercalation movements. The research presented here is the first examination of β-parvin during gastrulation in *Xenopus* embryos. I have used an over-expression approach to examine the role that the two CH domains of β-parvin play downstream of integrin ligation. My results demonstrate that β-parvin is actively involved in regulating morphogenetic movements required for proper gastrulation. The CH1 domain of

β-parvin is required for the modulation of cadherin adhesion, while the CH2 domain regulates integrin adhesion during *Xenopus* gastrulation. Over-expression of either CH domain results in the loss of integrin-cadherin cross-talk, leading to an inhibition of FN matrix assembly on the BCR, and consequently a failure in morphogenetic movements that define gastrulation. Although CH1 and CH2 domain over-expression results in a failure in gastrulation, both CH domains act in opposing fashion. Interestingly over-expression of full-length β-parvin acts as an intermediate, exhibiting no phenotype. In the DMZ over-expression of the CH1 domain inhibits TS in post-involution mesoderm via activation of Rac, while CH2 over-expressed embryos exhibit TS behavior in both the pre- and post-involution mesoderm via activation of Rho. β-parvin localizes to sites of integrin-ECM adhesion in the pre-involution mesoderm, and translocates to sites of cell-cell adhesion in post-involution mesoderm, indicating that β-parvin is intimately involved in regulating cell adhesion receptor cross-talk during *Xenopus* gastrulation.

1.4 Experimental Objectives

The *Xenopus* gastrula stage embryo has proven to be a robust *in vivo* system for the investigation of integrin adhesion. There is a single functional integrin, α5β1, and a single ligand, FN. The cell and tissue movements of gastrulation that require integrin function have been extensively characterized (Keller et al., 2003). Together this provides a simple model to examine the signaling downstream of integrin ligation that regulates cell movements driving gastrulation. Furthermore, an integrin-cadherin cross-talk that is critical to cell intercalation

movements has been described (Dzamba et al., 2009). This receptor cross-talk lies downstream of integrin ligation, suggesting that integrin associated molecules are key players in the modulation of cell adhesion during gastrulation. In *Xenopus* there is no α-parvin ortholog, suggesting that β-parvin plays critical roles downstream of integrin. β-parvin is expressed in the BCR and on the dorsal side of the embryo in tissues undergoing rearrangements during gastrulation. As such it is a good candidate for a molecule intimately involved in the integrin mediated cell behaviors. I hypothesized that β-parvin could regulate integrin function during *Xenopus* gastrulation; therefore my goal was to examine the role that β-parvin plays in integrin mediated signaling during gastrulation. My experimental objectives were to complete *in vitro* localization assays in *Xenopus* A6 cells, followed by determining temporal and spatial expression of β-parvin in *Xenopus* embryos using reverse transcription-polymerase chain reaction (RT-PCR) and *in situ* hybridization. My next objective was to complete functional assays of β-parvin *in vivo* including FN cap assays, animal cap extensions, cell adhesion, and migration assays on FN substrates. Lastly I wanted to investigate the signaling properties of β-parvin *in vivo* using co-immunoprecipitation assays for members of the IPP complex, as well as Rac and Rho activation assays.

Chapter 2
Materials and Methods

2.1 Plasmid Constructs and Generation of *in vitro* Transcripts

2.1.1 β-parvin Constructs

A full-length *Xenopus laevis* β-parvin cDNA EST was obtained from American Type Culture Collection (ATCC) as an Image Consortium clone (Open Biosystems, Waltham Massachusetts, clone 5542473). The protein coding open reading frame of β-parvin was amplified by PCR using primers β-parvin forward (*Bam*HI) and β-parvin reverse (*Xho*I; Table 2.1; Isahaq Abdullaahi, Unpublished). The PCR product was inserted into the *Bam*HI and *Xho*I sites of pCS107 (XBP CS107). A full-length β-parvin GFP fusion was then generated by subcloning the protein coding sequence of β-parvin into the *Bam*HI and *Stu*I sites of pCS107 CGFP (plasmid was created by inserting GFP into the *Stu*I-*Xho*I sites of pCS107; Isahaq Abdullaahi; XBP-GFP CS107; Figure 2.1).

Two deletion constructs termed RP1 and RP2 were previously created (Hyder Al-Attar, Unpublished). RP1 consists of amino acids 1-212, and RP2 consists of amino acids 213-364 (Figure 2.2). Both RP1 and RP2 sequences were amplified by PCR using *Pfu* polymerase (Table 2.1; Hyder Al-Attar, Unpublished) in an Eppendorf personal thermocycler (Eppendorf, Mississauga, Ontario). These sequences were cloned into the pCS2 vector (Figure 2.3) using *Bam*HI and *Stu*I (*Eco*147I) restriction sites (XRP1 CS2; XRP2 CS2).

Table 2.1 PCR primers used to clone *Xenopus laevis* β-parvin, RP1, and RP2.

Clone	Primer DNA Sequence	Restriction Enzyme
β-parvin	Forward 5’	*Bam*HI
	CGGATCCATGTCCAGCACCCCAGTC 3’	
	Reverse 5’	
	GGCTCGAGTCAGTCGAGGTGCTTGTACTTTG 3’	*Xho*I
RP1	Forward 5’	*Bam*HI
	CGGATCCATGTCCAGCACCCCAGTC 3’	
	Reverse 5’	
	CCAGGCCTCTTCACTACTACCACTTGTACAC 3’	*Stu*I
RP2	Forward 5’	*Bam*HI
	CCGGATCCATGAAGAAACGCGAGGGGC3’	
	Reverse 5’	
	CCAGGCCTGTCGAGGTGCTTGTACTTTG 3’	*Stu*I

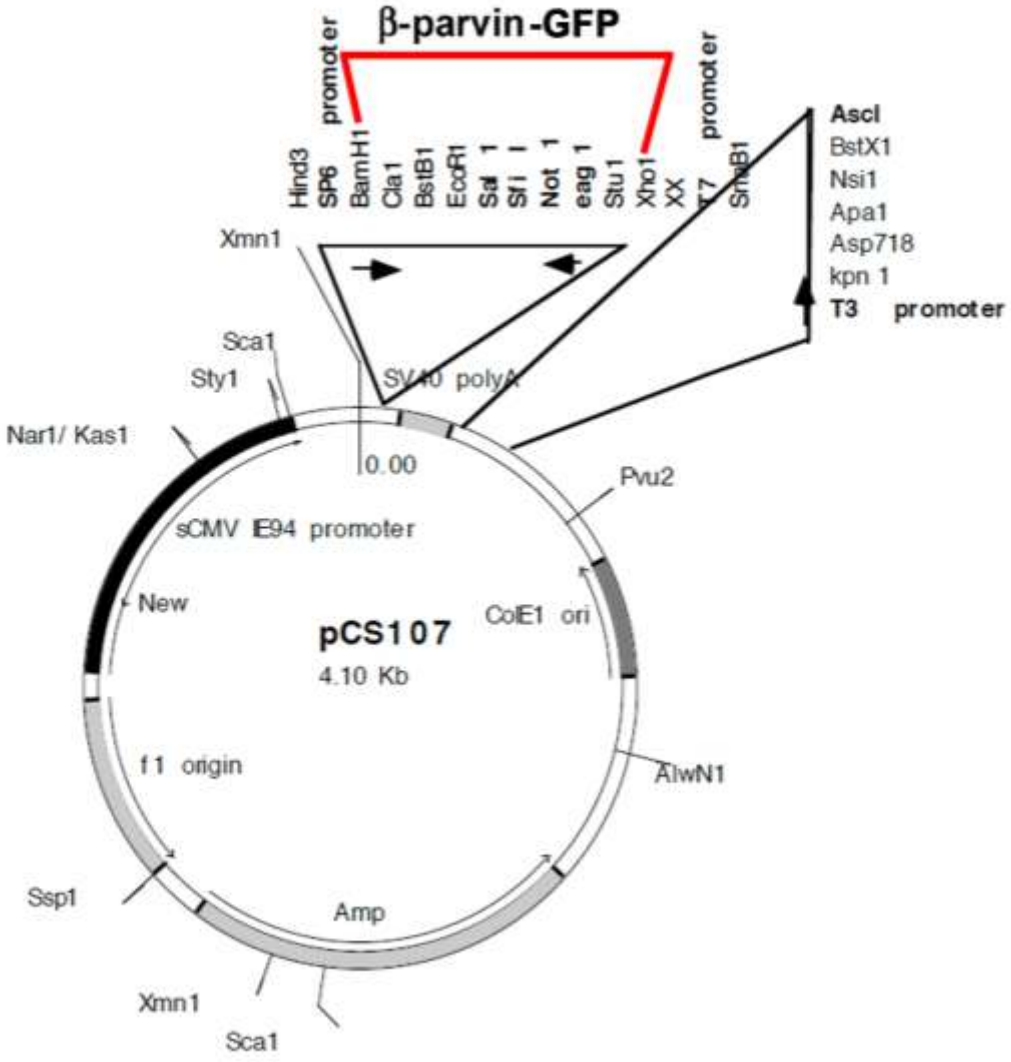

Figure 2.1 XBP-GFP CS107. The coding sequence of β-parvin was directionally cloned into the *Bam*HI and *Stu*I sites of pCS107. GFP was directionally cloned into the *Stu*I and *Xho*I sites of pCS107. This construct is used for *in vitro* transfections, and *in vitro* transcription with SP6 polymerase, following linearization with *Asc1*. pCS107 was a gift from Dr. Richard Harland.

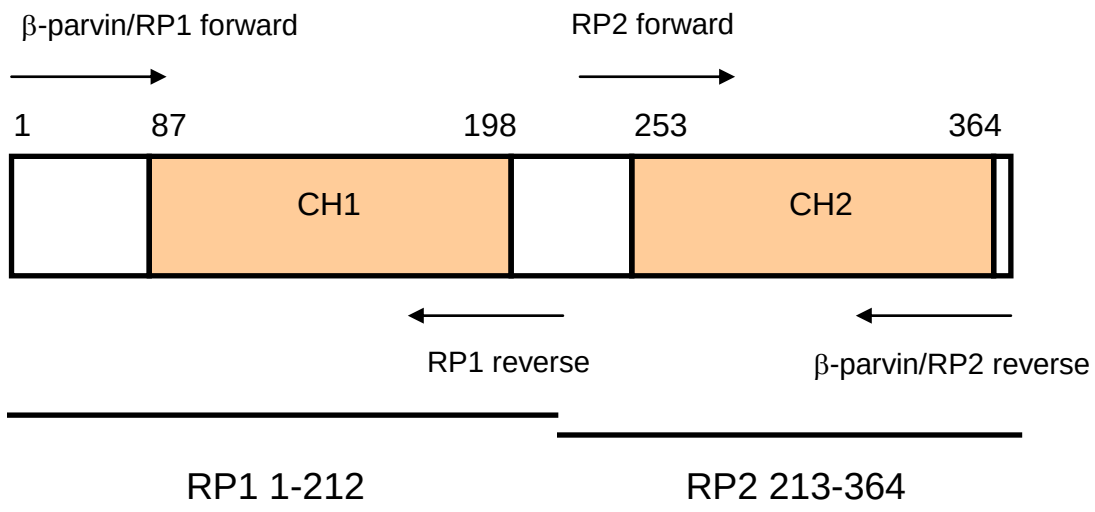

Figure 2.2 β-parvin deletion constructs. β-parvin contains two calponin homology (CH) domains. Two deletion constructs were generated, RP1 and RP2. RP1 contains the first CH domain, and RP2 contains the second CH domain. Numbers indicate amino acid positions. Arrows indicate forward and reverse primers. RP1 and RP2 are indicated with a horizontal line.

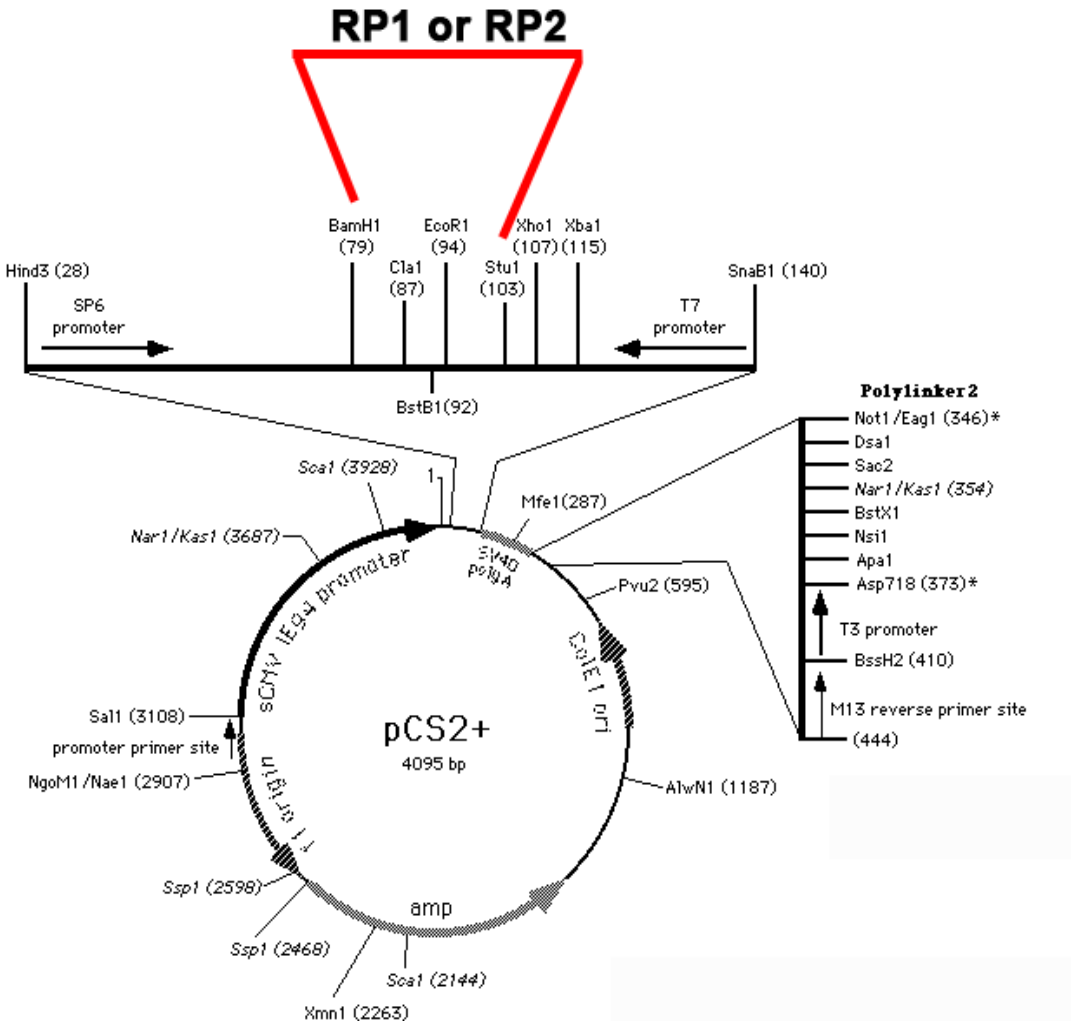

Figure 2.3 XRP1 CS2 and XRP2 CS2. The coding sequence of the RP1 and RP2 constructs were directionally cloned into the *Bam*HI and *Stu*I sites in pCS2.

2.1.2 Subcloning

XL-1 Blue *E. coli* (Stratagene, La Jolla, California) containing the plasmid of interest were incubated overnight at 37°C in 3mL of Luria-Bertani Medium (LB; 1% tryptone (w/v), 0.5% yeast extract (w/v), 1% NaCl (w/v)) supplemented with 100μg/mL ampicillin (Calbiochem, Mississauga, Ontario). Overnight cultures were pelleted by centrifugation for five minutes, and plasmids were isolated using a High-Speed Plasmid Mini Kit (FroggaBio Scientific Solutions, Toronto, Ontario). Plasmids were separated on a 1% TAE (40mM Tris-acetate, 1mM EDTA) agarose (w/v) gel containing 0.2μg/mL ethidium bromide to confirm size, quantity, and integrity.

Unless otherwise specified the following reaction concentrations were used for PCR amplification: 50ng DNA template, 1X *Pfu* polymerase buffer with $MgSO_4$ (Fermentas, Burlington, Ontario), 50ηg forward primer, 50ηg reverse primer, and 0.2mM dNTPs.

PCR was performed using the hot start method. Briefly, an initial two minute cycle at 95ºC, following which 2.5 units of *Pfu* polymerase (Fermentas, Burlington, Ontario) was added to the reaction. This was followed by 30 cycles of: 30 seconds at 95ºC, 30 seconds at 50ºC, and 90 seconds at 68 º C. An additional 5 minutes at 68ºC was included after the last cycle. PCR products were separated on a 1% agarose gel and visualized as described earlier.

For subcloning of PCR products, 10μl of the PCR reaction was digested with restriction enzymes (see Table 2.1) in a total volume of 50μl and incubated at 37°C. The digested product was separated on a 1% agarose gel as previously described. The band representing the PCR product of interest was isolated and purified using the Gel Extraction

Protocol in the Gel/PCR DNA Fragments Extraction Kit from FroggaBio Scientific Solutions (Toronto, Ontario). Yield and quality of purified PCR products was estimated on an agarose gel as described earlier.

The concentration of each insert was visually estimated on an agarose gel by comparing the intensity of the band to the λ/HindIII DNA ladder marker bands, and a 3:1 insert to vector molar ratio was used for ligation. Ligations were performed with 1X T4 DNA Ligase buffer (Fermentas, Burlington, Ontario) and one unit of T4 DNA Ligase (Fermentas, Burlington, Ontario) per 20μL reaction for two hours at room temperature. 100μL of frozen chemically competent XL1-Blue *E. coli* were thawed and 10μL of the ligation reaction was added. The reaction was incubated for ten minutes on ice, followed by 45 seconds heat-shock at 42°C, and two minutes on ice, after which 300μL of LB media was added, and the transformation incubated with agitation for 30 minutes at 37°C. The transformation was spread onto LB-agar plates (LB with 1.5% agar (w/v)) containing 50μg/mL ampicillin (Calbiochem, Mississauga, Ontario). Two plates were made, one at a low density (50μL) and one with a high cell density (250μL). Bacterial plates were incubated overnight at 37°C. Two isolated colonies were selected and inoculated into 3mL LB containing 50μg/mL ampicillin (Calbiochem, Mississauga, Ontario), and incubated overnight at 37°C with agitation. The plasmids were isolated and separated on an agarose gel as previously described.

2.1.3 Generation of Plasmid Constructs

GFP-XRP1 CS2 and GFP-XRP2 CS2 (Figure 2.4) fusion constructs were generated by

digestion of RP1 and RP2 PCR-amplified sequences with *Bam*HI and *Stu*I restriction enzymes. These PCR products were then ligated into the *Bam*HI and *Stu*I sites of pCS2-GFP-N1, fusing GFP to the N-terminus of the RP1 and RP2 constructs.

β-parvin was removed from pCS107 using *Bam*HI and *Xho*I restriction enzymes and ligated into the *Bam*HI and *Xho*I restriction sites in Bluescript II KS +/- (BS; Figure 2.5; XBP BS). XBP BS was used for generation of sense and anti-sense riboprobes.

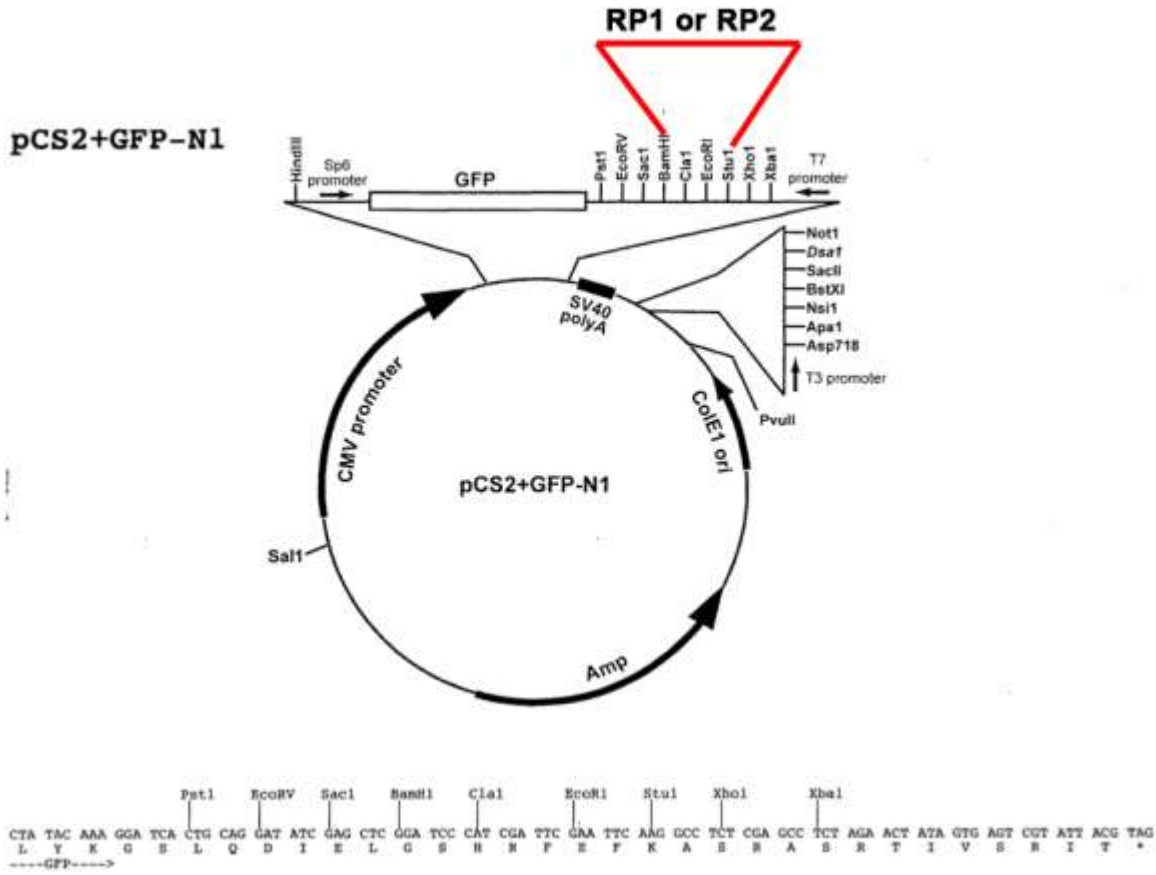

Figure 2.4 GFP-XRP1 CS2 and GFP-XRP2 CS2. This plasmid was used to generate N-terminal tagged GFP constructs. The coding sequence of RP1 and RP2 constructs were directionally cloned into the *Bam*HI and *Stu*I sites. Plasmid was a gift from Dr. Jeff Miller.

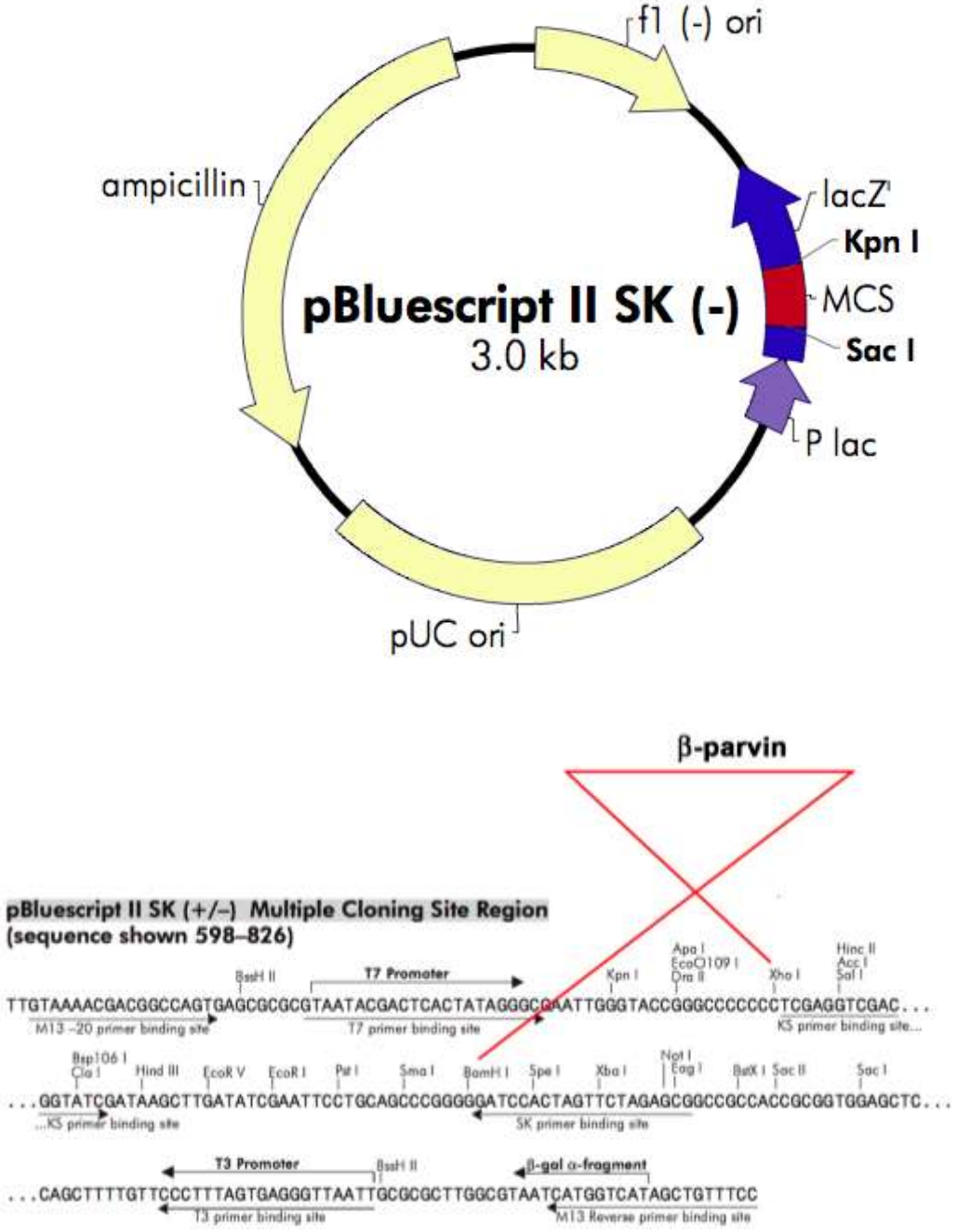

Figure 2.5 XBP BS. This plasmid was used to generate sense and anti-sense riboprobes (section 2.5.1). β-parvin coding sequence was directionally cloned into the *Bam*HI and *Xho*I restriction sites found within the multiple cloning site (MCS).

A red fluorescent protein (RFP) sequence (Campbell et al., 2002) was removed from pSB1A2 (registry of biological parts, Tom Knight) using *Bgl*II and *Bam*HI restriction enzymes. The isolated and purified RFP sequence was ligated into the *Bam*HI site of pCS2 to create pCS2-RFP.

ILK-pSPORT was obtained as an Image Consortium clone (Open Biosystems, Waltham Massachusetts, clone 731117). ILK sequence was amplified by PCR using *Pfu* polymerase (primers listed in Table 2.2), digested using *Bgl*II and *Xba*I restriction enzymes, and ligated into the *Bam*HI and *Xba*I sites of pCS2-RFP, fusing the RFP tag to the N-terminus of ILK (RFP-XILK CS2).

Table 2.2 PCR primers used to clone *Xenopus* ILK

Clone	Primer DNA Sequence	Restriction Enzyme
ILK	Forward 5’	*Bgl*II
	CGCAGATCTGATGACATTTTCGCTCAGTGTC 3’	
	Reverse 5’	
	CGCTCTAGATTTCTCCTGCATCTTCTCCAG 3’	*Xba*I

2.1.4 *in vitro* mRNA Transcription

GFP-XRP1 CS2, GFP-XRP2 CS2, and pCS2-GFP-N3 (Figure 2.6) were linearized using *Not*I restriction enzyme, and XBP-GFP CS107 was linearized using the *Asc*I enzyme. Digested DNA was purified from solution using PCR Clean Up Protocol in the Gel/PCR

DNA Fragments Extraction Kit from Froggabio Scientific Solutions (Toronto, Ontario). Purified DNA was separated on an agarose gel to estimate size, visualize quantity, and integrity as described earlier.

Transcription reactions were carried out in a 50μL volume including: 5μg of linearized purified DNA, 1X Reaction Buffer (New England Biolabs, Toronto, Ontario), 1mM rATP, 1mM rCTP, 1mM rUTP, 0.1mM rGTP (all ribonucleotide triphosphates from Fermentas, Burlington, Ontario), 1mM G(5')ppp(5')G RNA Cap Structure Analog (New England Biolabs, Toronto, Ontario), and 40 units Ribolock RNase Inhibitor (Fermentas, Burlington, Ontario), followed by the addition of 100 units SP6 RNA Polymerase (New England Biolabs, Toronto, Ontario) and incubation at 40°C for 30 minutes. An additional 0.5mM rGTP (Fermentas, Burlington, Ontario) was added and the transcription reaction was incubated for one hour at 40°C, followed by the addition of three units of RQ1 RNase-Free DNase (Promega, Madison, Wisconsin), incubation for 30 minutes at 37°C, and subsequent addition of 2μL of 0.5M EDTA. The mRNA was purified using Ambion Mega Clear Kit following manufacturer instructions (Invitrogen, Burlington, Ontario). Yields were assessed using Ultrospec 2100 pro at 260/280nm (GE Healthcare, Baie-D'Urfe, Quebec).

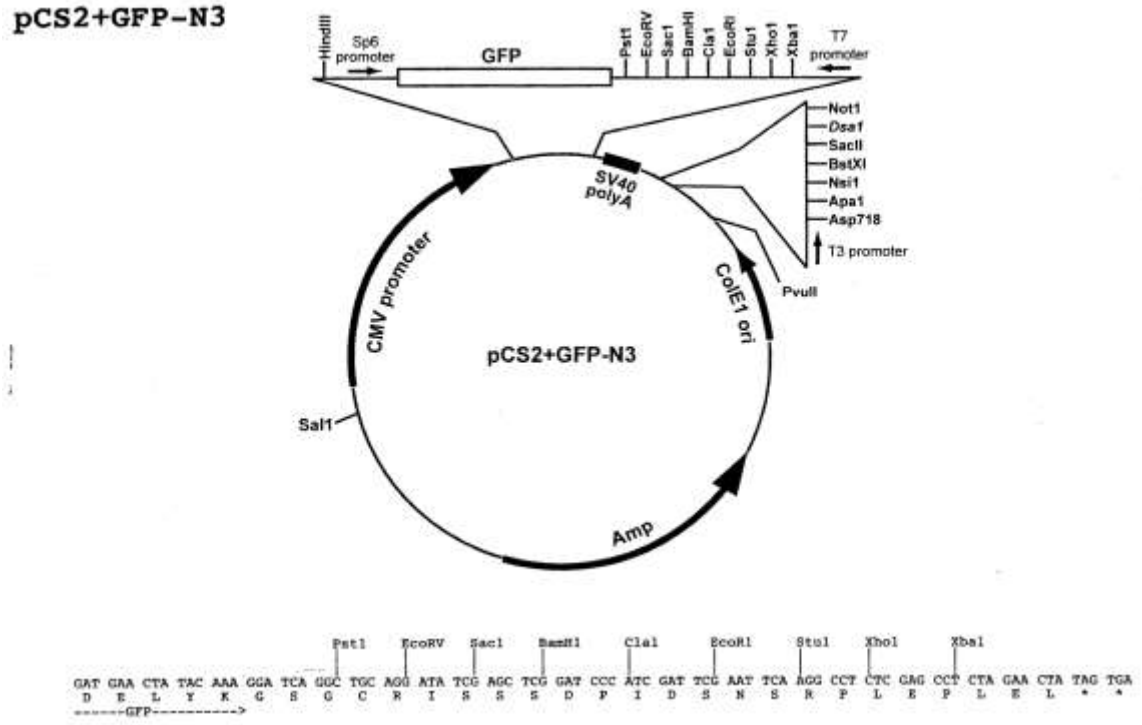

Figure 2.6 pCS2-GFP-N3. No insert was cloned into this plasmid. This plasmid was used as control for DNA transfections and mRNA microinjections.

2.2 Maintenance and Manipulations of *Xenopus laevis* Embryos

Sexually mature *Xenopus laevis* were purchased from Nasco (Fort Atkinson, Wisconsin) and housed in the Department of Biology Aquatic Facility at the University of Waterloo. Three to seven days prior to spawning female frogs were pre-primed with 50 units HCG (Chorulon; Intervet, Kirkland, Quebec), and spawning was induced with subcutaneous injection with 600 units of HCG. Eggs were obtained by manual stripping, and fertilized *in vitro* following standard protocol (Sive et al., 1996). Fertilized embryos were dejellied in 2% cysteine

hydrochloride (w/v; BioShop, Burlington, Ontario; pH 8.3) with gentle agitation. Embryos were rinsed three times with deionized water, and two times in 0.1X MBS (Modified Barth's Saline; 1X MBS; 88mM NaCl, 1mM KCl, 0.7mM $MgSO_4$, 1mM HEPES, 5mM $NaHCO_3$, 0.1mM $CaCl_2$, pH 7.6) prior to transfer to a 100mm Petri dish. Embryos were cultured in 0.1X MBS and staged according to Nieuwkoop and Faber (1994).

2.2.1 Microinjections and Imaging

Injections were performed using a Narishige IM300 pressure injector (East Meadow, New York) with glass microinjection needles created using a Narishige PC-10 puller (East Meadow, New York). Embryos were transferred and arranged on a mesh grid in 0.5X MBS containing 4% Ficoll 400 (BioShop, Burlington, Ontario), and mRNA (section 2.1.5) was microinjected into the animal cap of a two-cell embryo or dorsal marginal zone of a four-cell embryo. Two nanograms of each mRNA construct were injected, and some co-injections with Rac1 and RhoA constructs were performed as described in the Results section. Following injection embryos were transferred to 0.1X MBS and cultured until the desired stage for manipulation or imaging. Embryos were imaged on a Zeiss Lumar V12 stereo microscope (Zeiss, Mississauga, Ontario) with a Qimaging Micropublisher 5.0 RTV digital camera (Qimaging, Burnaby, BC).

Embryos were injected with constructs and fixed in MEMFA (100mM MOPS, 2mM EGTA, 1mM $MgSO_4$, 4% formaldehyde; Sive et al., 2000) at stage 11. Embryos were bisected along the sagittal plane using a scalpel blade and Brachet's cleft or cell layers in the

BCR imaged using the Zeiss Lumar microscope as previously described.

Embryos were injected with constructs at the four cell stage and cultured until stage 11, where pre- and post- involution mesoderm were excised, and Z-stack series imaged using Nikon Eclipse 90i fitted with a Nikon D-eclipse C1 scan head using Nikon EZ-C1 software (Nikon Canada Inc., Mississauga, Ontario).

Embryos were injected with constructs at the two-cell stage and animal caps excised at stage 11 as described previously (Sive et al., 1996). Animal caps were permeabilized with 1X PBS (Phosphate Buffered Saline; 130mM NaCl, 3mM KCl, 10mM Na_2HPO_4, 2mM KH_2PO_4, 1mM $CaCl_2$ and 1mM $MgCl_2$) with 0.1% Tween20 (v/v; PBST), and actin detected using 10μg/mL rhodamine-phalloidin (Sigma, Oakville, Ontario) in 1X PBS for 15 minutes at room temperature. Caps were rinsed three times 20 minutes each in 1X PBS, mounted onto coverslips, and imaged using Nikon Eclipse 90i as previously described.

2.2.2 Animal Cap Experiments

Animal caps were isolated and treated with activin-A as described previously (Sive et al., 1996). Briefly animal caps were excised from stage eight embryos in 1X MBS. Animal cap explants were transferred to a 60mM dish containing 0.5X MBS supplemented with antimycotic (Sigma, Oakville, Ontario) in the presence or absence of 50pM activin-A (R&D Systems, Burlington, Ontario) and cultured overnight at 18°C. Sibling embryos were cultured in 0.1X MBS at 18°C overnight as a control for normal development. Overnight explant extensions were either imaged using a Zeiss Lumar V12 microscope (Zeiss, Toronto,

Ontario) or fixed in 1X PBS containing 4% paraformaldehyde for immunocytochemistry.

Assembly of a FN matrix was monitored using immunocytochemistry. Animal cap explants and animal cap extensions were fixed in 1X PBS containing 4% paraformaldehyde. Explants were stained with a monoclonal antibody directed against FN (4B12; Ramos et al., 1996) in PBST containing1μg/mL of BSA. Primary antibodies were detected using Alexa Fluor 488 Conjugated Goat Anti-Mouse secondary antibody (Invitrogen, Burlington, Ontario). Explants were mounted on glass slides and imaged using a Zeiss Axiovert 200 (Zeiss, Mississauga, Ontario) using Open Lab Software (Improvision, Waltham, Massachusetts), or 3D FN matrix was visualized using Z-stack series imaging as described previously.

2.2.3 Tissue Separation

Ectoderm-mesoderm cell repulsion was tested by placing small cell aggregates of ectoderm and mesoderm on the inner surface of a BCR. Animal caps were removed from stage 11 control uninjected embryos as previously described (Sive et al., 1996). Embryos were injected with constructs at the four-cell stage. Explants of pre- and post-involution mesoderm tissues were removed from stage 11 embryos and placed on the control uninjected animal cap (Figure 2.7). Explants were covered with a small piece of coverslip to prevent the BCR explants from rolling up. Separation behavior was scored after 45-75 minutes as either reintegration or tissue separation.

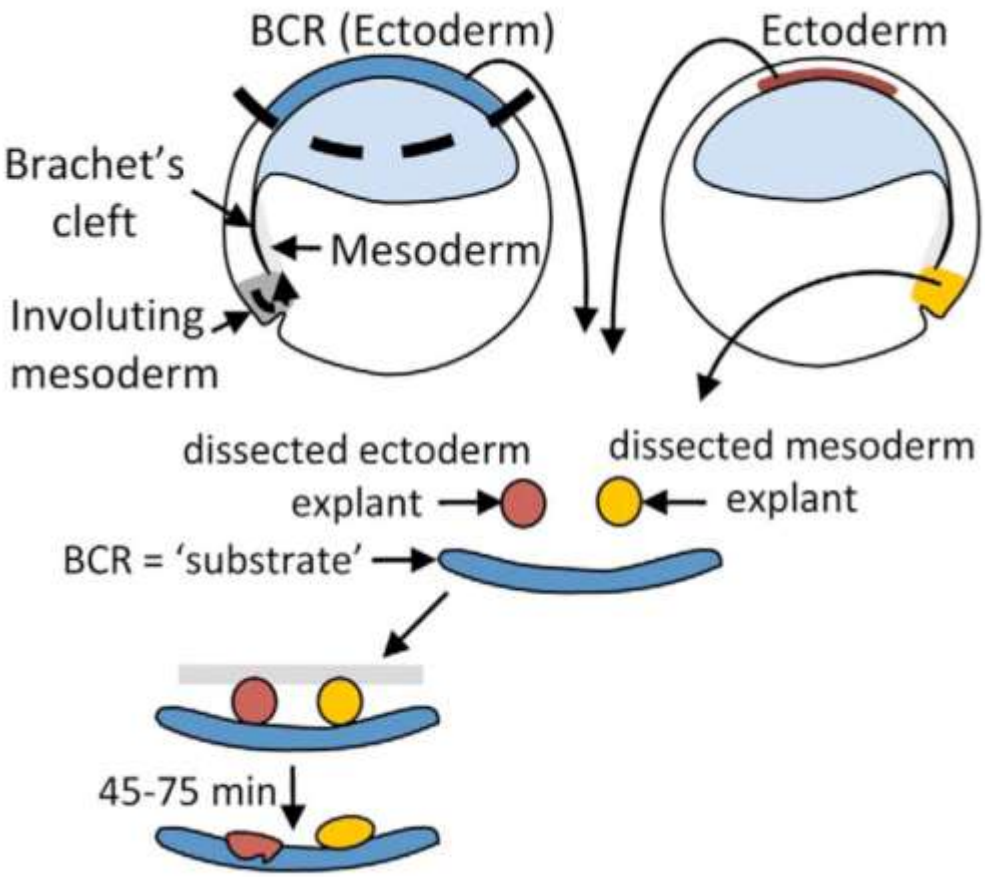

Figure 2.7 Tissue Separation Protocol. Sagittal view of stage 11 embryos. The blastocoel roof (BCR) is removed and placed in a dish with the inside surface of the BCR facing upwards. Small cell aggregates of ectoderm and mesoderm taken from a second embryo expressing the construct of interest are placed on the roof. Grey bar indicates a coverslip, which prevents rolling up of the BCR. *Adapted from Rohani et al., 2011*.

2.3 Cell Adhesion Assays

2.3.1 Preparation of Substrates

Petri dishes (60mm) were coated for six hours at room temperature with 25μg/mL human plasma FN (BD Biosciences, Bedford, Massachusetts) in 1X PBS. Substrates were blocked with 1% BSA (w/v; Bovine serum albumin; BioShop, Burlington, Ontario) in 1X PBS and washed three times with 1X MSS (3.75mM NaCl, 0.01mM Na_2SO_4, 0.25mM HEPES, 0.12mM KCl, 30mM Na_2HPO_4, 0.07mM KH_2PO_4, pH 8.3 supplemented with 1mM $CaCl_2$ and 0.5mM $MgCl_2$) before being used in adhesion and migration assays.

Coverslips were coated with 0.25μg/mL FC-cadherin in 1X MSS at 4ºC overnight. Coverslips were washed two times with 1X MSS, and blocked with 1X MSS (supplemented with 1mM $CaCl_2$ and 0.5mM $MgCl_2$) with 1 mg/mL BSA (pH 8.3) for ten minutes before being used in adhesion assays.

2.3.2 Cell Adhesion and Migration Assays

Animal caps were dissociated in MSS lacking $CaCl_2$ and $MgCl_2$, and the superficial ectoderm was removed after ten minutes. The remaining cells were cultured until sibling embryos reached stage 10, following which cells were plated onto cadherin substrates for cell adhesion assays. Cells were incubated on the substrate for 20 minutes, imaged using Zeiss Axiovert 200 inverted microscope (Zeiss, Mississauga, Ontario), Qimaging retiga 1494

digital camera (Burnaby, British Columbia), and OpenLab software (Improvision, Waltham, Massachusetts), following fixation in 4% paraformaldehyde and imaged as described. Cell adhesion counts were performed prior to and after fixation to determine percent cell adhesion counts. The same protocol with one deviation was used to measure integrin adhesion on FN substrates: dissociated cells were cultured with 50 pM activin-A until sibling embryos reached stage 10. Dissociated cells were then plated on FN substrates in 1X MSS at low density. Cells were allowed to adhere to the FN substrate for 20 minutes before imaging. For cell migration, cells were not fixed after initial imaging, and migration tracks were recorded for 2.8 hours on a Zeiss Axiovert microscope (Zeiss, Mississauga, Ontario), with a Qimaging retiga 1494 digital camera (Burnaby, British Columbia), using Open Lab Software (Improvision, Waltham, Massachusetts). At least four cells per substrate field were tracked at one minute time-lapse intervals.

2.4 RT-PCR

Embryos were cultured until stages 2, 5, 9, 10.5, 17, and 28, collected, and frozen at -80°C. RNA extractions were performed following the method of Chomczynski and Sacchi (1987) with minor modifications. Briefly, twenty-five embryos were homogenized in 500μL denaturing solution (4M guanidinium thiocyanate, 25mM sodium citrate (pH 7.0), 0.5% sarcosyl lauryl sarcosine (v/v), 100mM dithiothreitol (DTT)), followed by addition of 50μL 2M NaAc (pH 4.0), 500μL water saturated phenol, and 90μL chloroform/isoamyl alcohol (49:1). After 15 minute incubation the lysate was subjected to centrifugation for 20 minutes,

the supernatant removed and an equal volume isopropanol added, followed by one hour incubation at -20°C and centrifugation for 20 minutes. The pellet was resuspended in 500µL denaturing solution, followed by addition of 500µL isopropanol and centrifugation for 20 minutes. The pellet was then washed in 200µL 70% ethanol, followed by centrifugation for 10 minutes. Next, the pellet was resuspended in 75µL RNase DNase free water, followed by addition of 2.5µL of 4M LiCl and 125µL 100% EtOH and incubation overnight at -20°C. RNA was pelleted via centrifugation for 20 minutes and resuspended in 50µL RNase DNase free water with 5µL 1M NaAc and 125µL 100% EtOH, followed by incubation at -20°C overnight. RNA was pelleted via centrifugation for 20 minutes, pellet washed with 70% EtOH, and RNA resuspended in 50µL RNase DNase free water. Concentration, purity and integrity of RNA was estimated via separation on an agarose gel and analyzed via Ultrospec 2100 pro at 260/280nm (GE Healthcare, Baie-D'Urfe, Quebec).

First strand cDNA was created from 2µg total RNA extracted from each stage listed above using RevertAid H Minus First Strand cDNA Synthesis Kit (Fermentas, Burlington, Ontario) using a random hexamer primer (0.2µg). PCR reactions (50µL) were performed using *Taq* DNA polymerase (1.25 units) and 1X *Taq* buffer (Fermentas, Burlington, Ontario), 2µL first strand cDNA template, 50ηg of each forward and reverse primers (β-parvin Table 2.1; Table 2.3) and 0.2mM dNTPs.

PCR was initiated with a two minute hot start at 95ºC, followed by 30 cycles of: 30 seconds at 95ºC, 45 seconds at 50ºC, and 30 seconds at 72ºC. An additional incubation for 5 minutes at 72ºC was added at the end of the last cycle. A sample containing no cDNA was

included as a negative control. PCR products were separated on an agarose gel to visualize the presence of amplified cDNA.

Table 2.3 *Xenopus laevis* primers used to test mesoderm induction

Clone	Primer DNA Sequence
Xenopus Brachyury	Forward 5' GGATCGTTATCACCTCTG 3'
	Reverse 5' GTGTAGTCTGTAGCAGCA 3'
Xenopus Chordin	Forward 5' AACTGCCAGGACTGGATGGT 3'
	Reverse 5' GGCAGGATTTAGAGTTGCTTC 3'
Xenopus EF-1α	Forward 5' CAGATTGGTGCTGGATATGC 3'
	Reverse 5' ACTGCCTTGATGACTCCTAG 3'

2.5 Whole Mount *in situ* Hybridization

2.5.1 Riboprobe Preparation

DIG-UTP labeled probes were generated in a 20μL volume using 1μg linearized DNA (Table 2.4), 1X DIG RNA Labeling mix (Roche, Mississauga, Ontario), 2X transcription buffer (New England Biolabs, Toronto, Ontario), 40 units RNA polymerase (Table 2.4), and 10 units RNasin, followed by incubation at 37°C for two hours. Two units DNase 1 was added to the transcription reaction, followed by incubation at 37°C for 15 minutes, and addition of 2μL 0.2M EDTA pH 8.0. RNA transcripts were precipitated using 2.5μL of 4M LiCl and 75μL 100% EtOH at -20°C overnight, and DIG labeled probes were pelleted by centrifugation for 15 minutes. The pellet was washed with 300μL 70% EtOH (v/v), followed

by centrifugation at for 15 minutes, and the pellet resuspended in RNase DNase free water.

Table 2.4 Specific riboprobe generation conditions

Gene Insert	Orientation	Restriction Enzyme	RNA Polymerase
β-parvin	Anti-sense	*Bam*HI	T7
β-parvin	Sense	*Xho*I	T3
Xenopus Brachyury	Anti-sense	*Eco*RV	T7

Embryos were collected at stages 2, 8, 10.5, 12, 17, and 28 and fixed in MEMFA (Sive et al., 2000). Fixed embryos were subsequently used in whole mount *in situ* hybridizations with antisense or sense DIG-labeled RNA probes following standard protocol (Sive et al., 2000). Hybridized probe was detected via overnight incubation with alkaline phosphatase-coupled anti-DIG antibody (Roche, Mississauga, Ontario), followed by visualization with BM purple (Roche, Mississauga, Ontario).

2.6 Immunoblot Analysis

2.6.1 Western Blotting

Western blotting was performed using standard techniques (Sambrook and Russell, 2001). Briefly, embryos were homogenized in embryo solubilization buffer (ESB; 25mM Tris (pH 7.5), 50mM NaCl, 1% TritonX-100 (v/v), 1mM PMSF (phenylmethyl sulfonyl fluoride), 1X protease inhibitor cocktail (Roche, Mississauga, Ontario)). Equal embryo equivalents were

separated using 12% SDS-PAGE (Sambrook and Russell, 2001), and transferred onto nitrocellulose. Efficiency of transfer was confirmed with Ponceau S staining. The nitrocellulose membrane was incubated overnight in blocking solution (5% skim milk powder (w/v) in TBST (2mM Tris, pH 7.5, 30mM NaCl, 0.1% Tween20 (v/v))). Membranes were incubated with primary antibody (listed in Table 2.5) in blocking solution for one hour at room temperature, followed by three ten minute washes in blocking solution. Secondary antibody diluted to 1:3000 in blocking solution was incubated on membranes for 45 minutes at room temperature. Membranes were washed three times ten minutes each in blocking solution, and two washes five minutes each in TBS, followed by detection using enzymatic chemiluminescence (1.25mM luminol (Sigma #A-8511), 0.2mM p-coumaric acid (Sigma #C-9008), 10mM Tris-HCl (pH 8.5), 0.00018% hydrogen peroxide (v/v)) and exposure to RXB x-ray film (Labscientific; Livingston, New Jersey).

Proteins of interest were detected using primary antibodies listed in Table 2.5. Secondary antibodies used were anti-mouse or anti-rabbit horseradish peroxidase (HRP) conjugates (Jackson Labs; Bar Harbor, Maine).

2.6.2 Biotinylation

Animal caps were excised from stage eight embryos and placed in 300µL 1X PBS at 4°C. Half of the volume was removed and replaced with 150µL of 1mg/mL biotin (Thermo Fisher Scientific, Ottawa, Ontario) in 1X PBS at 4°C. Caps were mixed gently and incubated at 4°C for 30 minutes. Biotin was quenched with 100mM glycine in 1X PBS at 4°C for ten minutes. Animal caps were washed three times in 500µL 1X PBS at 4°C. Cells were lysed in 50µL

ESB and frozen at -80°C. Immunoprecipitations were performed using Protein G beads (Protein G Agarose Fast Flow, Millipore, Temecula, California) and 2μL X-Cad antibody (Table 2.5). Western blotting was performed as previously described except 5% BSA in TBST was used instead of 5% milk in TBST. Strepavidin-horseradish peroxidase conjugate (GE Healthcare, Baie-D'Urfe, Quebec) was used (1:1000) to detect biotinylated protein.

2.6.3 Co-Immunoprecipitation Assay

Embryos were homogenized in 10μL ESB (with 87.5mM NaCl)/embryo. Embryo lysates were incubated on ice for ten minutes followed by centrifugation at 4ºC for 20 minutes. Lysate was moved to a new microfuge tube. One fifth of each sample was kept on ice while the remainder was added to 500μL ESB (with 87.5mM NaCl) and pre-cleared with 10μL of either Protein G beads (Protein G Agarose Fast Flow, Millipore, Temecula, California) for use with mouse antibodies, or Protein A beads (Protein A Agarose Resin, Agarose Beads Technology, Tampa, Florida) for use with rabbit antibodies. Lysate-bead mixture was rocked at 4ºC for 60 minutes, followed by centrifugation for one minute at 4ºC, 3000 rpm. Lysate was moved to a new microfuge tube and rocked for 60 minutes at 4ºC after the addition of primary antibody, followed by two hours of rocking at 4ºC after the addition of 15μL Protein G or Protein A beads. Lysates were centrifuged to retrieve beads, supernatants removed, and beads rinsed three times with 500μL ESB. Immunoprecipitations were subjected to Western blotting as previously described.

Table 2.5 Antibodies

Antibody	Animal	Dilution	Manufacturer
GFP 7.1 and 13.1	Mouse	1:1000	Roche, Mississauga, Ontario
ILK 4G9	Rabbit	1:1000	Cell Signaling Technology, Danvers Massachusetts
PINCH C58	Mouse	1:2000	Abcam, Cambridge, Massachusetts
β-Tubulin	Mouse	1:5000	Gift from R. Bloodgood, University of Virginia
Paxillin	Mouse	1:2000	Transduction Laboratories, Mississauga, Ontario
X-Cad	Rabbit	1:2500	Gift from B. Gumbiner, University of Virginia
RhoA (119)	Rabbit	1:500	Santa Cruz Biotechnology, Dallas, Texas
Rac1 (23A8)	Mouse	1:1000	Millipore, Temecula, California

2.7 Rac1 and RhoA Activation Assays

2.7.1 Preparation of GST-PBD Beads for Rac1 Activation Assay

Six milliliters of LB with 100μL/mL ampicillin was inoculated with pGEX GST-PBD (Sander et al., 1998; Addgene, Cambridge Massachusetts) in BL21 *E. coli* bacterial cells and incubated overnight at 30°C. The overnight culture was diluted 1:10 in LB, and incubated for three hours at 30°C. GST-PBD (p21-binding domain) protein expression was induced with 0.3mM IPTG (isopropyl β-D-1-thiogalactopyranoside), for four hours at 30°C. Bacterial cells were centrifuged at 4000 rpm for ten minutes at 4°C. Supernatant was removed, and the pellet was resuspended in 500μL lysis buffer (20mM HEPES pH 7.5, 120mM NaCl, 10% glycerol (v/v), 2mM EDTA, 1mM PMSF, and 1X protease inhibitor cocktail (Roche,

Mississauga, Ontario)). The suspension was sonicated (Misonix, Farmingdale, New York) for 15 seconds twice, and lysate was centrifuged for 15 minutes at 4°C. Supernatant was moved to new 1.5mL microfuge tube and NP-40 was added to 0.5% (v/v). Glutathione-Sepharose 4B beads (GE Healthcare, Baie-D'Urfe, Quebec) were washed with lysis buffer, and 100μL of 50% slurry was added to the lysate, and incubated for one hour at 4°C with rotation. Beads were washed five times in lysis buffer with 0.5% NP-40 (v/v) with centrifugation at 2000 rpm for one minute at 4°C, followed by three washes in lysis buffer with no NP-40 with centrifugation at 2000 rpm for one minute at 4°C. Beads were stored as a 50% slurry for less than one week at 4°C.

2.7.2 Preparation of GST-RBD Beads for RhoA Activation Assay

Six milliliters of LB was inoculated with 100μg/mL ampicillin and pGEX GST-RBD (Ren et al., 1999; Addgene, Cambridge Massachusetts) in BL21 bacterial cells, and incubated overnight at 30°C. The overnight culture was diluted to 2% in pre-warmed LB, and incubated for three hours at 30°C. GST-RBD (Rhotekin-binding domain) protein expression was induced with 0.3mM IPTG, and the cell culture was incubated for four hours at 30°C. Bacteria were pelleted by centrifugation at 4000 rpm for ten minutes at 4°C. The pellet was resuspended in 2mL 1X PBS, 10μM dithiothreitol (DTT), and 1X protease inhibitor cocktail (Roche, Mississauga, Ontario). The suspension was sonicated for 20 seconds three times, and 2.25 μL Triton-X 100, 22.5 μL $MgCl_2$, and 22.5 units DNase1 was added, and the lysate was

incubated for 30 minutes at 4°C. The lysate was centrifuged at 12000 rpm for ten minutes at 4°C. Supernatant was moved to a new tube and 100μL of 50% slurry of washed Glutathione Sepharose 4B beads (GE Healthcare, Baie-D'Urfe, Quebec) were added and the suspension incubated for one hour at 4°C with rotation. Beads were washed three times in 1X PBS, 10 mM DTT, 1% Triton-X 100 (v/v), and stored at 4°C for up to one week.

2.7.3 GTPase Activation Assays

Embryos were injected with constructs as described in the Results section. Seventy-five animal caps from each sample were excised as previously described (Sive et al., 1996) and stored at -80°C. Each sample was lysed in 500μL of Rac1 or RhoA lysis buffer (Rac1: 50mM Tris pH 7.5, 200mM NaCl, 2% NP40 (v/v), 10% glycerol (v/v), 10mM $MgCl_2$, and 1X protease inhibitor cocktail (Roche, Mississauga, Ontario), RhoA: 50mM Tris pH 7.5, 500mM NaCl, 1% Triton-X 100 (v/v), 0.5% sodium deoxycholic acid (w/v), 0.1% SDS (v/v), 10mM $MgCl_2$ and 1X protease inhibitor cocktail (Roche, Mississauga, Ontario)) and ten units of RQ1 DNase was added to each sample. Lysates were incubated on ice for ten minutes, followed by centrifugation for 15 minutes at 14000 rpm at 4°C, 40μL of each supernatant was removed to a new microfuge tube as a control for total GTPase. An additional 360μL of supernatant was removed from each sample and placed in a new microfuge tube. To this, 50μL GST-beads coupled to PBD or RBD were added, and the solutions rocked for one hour at 4°C. Bead suspensions were centrifuged for one minute at 2000 rpm at 4°C, and

supernatant removed. GST-beads were washed three times in 1mL wash buffer (Rac1: 25mM Tris pH 7.5, 40mM NaCl, 1% NP40 (v/v), 30mM $MgCl_2$; RhoA: 50mM Tris pH 7.5, 1% Triton-X 100 (v/v), 150mM NaCl, and 10mM $MgCl_2$). After the final wash, Western blotting was performed as previously described using Rac1 and RhoA antibodies listed in Table 2.5.

2.8 Tissue Culture

2.8.1 Maintenance of *Xenopus* A6 Cells

Xenopus laevis A6 kidney cells (ATCC# CCL-102; Rockville, Maryland) were cultured at room temperature in Leibovitz (L)-15 media (Sigma, Oakville, Ontario), diluted to 66% (v/v), and supplemented with 10% fetal bovine serum (v/v; FBS; Wisent, St. Bruno, Quebec), 1mM sodium pyruvate (Wisent, ST. Bruno, Quebec), 1% (w/v) L-glutamine (Wisent, St. Bruno, Quebec), 100units/mL penicillin and 100μg/mL streptomycin (Wisent, St. Bruno, Quebec).

Cells were cultured until 60-70% confluencey before detachment using Trypsin/EDTA (Wisent, St. Bruno, Quebec; 0.05% Trypsin, 0.53mM EDTA), and replated on 60mm glass bottom dishes or coverslips in 66% L-15 media with 10% FBS (v/v).

2.8.2 Transfection of *Xenopus* A6 Cells

Cells plated on glass bottom dishes were transfected with various constructs as described in

the Results section. Purified DNA constructs were incubated with 35μL lipofectamine (Invitrogen, Burlington, Ontario) in 200μL 66% L-15 media for 30 minutes. Confluent cells were rinsed with 3mL 66% L-15 media, and covered with 1mL 66% L-15 media prior to transfection. The DNA-lipofectamine mixture was added to the confluent cells followed by six hours of incubation at room temperature. Transfection media was removed, and cells were cultured overnight in 66% L-15 media containing 10% FBS (v/v). After a 48-hour incubation period transfected cells were imaged using a Zeiss Axiovert 200 microscope (Zeiss, Mississauga, Ontario), Qimaging retiga 1494 digital camera (Burnaby, British Columbia), with Open Lab Software (Improvision, Waltham Massachusetts).

2.9 Statistics

All statistical analysis was completed by comparing numerical results using a two-tailed Student's unpaired *t* test. Values below $p < 0.05$ were considered to be statistically significant.

Chapter 3
Results

3.1 Phylogenetic Analysis of *Xenopus* β-parvin

β-parvin has not been previously described in *Xenopus laevis*. The amino acid sequence of *Xenopus* β-parvin (Accession NP_001089519.1) was compared to a variety of β-parvin orthologs. All orthologs contain a similar number of amino acids (365), and the locations of CH1 (orange) and CH2 (green) domains are conserved (Figure 3.1). Alignment of the amino acid sequences shows *Xenopus* β-parvin to be highly conserved between *Gallus gallus* (88.8% identity), *Homo sapiens* (85.5% identity), *Mus musculus* (83.3% identity), and *Danio rerio* (77.3% identity), whereas the sequence is more divergent in *Drosophila melanogaster* (56% identity; Figure 3.2 A).

Evolutionary relationships were visualized as a dendrogram (Figure 3.2B), demonstrating *Xenopus* β-parvin is more closely related to the β-parvin sequence found in birds and fish than the orthologs found in mammals and insects (Figure 3.2 B).

Figure 3.1 Alignment of *Xenopus* β-parvin with known β-parvin orthologs. Amino acid sequence of *Xenopus laevis* β-parvin (accession number NP_001089519.1) was aligned with *Gallus gallus* (accession number XP_416459.2), *Homo sapiens* (accession number AAG27171.1), *Mus musculus* (accession number AAG27172.1), *Danio rerio* (accession number NP_956020.1), and *Drosophila melanogaster* (accession number AE014298.4). The CH1 domain is highlighted in orange and encompasses 111 amino acids. The CH2 domain is highlighted in green and encompasses 111 amino acids.

Formatted Alignments

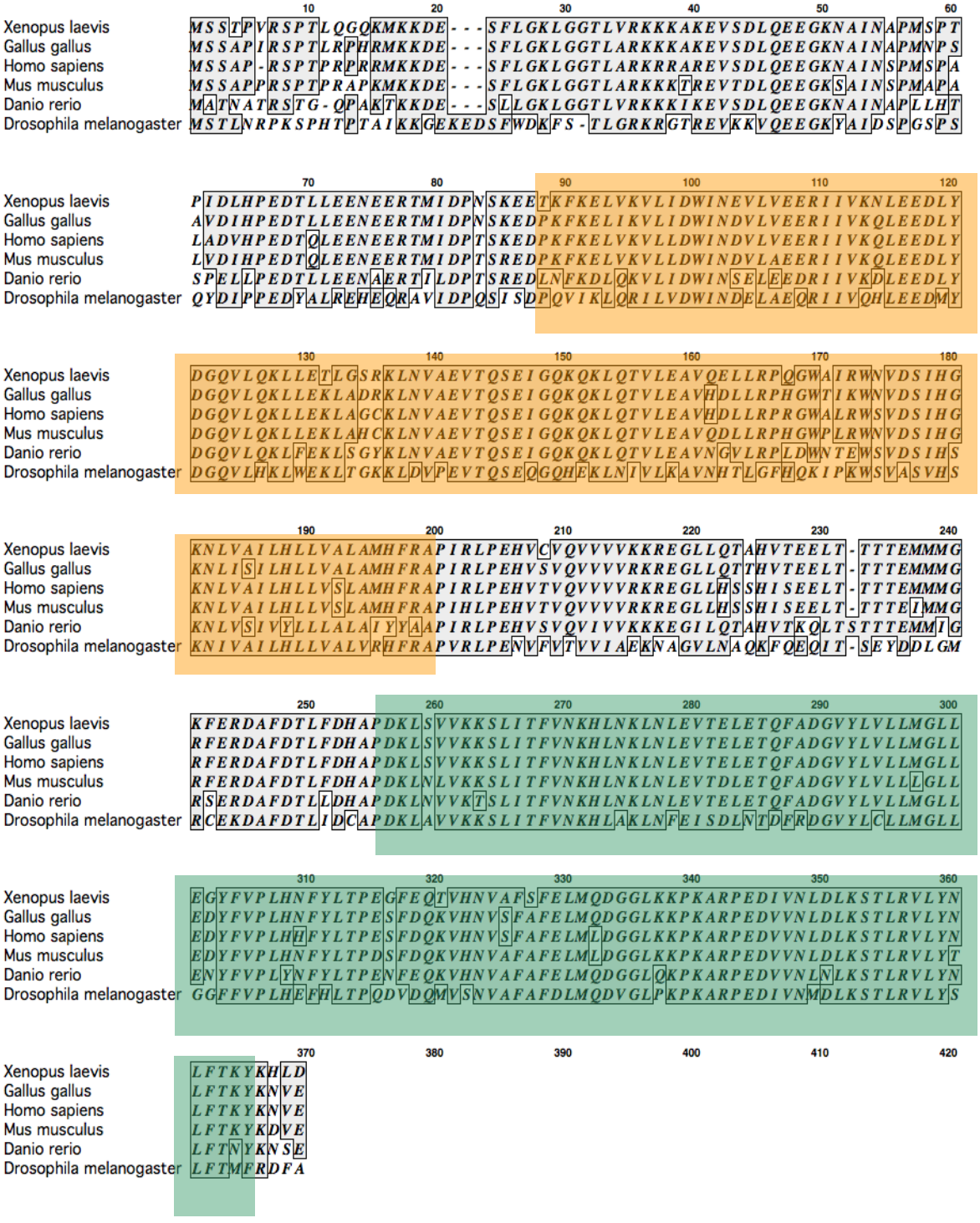

A

Percent Identity

	Xenopus laevis	Gallus gallus	Homo sapiens	Mus musculus	Danio rerio	Drosophila melanogaster
Xenopus laevis		88.8	85.5	83.3	77.3	56
Gallus gallus	97		90.7	87.7	77.6	57.6
Homo sapiens	95.3	97.3		91.8	74.6	58.2
Mus musculus	94.2	95.9	97		73	57.9
Danio rerio	86.3	86.9	86.3	85.2		53.7
Drosophila melanogaster	72.3	72.8	72.8	72.3	69.6	

Percent Similarity

B

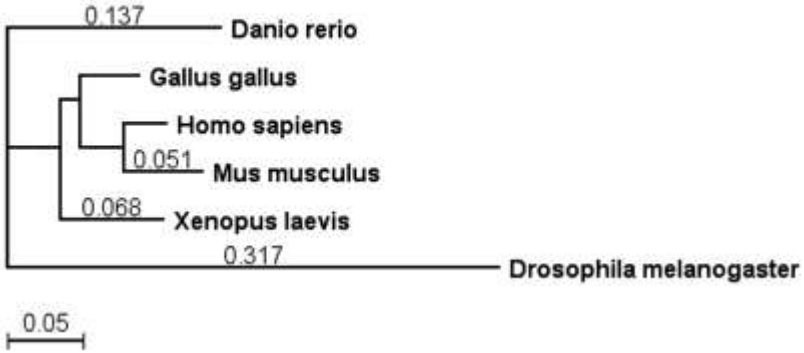

Figure 3.2 Comparison of *Xenopus* β-parvin with known β-parvin orthologs. Sequences were aligned using ClustalW and percent identity and similarity values calculated between *Xenopus laevis*, *Gallus gallus*, *Homo sapiens*, *Mus musculus*, *Danio rerio*, and *Drosophila melanogaster* (A). A dendrogram was created from the ClustalW using MacVector software (MacVector Inc, Cary, North Carolina) showing relative divergence between species (B).

3.2 Temporal and Spatial Expression of *Xenopus* β-parvin

RT-PCR and *in situ* hybridizations were employed to determine the temporal and spatial expression of *Xenopus* β-parvin transcripts during early embryogenesis.

RT-PCR was used as a qualitative measure to determine whether β-parvin transcripts were present through early development. β-parvin is expressed as maternal mRNA prior to the midblastula transition (stage 2, 5), and continues to be zygotically expressed during gastrulation (stage 10.5), neurulation (stage 17), and organogenesis (stage 28; Figure 3.3). This indicates that β-parvin is expressed during all stages of early development.

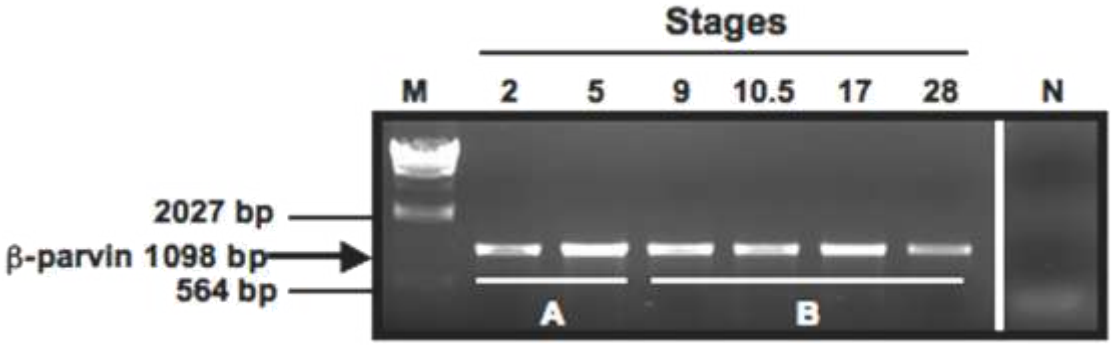

Figure 3.3 β-parvin mRNA is expressed throughout early *Xenopus* embryogenesis. RT-PCR was used to amplify endogenous β-parvin transcripts using total RNA isolated from key developmental stages (indicated along top of figure) during *Xenopus* development. β-parvin is expressed as a maternal transcript (A; Stages 2 and 5) prior to the midblastula transition, and continues to be zygotically expressed (B) prior to gastrulation (Stage 9), during gastrulation (Stage 10.5), neurulation (Stage 17), and organogenesis (Stage 28). A negative control containing no template cDNA (N). λ/HindIII DNA ladder was used as a size marker (M) with the bottom two bands corresponding to 564 and 2027 base pairs (bp).

Spatial localization of *Xenopus* β-parvin transcripts was visualized using *in situ* hybridizations. β-parvin transcripts were localized in the animal pole of stage two *Xenopus* embryos (Figure 3.4 A). Expression persisted on the dorsal side of blastula and gastrula stage embryos (Figure 3.4 B, C). In gastrulae, expression was localized to deep BCR cells and in DMZ mesodermal cells (Figure 3.4 C). β-parvin transcripts localized to newly forming somites during neurulation, and in myotomes in hatched tadpoles (Figure 3.4 D, E).

Figure 3.5 shows a higher magnification view of the dorsal marginal zone where gastrulation movements are initiated. β-parvin is expressed in BCR cells of stage 10 and 10.5 embryos where FN matrix assembly occurs (Figure 3.5). β-parvin transcripts are present in the pre-involution mesoderm in stage 10 and 10.5 embryos (Figure 3.5, white arrows), and expression persists in post-involution mesoderm at the dorsal lip. However, expression is decreased in the anterior mesoderm (Figure 3.5, black arrows).

Temporal and spatial expression experiments reveal that β-parvin is expressed throughout early *Xenopus* embryogenesis. Localization of transcripts in *Xenopus* gastrulae indicates that β-parvin is expressed in tissues that are involved in FN matrix assembly, and morphogenetic movements. This suggests β-parvin may play a role in the cell movements that drive gastrulation.

Figure 3.4 β-parvin mRNA is expressed in tissues that undergo morphogenetic movements during *Xenopus* gastrulation. Whole-mount *in situ* hybridization using a β-parvin anti-sense RNA probe reveals localization of transcript expression. β-parvin expression is localized to the animal pole of a two-cell embryo (A, red arrow), in the future dorsal side at stage 9 (B, red arrow), in the blastocoel roof and dorsal marginal zone at stage 10.5 (C, red arrows) in the somites at stage 17 (D, red arrow), and in the myotomes at stage 28 (E, red arrow). β-parvin sense RNA probe was used as a negative control in embryos at stage 2 (F), 10.5 (G), and 28 (H), demonstrating no unspecific binding.

β-parvin Anti-Sense

β-parvin Sense Control

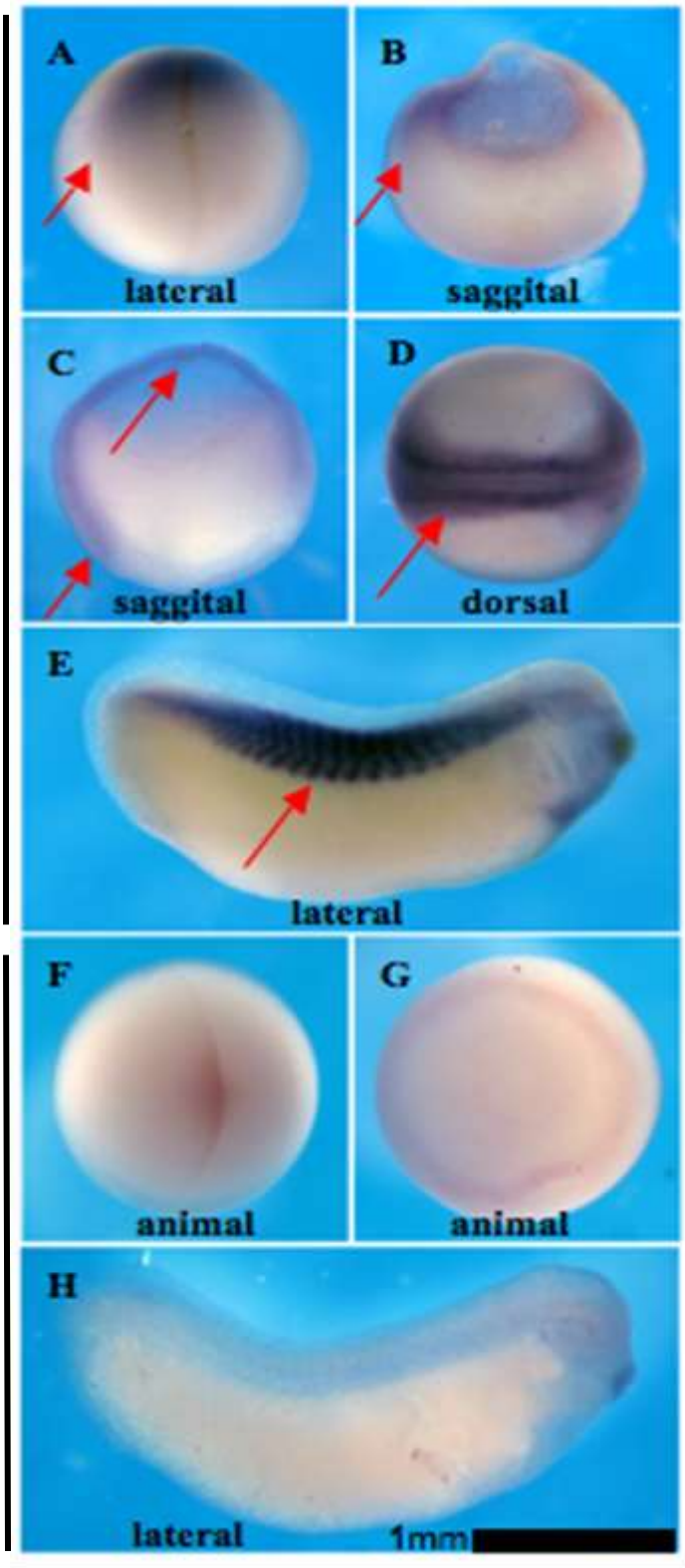

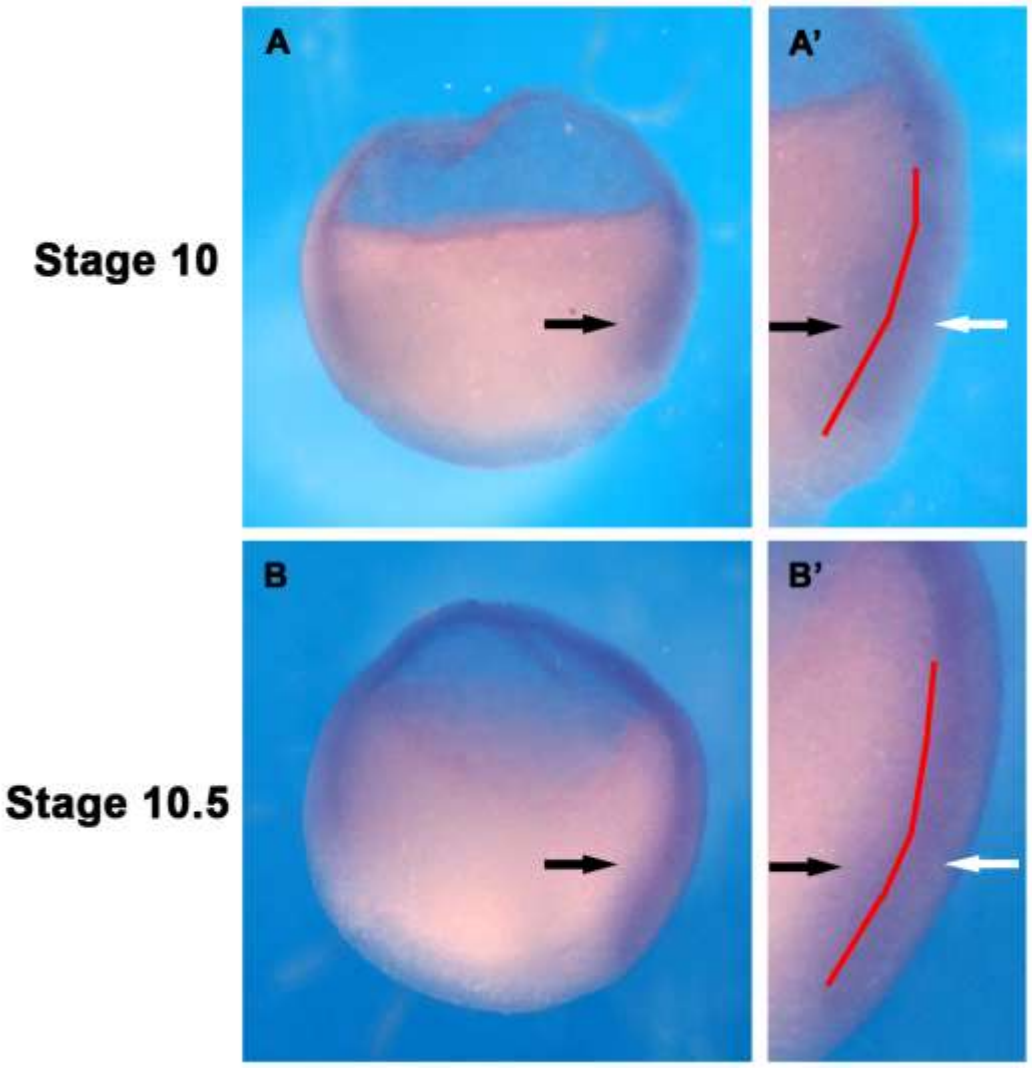

Figure 3.5 β-parvin is expressed in the dorsal marginal zone that undergoes convergent extension movements during gastrulation. Whole-mount *in situ* hybridization using a β-parvin anti-sense RNA probe demonstrates the localization of transcripts during early *Xenopus* gastrulation. Transcripts are present in blastocoel roof cells at stage 10 and 10.5 (A, B). Transcripts are present in pre-involution mesoderm at stage 10 and 10.5 (A', B', white arrows). Expression persists in post-involution mesoderm at stage 10 and 10.5 (A', B', black arrows). Red line indicates Brachet's cleft, the tissue separation boundary between pre- and post-involution mesoderm.

3.3 β-parvin, ILK, and PINCH Co-localize *in vitro*

The IPP complex is recruited to sites of focal adhesions (FA) in mammalian tissue culture cells (Wickstrom et al., 2010; Stanchi et al., 2009). The CH2 domain of β-parvin is necessary for localization to the IPP as well as FAs (Yamaji et al., 2001; Tu et al., 2001; Olski et al., 2001). There is no commercial antibody that recognizes *Xenopus laevis* β-parvin, therefore I created GFP-tagged constructs of β-parvin, RP1, and RP2 to visualize localization of β-parvin constructs both *in vitro* (tissue culture) and *in vivo* (embryos). Prior to utilization of tagged constructs *in vivo*, localization of constructs was tested *in vitro*. *Xenopus* A6 cells which use integrin α5β1 to bind on exogenously supplied FN subtrates were transfected with pCS2-GFP-N3 GFP, XBP-GFP CS107, GFP-XRP1 CS2, or GFP-XRP2 CS2 plasmids. pCS2-GFP-N3 with no insert was used as a control, and GFP protein expression was visualized throughout the cell. β-parvin-GFP and GFP-RP2 proteins localized to FAs (Figure 3.6), whereas GFP-RP1 proteins localized to the leading edge (Figure 3.6). Localization of GFP-tagged constructs to the nucleus is non-specific as control GFP also localizes to the nucleus (Figure 3.6).

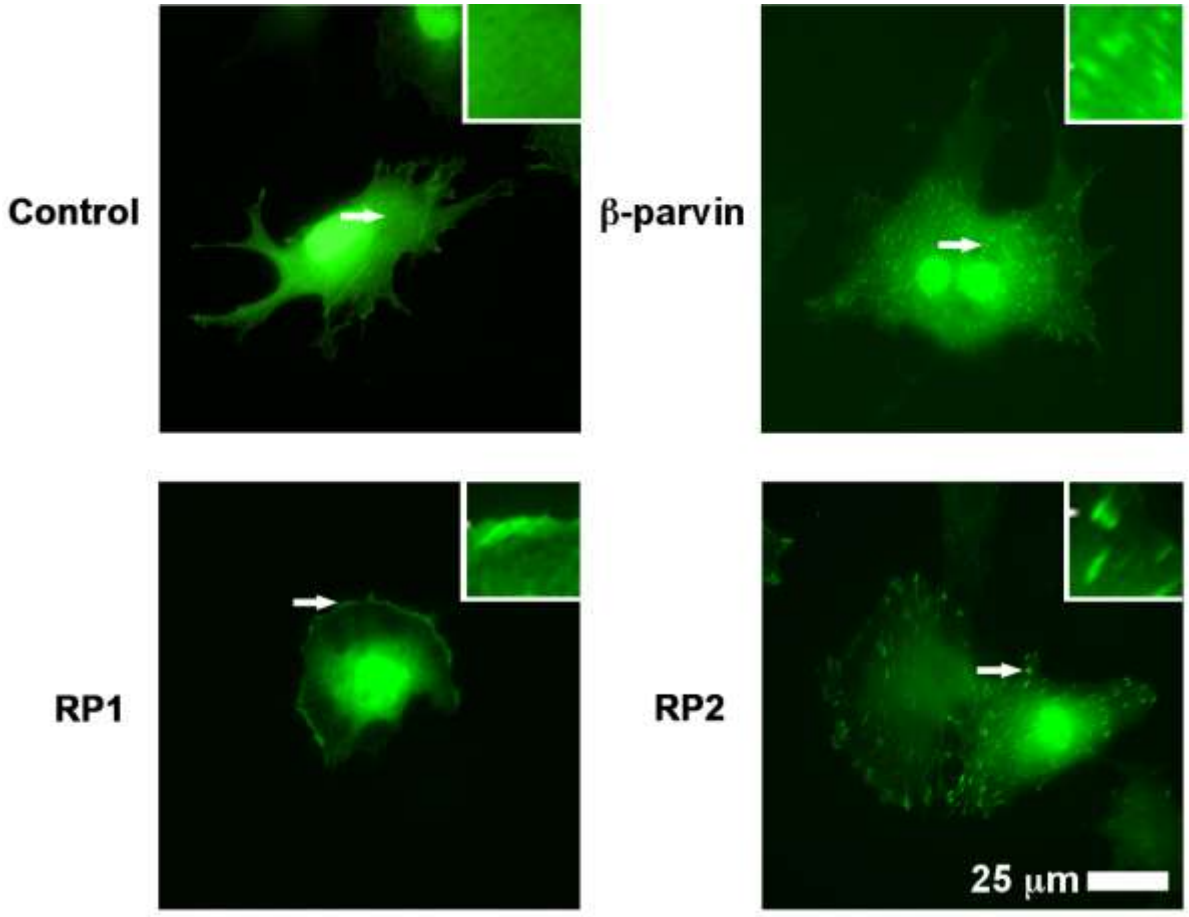

Figure 3.6 β-parvin and RP2 localize to focal adhesions in *Xenopus* A6 cells. *Xenopus* A6 cells were transfected with pCS2-GFP-N3 GFP, XBP-GFP CS107, GFP-XRP1 CS2, or GFP-XRP2 CS2 plasmids, and protein expression and localization visualized. GFP protein expression was dispersed throughout the cell (control). β-parvin-GFP and GFP-RP2 proteins localized to focal adhesions. GFP-RP1 proteins localized to the leading edge. Arrows indicate magnified areas shown as insets.

Co-transfections of pCS2-GFP-N3 GFP, XBP-GFP CS107, GFP-XRP1 CS2, or GFP-XRP2 CS2 with RFP-XILK CS2 were performed to determine if β-parvin constructs would co-localize with ILK to FAs in *Xenopus* A6 cells. Both β-parvin-GFP and GFP-RP2 proteins

co-localize with RFP-ILK to sites of integrin adhesion (Figure 3.7). GFP-RP1 proteins do not co-localize with RFP-ILK (Figure 3.7).

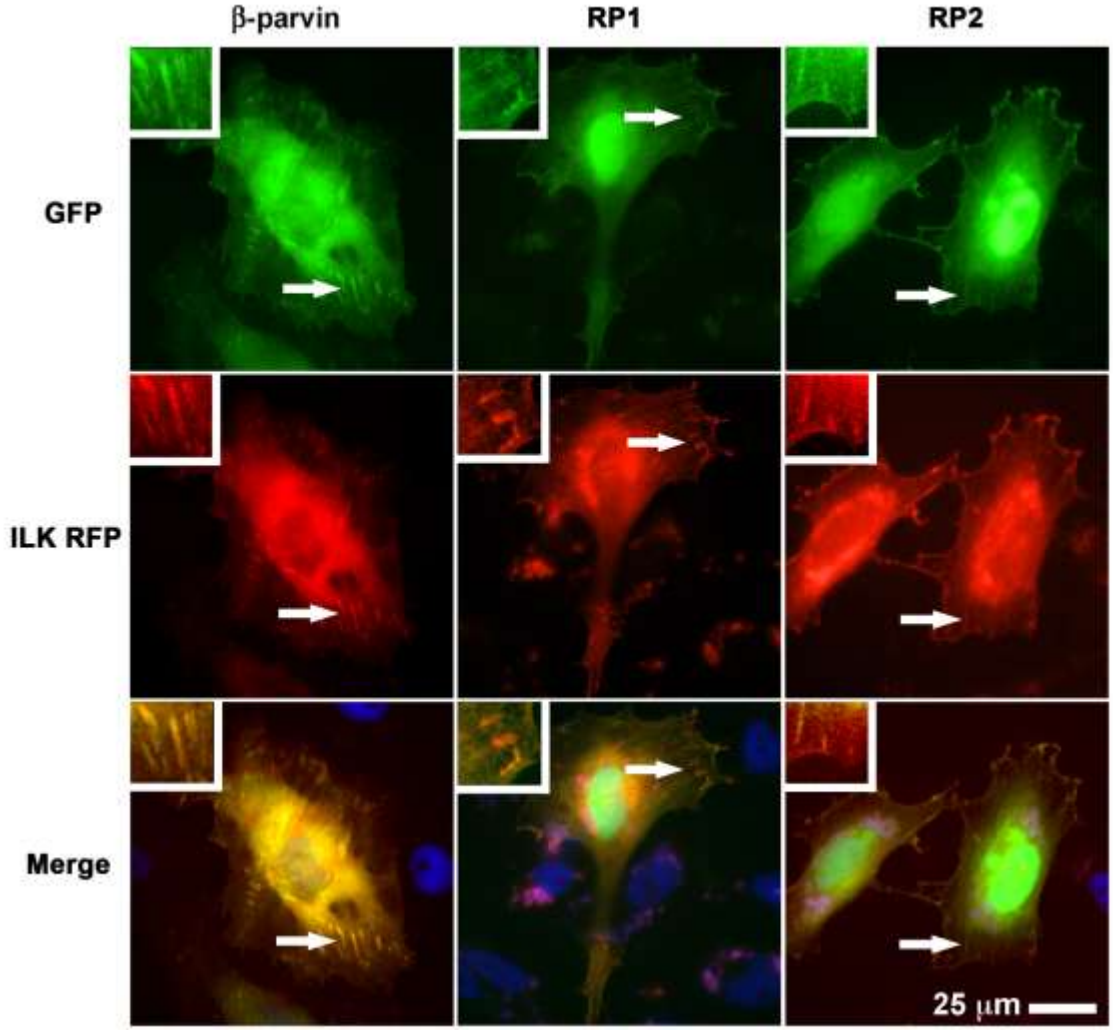

Figure 3.7 β-parvin and RP2 co-localize with ILK to focal adhesions in *Xenopus* A6 cells. pCS2-GFP-N3 GFP, XBP-GFP CS107, GFP-XRP1 CS2, or GFP-XRP2 CS2 plasmids were co-transfected with RFP-XILK CS2 into *Xenopus* A6 cells, and localization was visualized. ILK co-localized with β-parvin and RP2 proteins to focal adhesions. RP1 did not co-localize with ILK. Arrows indicate magnified areas shown as insets.

I next tested whether PINCH is able to co-localize with β-parvin to sites of integrin adhesion. Co-localization of β-parvin-GFP and RFP-PINCH was observed in *Xenopus* A6 cells upon co-transfection of XBP-GFP CS107 with RFP-XPINCH CS2 (created by Pilli, 2012; Figure 3.8). These experiments were not performed with GFP-XRP1 CS2 or GFP-XRP2 CS2.

My results suggest that the GFP and RFP tags have no effect on protein localization within the cells, since β-parvin, RP2, ILK, and PINCH all localized to focal adhesions whereas RP1 remained absent from sites of integrin adhesion as expected (Tu et al., 2001; Zhang et al., 2004, 2002a). Since these proteins behave as expected *in vitro*, I then used these tagged constructs to perform over-expression studies in *Xenopus* embryos *in vivo*.

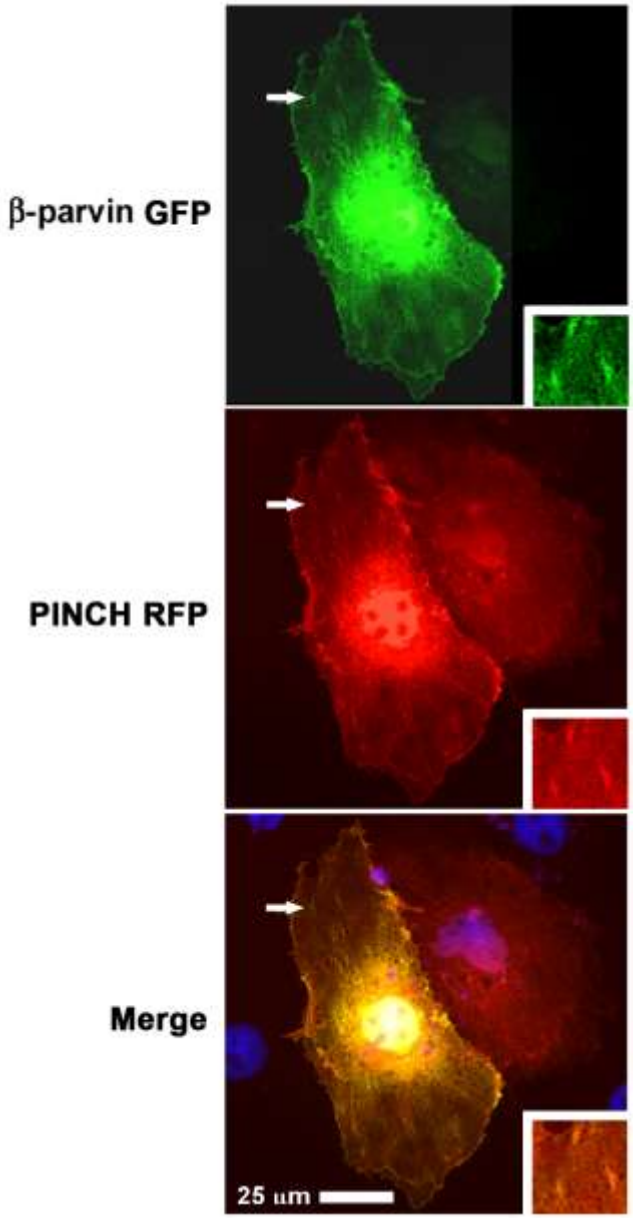

Figure 3.8 β-parvin and PINCH co-localize to focal adhesions in *Xenopus* A6 cells. XBP-GFP CS107 and RFP-XPINCH CS2 (Pilli, 2012) constructs were co-transfected into *Xenopus* A6 cells, and localization visualized. β-parvin-GFP and RFP-PINCH co-localized to focal adhesions. Arrows indicate magnified areas shown as insets.

3.4 RP1 and RP2 Constructs Inhibit Gastrulation

I over-expressed GFP-tagged β-parvin constructs in *Xenopus* embryos to elucidate a potential role for β-parvin during gastrulation. All experiments were performed using microinjections at the animal pole of stage two embryos (unless otherwise specified) with 2ng of mRNA of each GFP construct; GFP, β-parvin-GFP, RP1-GFP and RP2-GFP. This was the lowest amount of mRNA where full-length β-parvin had no affect on development, and protein expression levels between β-parvin constructs is similar, as demonstrated by Western blot analysis (Appendix B).

Gastrulation was measured by the ability of embryos to close the blastopore and continue developing into tadpoles. All embryos expressing GFP (control) showed a normal progression of blastopore closure (Figure 3.9, Figure 3.10). Embryos over-expressing β-parvin-GFP (β-parvin) are phenotypically similar to control embryos (Figure 3.9), with 88% of embryos exhibiting normal blastopore closure (Figure 3.10). Embryos over-expressing GFP-RP1 (RP1) or GFP-RP2 (RP2) exhibit a delay in blastopore closure (Figure 3.9). RP1 over-expression reduced normal blastopore closure to 15% (Figure 3.10), and in RP2 over-expressing embryos normal blastopore closure was reduced to 19% (Figure 3.10). When RP1 and RP2 were co-injected into the animal pole of stage two *Xenopus* embryos, blastopore closure was inhibited as the embryos failed to develop further (Figure 3.11). This suggests that expression of either CH domain of β-parvin can inhibit blastopore closure, and that for normal function the CH1 and CH2 domains need to be part of the same polypeptide.

GFP and β-parvin over-expressing embryos developed into tadpoles that extended along the anterior-posterior axis (Figure 3.12). Tadpoles over-expressing either RP1 or RP2 were truncated along the anterior-posterior axis (Figure 3.12), indicative of a failure in CE.

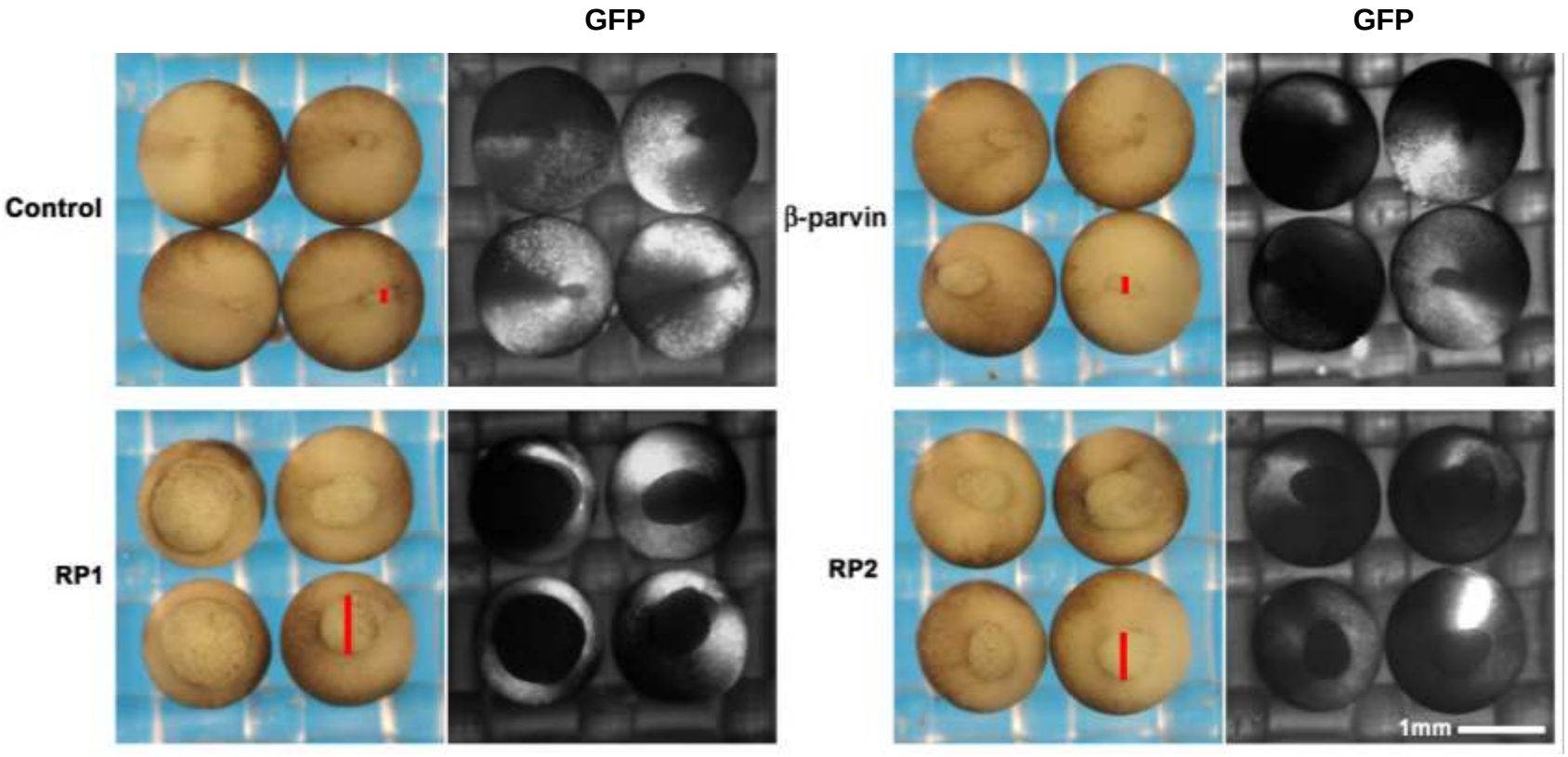

Figure 3.9 Expression of RP1 or RP2 delays blastopore closure during *Xenopus* gastrulation. Embryos were injected with 2ng mRNA of GFP or β-parvin GFP constructs in the animal pole of stage two embryos, and blastopore closure imaged at stage 12. The red line in each left panel indicates blastopore diameter. Over-expression of each GFP construct is shown in the panels on the right. Control and β-parvin over-expressing embryos display normal progression of blastopore closure as indicated by the short red lines. RP1 and RP2 over-expressing embryos display a delay in blastopore closure as indicated by the longer red lines.

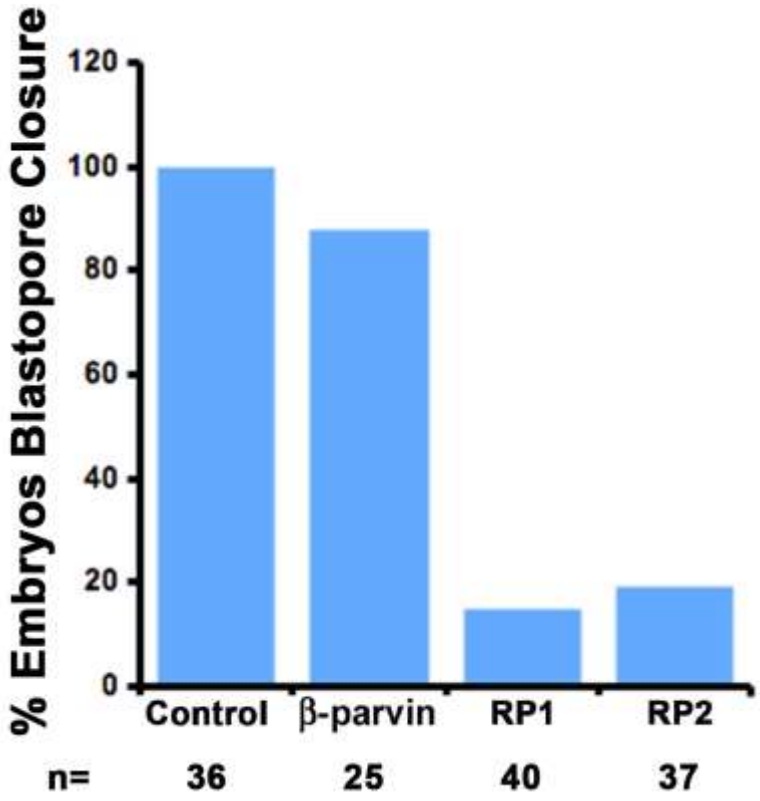

Figure 3.10 Expression of RP1 or RP2 delays blastopore closure. Blastopore closure was qualitatively measured in embryos over-expressing GFP and β-parvin-GFP constructs through comparison of blastopore diameters to control. All GFP expressing embryos (control) displayed normal blastopore closure. Blastopore closure was normal in 88% of β-parvin, 15% of RP1, and 19% of RP2 over-expressing embryos.

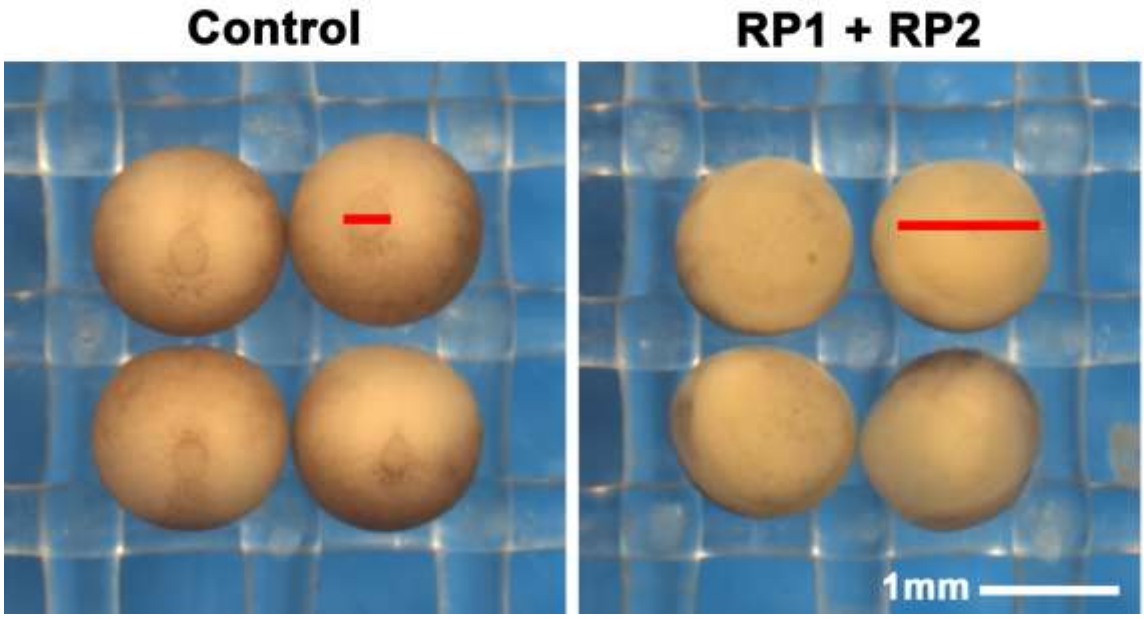

Figure 3.11 Co-expression of RP1 and RP2 inhibits blastopore closure. Stage two embryos were injected in the animal pole with GFP, or co-injected with GFP-RP1 and GFP-RP2 mRNA and cultured until stage 12. Control embryos exhibit normal development as the blastopore is almost closed. RP1 and RP2 co-injected embryos exhibit an inhibition in blastopore closure. Red lines indicate blastopore diameter.

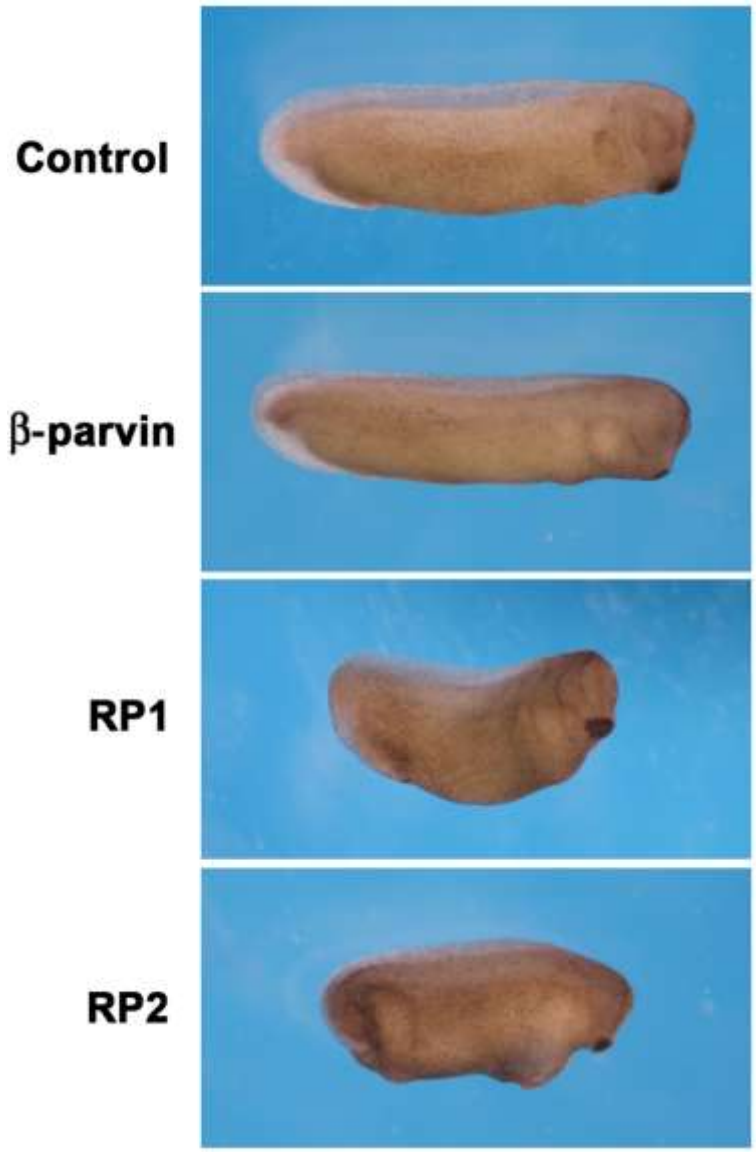

Figure 3.12 Expression of RP1 or RP2 inhibits axial extension. Stage two embryos were injected in the animal pole with 2ng of GFP or β-parvin-GFP constructs and cultured until stage 28. Control and β-parvin over-expressing embryos exhibit normal development. RP1 and RP2 over-expressing embryos exhibit a shortened anterior-posterior axis.

3.5 RP1 and RP2 Constructs Inhibit FN Fibrillogenesis

FN matrix assembly is required for normal morphogenetic movements during gastrulation including blastopore closure and axial extension (Marsden and DeSimone, 2001; Rozario et al., 2009). Since RP1 and RP2 over-expressing embryos exhibited a delay in blastopore closure and shortened anterior-posterior axis, I asked whether RP1 or RP2 over-expression would affect FN fibrillogenesis. Animal caps were excised from embryos over-expressing GFP, β-parvin, RP1, or RP2 and FN fibrillogenesis visualized on the blastocoel roof. Both control and β-parvin expressing embryos exhibited a mature fibrillar FN matrix (Figure 3.13). RP1 and RP2 over-expressing embryos displayed an inhibition of FN matrix assembly, having short and sparse FN fibrils (Figure 3.13).

Figure 3.13 RP1 and RP2 inhibit FN matrix assembly. Stage two embryos were injected with GFP, β-parvin-GFP, GFP-RP1, or GFP-RP2 constructs and cultured until stage 12. Animal caps were removed and FN was visualized on the BCR using anti-FN antibody 4B12. GFP (control) and β-parvin over-expressing embryos exhibit normal FN fibril formation. Over-expression of RP1 or RP2 inhibits FN matrix assembly, with few FN fibers visible.

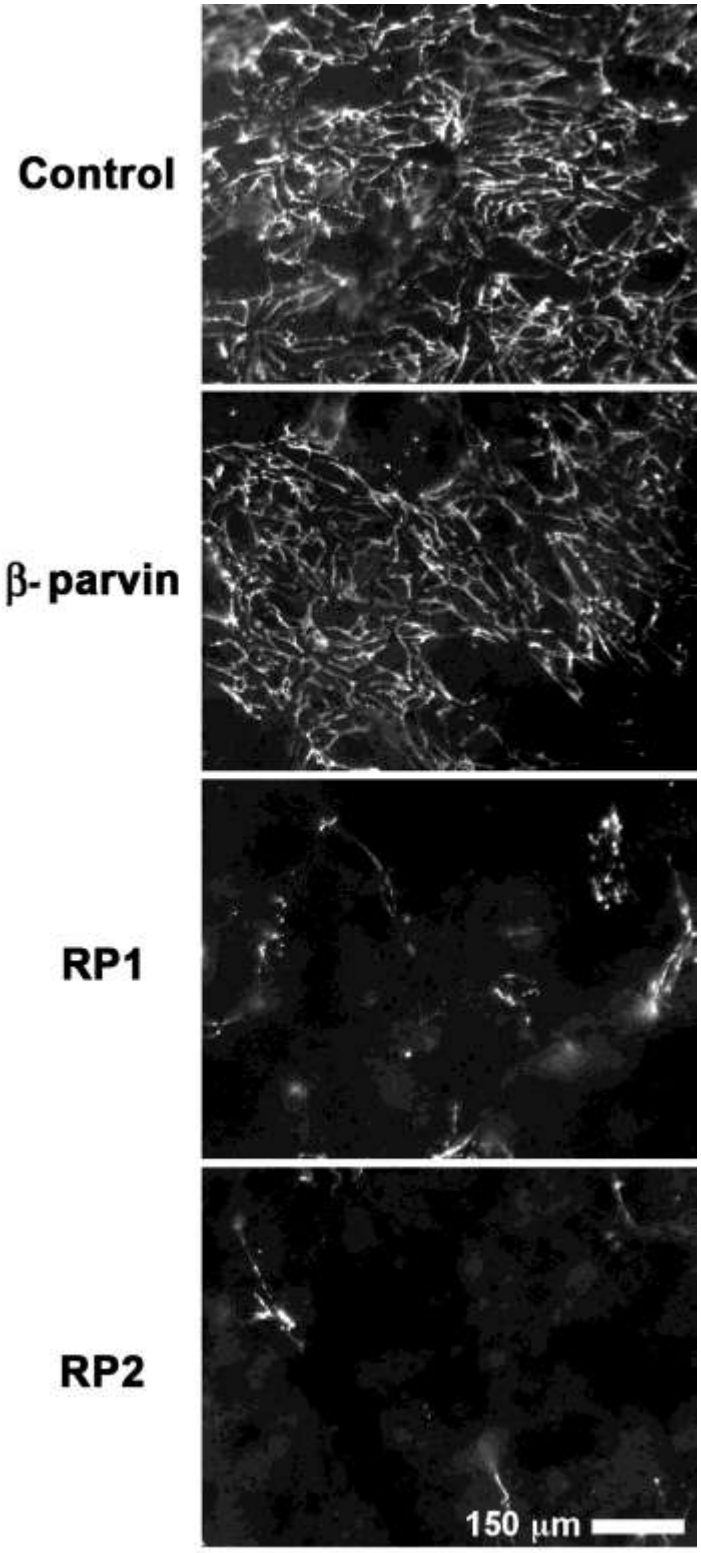
Control
β-parvin
RP1
RP2
150 μm

Previous studies have shown inhibition of FN matrix assembly on the BCR leads to defects in epiboly and mesendoderm adhesion to the BCR (Marsden and DeSimone, 2001; Rozario et al., 2009). Therefore, I investigated whether over-expression of RP1 and RP2 constructs would cause similar morphogenetic defects during *Xenopus* gastrulation. To investigate whether over-expression of RP1 or RP2 would inhibit epiboly, I examined BCR thickness of stage 12 embryos. In normal gastrulae, radial intercalation of deep BCR cells causes the BCR to thin from 5-6 to two cell layers, driving epiboly, as the cells spread to enclose the embryo in ectoderm (Keller, 1980; Marsden and DeSimone, 2001). Stage two embryos were injected with GFP or β-parvin GFP constructs in the animal pole and cultured until stage 12. In control and β-parvin over-expressing embryos, the BCR is thin, whereas embryos over-expressing RP1 or RP2 display a thicker BCR compared to controls (Figure 3.14). The mesendoderm mantle has closed in control, β-parvin, and RP2 over-expressing embryos, whereas the mesendoderm mantle in RP1 over-expressing embryos did not close (Figure 3.14). Mesendoderm in both RP1 and RP2 over-expressing embryos appears poorly adherent to the BCR, therefore I investigated whether mesoderm attachment was inhibited. When animal caps are excised from stage 12 control and β-parvin over-expressing embryos, the mesoderm remains attached to the blastocoel roof (Figure 3.15). When animal caps are excised from RP1 or RP2 over-expressing embryos the mesendoderm mantle falls free of the animal cap, clearly indicating that the mesoderm is not attached to the ectoderm (Figure 3.15).

Integrin α5β1-FN ligation is necessary for FN fibrillogenesis (Marsden and DeSimone, 2001; Davidson et al., 2006), and FN matrix assembly is required for epiboly

(Marsden and DeSimone, 2001; Rozario et al., 2009) and mesendodermal mantle closure and attachment to BCR (Marsden and DeSimone, 2001). Over-expression of RP1 and RP2 inhibit FN fibrillogenesis, mesendoderm attachment, and epiboly, suggesting that integrin $\alpha5\beta1$-FN ligation may be impaired either through inhibition of integrin function or FN matrix assembly.

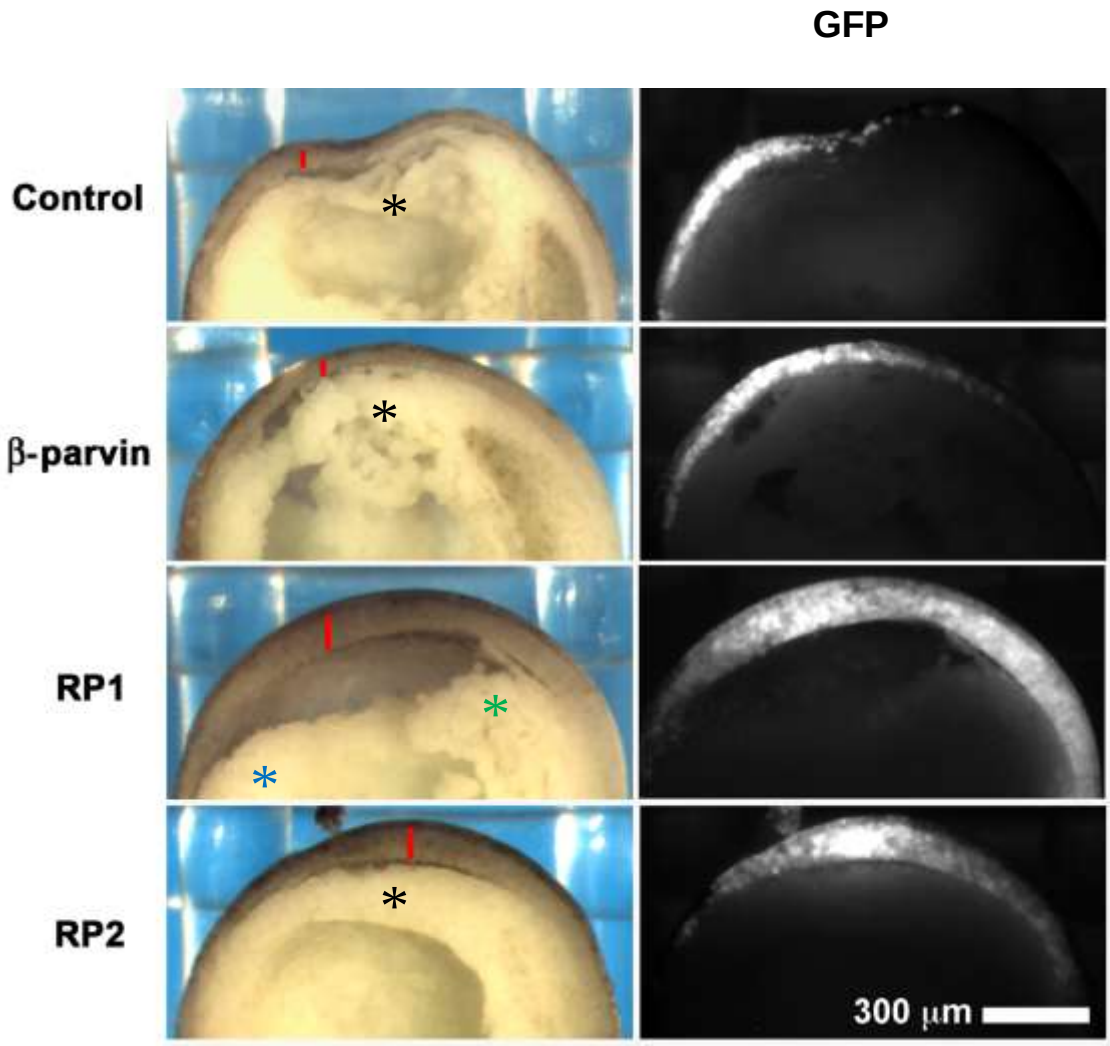

Figure 3.14 RP1 and RP2 inhibit epiboly in *Xenopus* gastrulae. Two-cell embryos were injected with GFP, or β-parvin GFP constructs in the animal pole and cultured until stage 12. Embryos were dissected along the sagittal plane to view BCR thickness. Control and β-parvin over-expressing embryos display a normal thinning of the blastocoel roof. RP1 and RP2 over-expression inhibits BCR thinning. Red lines indicate BCR thickness. The mesendodermal mantle has closed in control, β-parvin, and RP2 over-expressing embryos indicated by the black asterisk. Embryos expressing RP1 exhibit an inhibition of normal mesendodermal mantle closure as the dorsal (green) and ventral (blue) mantles remain separate. Localized expression of each GFP construct is shown in the panels on the right. These are representative examples of construct over-expression.

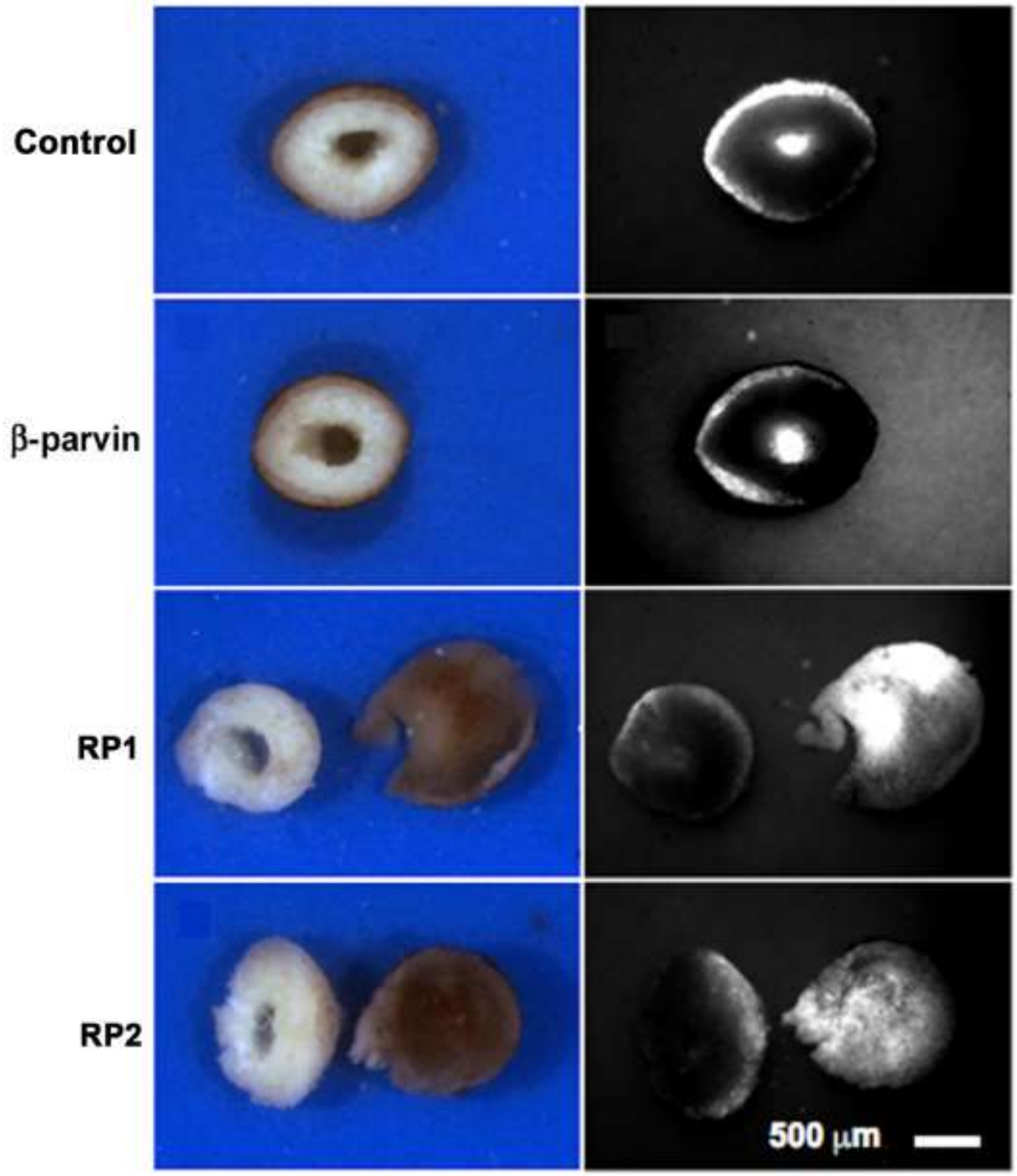

Figure 3.15 RP1 and RP2 inhibit mesoderm attachment to the BCR in *Xenopus* gastrulae. Two-cell embryos were injected with GFP, or β-parvin GFP constructs in the animal pole and cultured until stage 12. Control and β-parvin over-expressing embryos maintained attachment between the mesoderm and BCR upon animal cap excision. RP1 and RP2 over-expressing embryos displayed an inhibition of mesoderm-BCR attachment upon removal of the animal cap. Localized expression of each GFP construct is shown in the panels on the right.

In order to elucidate whether integrin α5β1-FN interactions were inhibited, I used confocal imaging to render 3-D images of FN fibrils on the BCR of stage 12 embryos. This method enables visualization of the entire FN matrix and the underlying BCR cells in one field of view. The absence of FN fibrils on cells over-expressing β-parvin constructs would indicate an inhibition of integrin function, whereas accumulation of FN would indicate inhibited fibrillogenesis but not integrin function. Two-cell embryos were injected with GFP, or β-parvin GFP constructs in the animal pole and cultured until stage 12. Animal caps were excised and FN visualized using anti-FN antibody 4B12 (Table 2.5). FN fibrils assembled into a dense matrix in control and β-parvin over-expressing embryos (Figure 3.16). FN is unable to assemble a fibrillar matrix in RP1 over-expressing embryos; however, FN is able to form short punctae on the cell surface, indicating accumulation at the cell surface likely through integrin α5β1-FN ligation (Figure 3.16). RP2 over-expressing embryos are unable to assemble a FN matrix (Figure 3.16). There are no punctae on the cell surface, indicating an inhibition in integrin α5β1-FN interactions. These results suggest that RP1 and RP2 inhibit FN matrix assembly via different mechanisms.

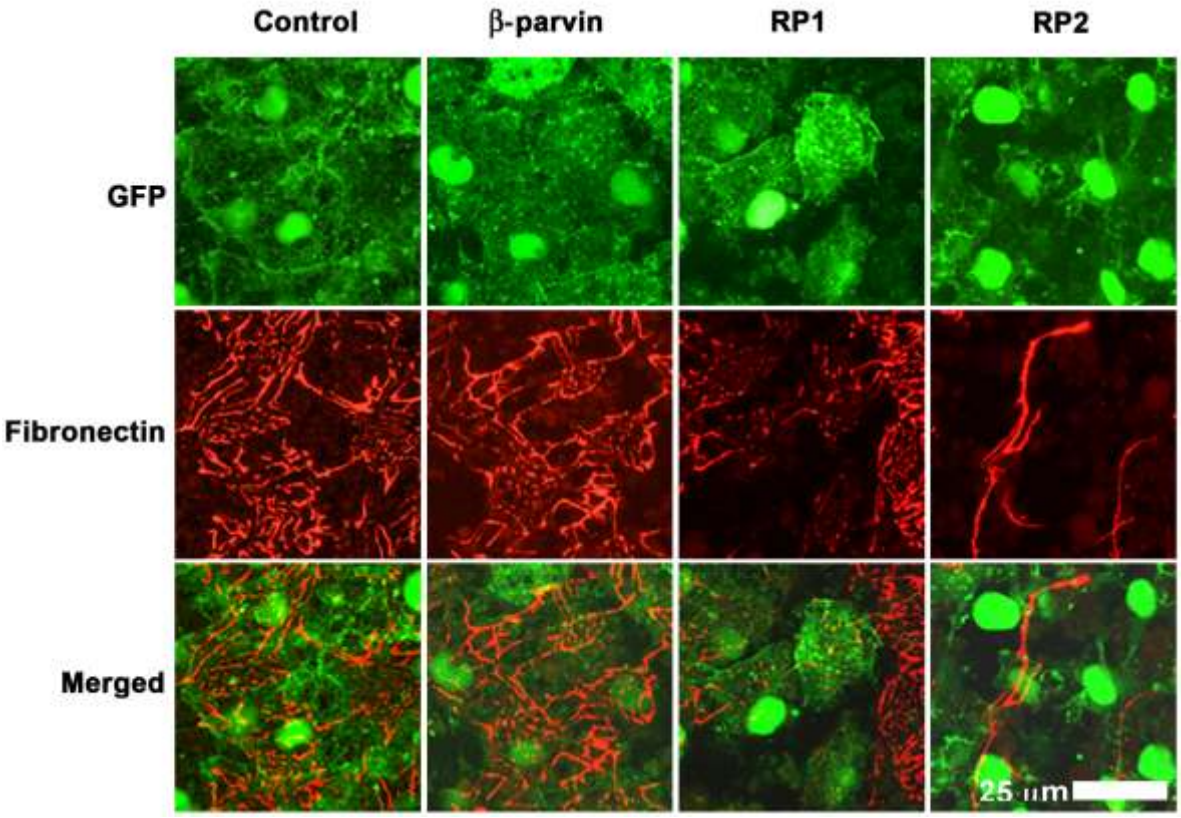

Figure 3.16 RP2 inhibits integrin α5β1-FN ligation. Stage two embryos were injected with GFP or β-parvin GFP constructs in the animal pole and cultured until stage 12. Animal caps were excised and FN visualized on the BCR using confocal imaging to produce a 3D image of fibrillar FN. Control and β-parvin over-expressing embryos exhibit a dense fibrillar network on the BCR. RP1 over-expressing embryos have reduced FN fibril assembly, and display short FN fibrils. RP2 over-expressing embryos inhibit integrin α5β1-FN ligation as the surface is free from short FN fibrils. A few large fibrils are visible on the BCR surface, spanning cells that do not express RP2.

3.6 The RP2 Construct Inhibits Convergent Extension

Extension of the anterior-posterior axis via CE has been shown to require integrin α5β1-FN ligation, (Marsden and DeSimone, 2001; Rozario et al., 2009; Davidson et al., 2006). In order to elucidate the role of β-parvin during CE separate from the other morphogenetic movements of gastrulation, CE was visualized *ex vivo*. Untreated animal cap explants will heal to form balls of ectoderm, while explants induced to become mesoderm via activin-A treatment are able to undergo CE *ex vivo* (Symes and Smith, 1987). Animal cap explants were removed from embryos over-expressing GFP or β-parvin GFP constructs and were utilized in animal cap extension assays. All untreated explants healed and formed balls of ectoderm (Figure 3.17). Animal caps excised from control, β-parvin, or RP1 over-expressing embryos that were induced to become mesoderm extended (Figure 3.17). 90% of activin induced control animal caps extended (Figure 3.18) and 89% of activin induced β-parvin or RP1 over-expressing caps extended (Figure 3.18). Activin induced animal caps excised from RP2 over-expressing embryos demonstrate inhibited CE (Figure 3.17), as only 13% of the caps extended (Figure 3.18). Animal cap extensions were immunostained to visualize FN fibrils. Interestingly, only control and β-parvin over-expressing explants show a dense FN matrix (Figure 3.17 inset) whereas RP1 and RP2 over-expressing explants lack a FN matrix (Figure 3.17 inset). Together with the previous experiments it suggests RP1 appears permissive for CE in the absence of a FN matrix, while RP2 inhibits CE likely through an inhibition of integrin α5β1-FN ligation and FN matrix assembly.

Figure 3.17 RP2 inhibits convergent extension in mesoderm induced animal caps. Stage two embryos were injected with GFP or β-parvin GFP constructs in the animal pole and animal caps excised from stage 8 embryos. Untreated animal caps did not extend (1st column). Mesoderm induced animal caps over-expressing GFP (control), β-parvin, or RP1 extended (2nd column). CE was inhibited by RP2 over-expression (2nd column). Localized expression of each GFP construct is visualized in the 3rd and 4th column. Mesoderm induced animal caps were immunostained for FN. Explants excised from control and β-parvin over-expressing embryos exhibit a fibrillar FN matrix (inset). FN matrix assembly is inhibited in explants excised from RP1 or RP2 over-expressing embryos (inset).

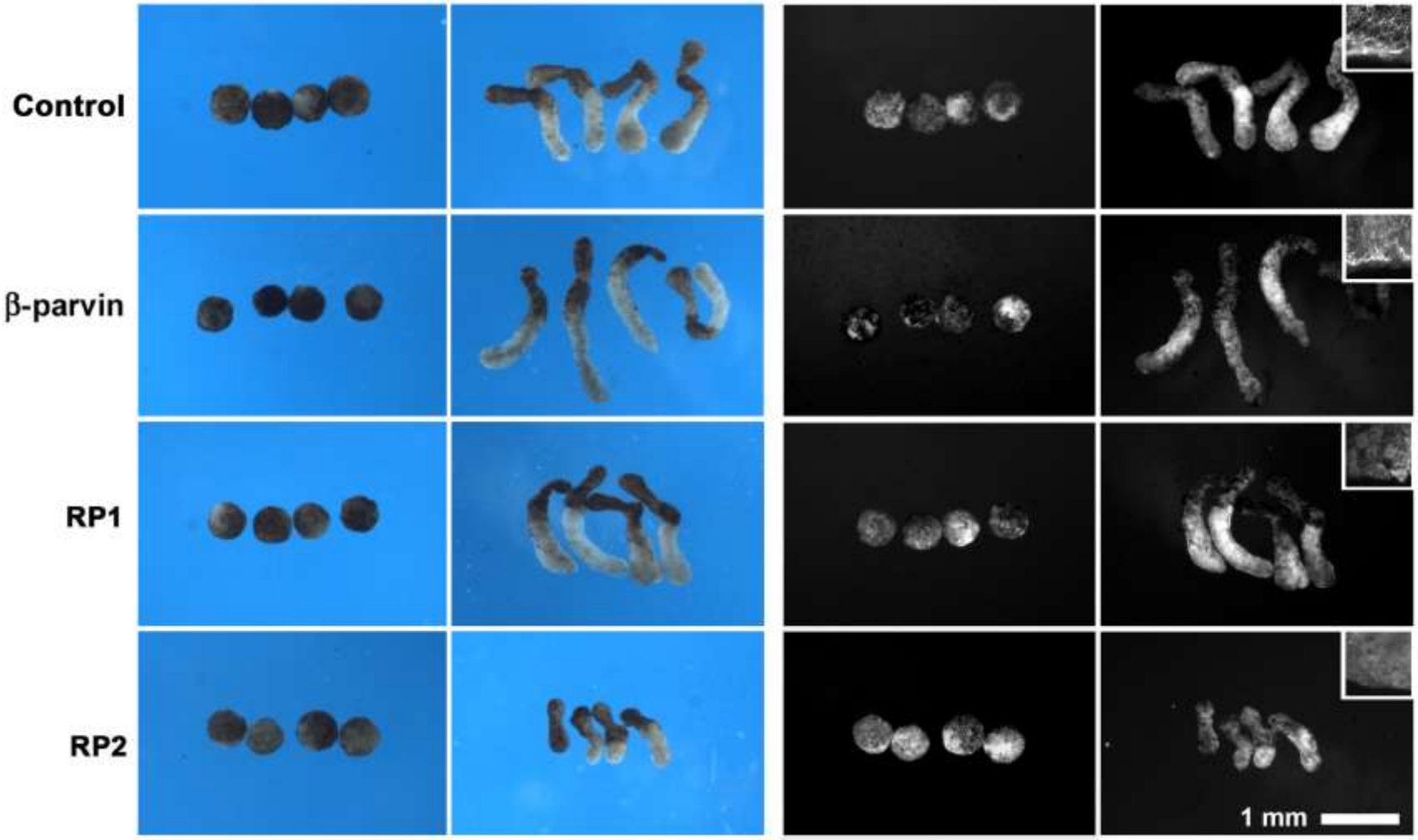
Control
β-parvin
RP1
RP2
1 mm

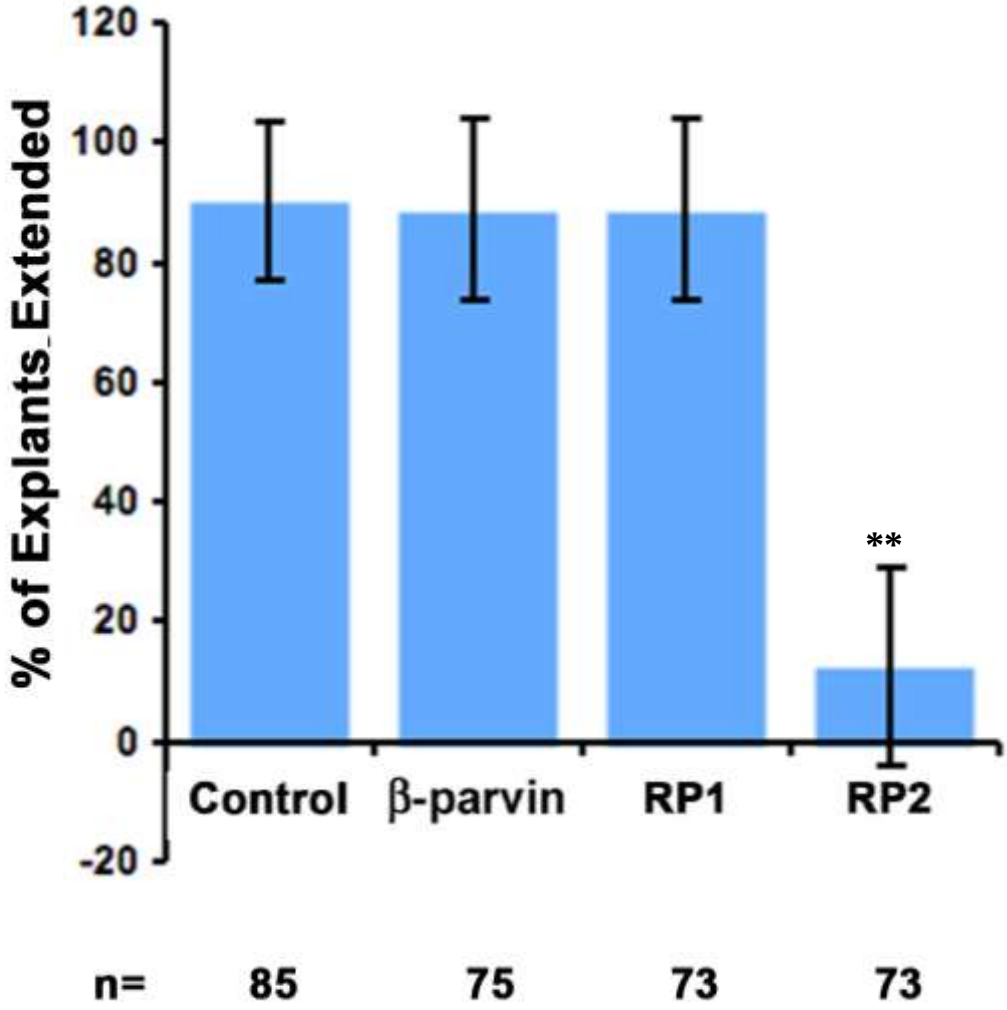

Figure 3.18 RP2 inhibits convergent extension. This is a summary of the number of extended mesoderm induced explants. Stage two embryos were injected with GFP, or β-parvin GFP constructs and animal caps excised at stage eight and cultured until stage 18 in the presence of Activin-A. Ninety percent of GFP (control) expressing caps extended. CE was normal in 89% of β-parvin or RP1 over-expressing explants and in 13% of RP2 over-expressing explants. ** indicates $p<0.01$ compared to controls.

3.7 β-parvin Regulates Morphogenesis

Changes in tissue patterning could affect CE indirectly though alteration of cell fates. To elucidate whether phenotypes of RP1 and RP2 expression were caused by possible effects on tissue patterning, I performed RT-PCR analysis looking at mesodermal markers that lie downstream of activin induction. I performed RT-PCR on total RNA isolated from animal caps of embryos over-expressing GFP or β-parvin GFP constructs. Animal cap cells are of undetermined cell fate, and if excised and left in isolation become ectoderm, while treatment with activin-A induces mesodermal cell fate (Symes and Smith, 1987). All untreated animal cap explants display very low levels of *Brachyury* (X*Bra*) and *Chordin* (X*Chd*) expression, while treatment with activin-A induces expression of these mesodermal marker genes (Figure 3.19). *Elongation Factor 1-α* (EF1-α) expression is used as a positive control, and is expressed in both uninduced and induced explants (Figure 3.19). These results demonstrate that the gastrulation defects seen in RP1 and RP2 over-expressing embryos is likely caused by a defect in morphogenesis, not tissue patterning.

Whole-mount *in situ* hybridization was performed with embryos injected with GFP or β-parvin GFP constructs in the animal pole of stage two embryos or in the two dorsal blastomeres of four-cell stage embryos. An X*Bra* probe was used to visualize mesoderm, and in embryos where GFP expression was dispersed throughout the animal cap, control and β-parvin over-expressing embryos exhibited normal X*Bra* expression in both pre- and post-involution mesoderm (Figure 3.20). Embryos over-expressing RP1 or RP2 exhibit normal X*Bra* expression in pre-involution mesoderm around the blastopore, however, mesoderm

involution is inhibited (Figure 3.20). To better visualize X*Bra* expression and mesoderm translocation around the blastopore lip, embryos were bisected along the sagittal plane at stage 11 and 12.5. Control and β-parvin over-expressing stage 11 embryos exhibit normal X*Bra* expression and mesoderm translocation (Figure 3.21). In RP1 and RP2 over-expressing stage 11 embryos, X*Bra* localization appears similar in the DMZ and ventral marginal zone, as mesoderm involution in the DMZ is delayed (Figure 3.21). Control and β-parvin over-expressing stage 12.5 embryos exhibit normal xBra expression and involuted mesoderm is undergoing CE as the mesendoderm translocates across the BCR (Figure 3.21). RP1 over-expressing stage 12.5 embryos display X*Bra* expression in pre-involution mesoderm; however, mesoderm involution continues to be inhibited. RP2 over-expressing stage 12.5 embryos exhibit X*Bra* expression in pre- and post-involution mesoderm, however, CE of post-involution mesoderm is inhibited and X*Bra* expressing tissue accumulated in the DMZ. This suggests that RP1 and RP2 do not inhibit tissue patterning, but inhibit morphogenesis via mechanisms that are independent of cell fate.

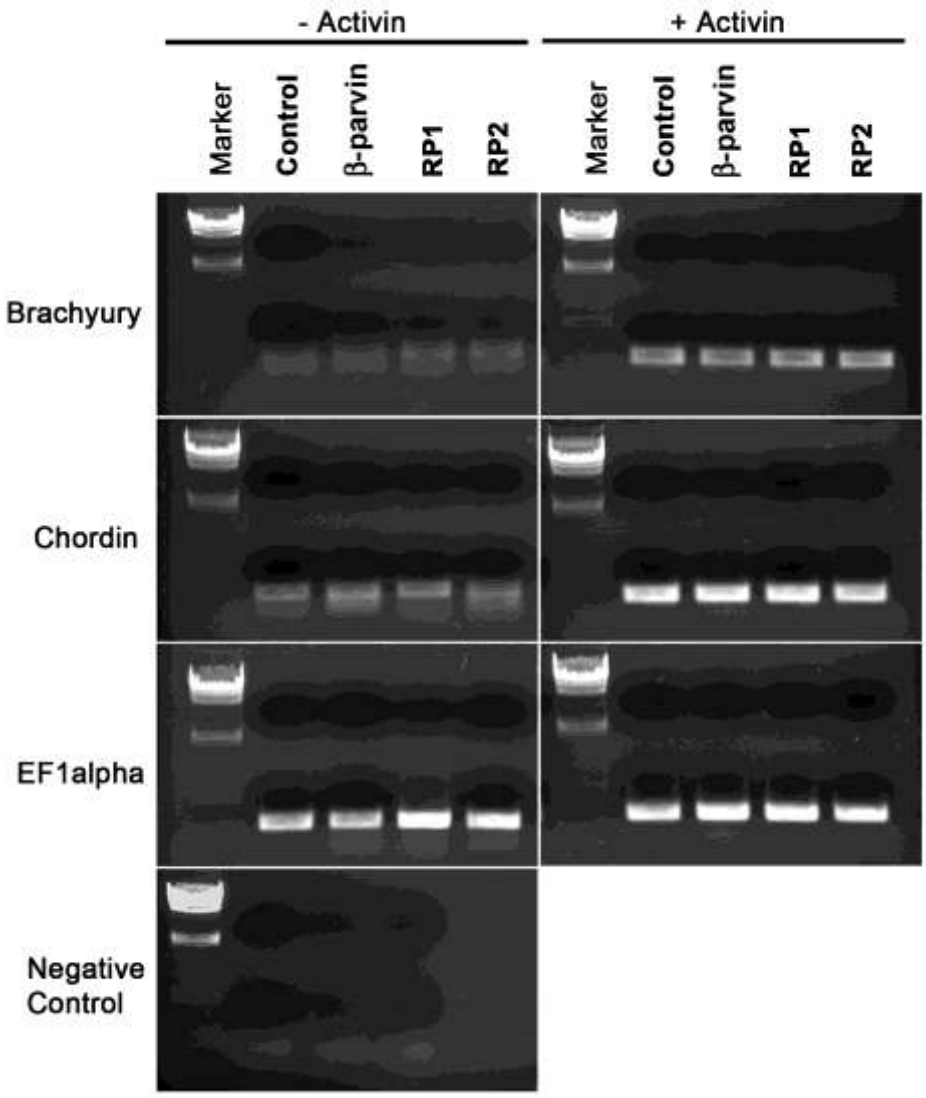

Figure 3.19 β-parvin expression does not affect tissue patterning. Animal cap explants expressing GFP (control) or over-expressing β-parvin GFP constructs were cultured in the presence or absence of activin-A. RT-PCR was performed on RNA isolated from each treatment group. Expression of mesodermal marker genes X*Bra* and X*Chd* was increased in all explants induced with activin-A. *EF1-α* expression did not change with activin-A treatment, or with construct over-expression. A negative control lacking template shows no expression.

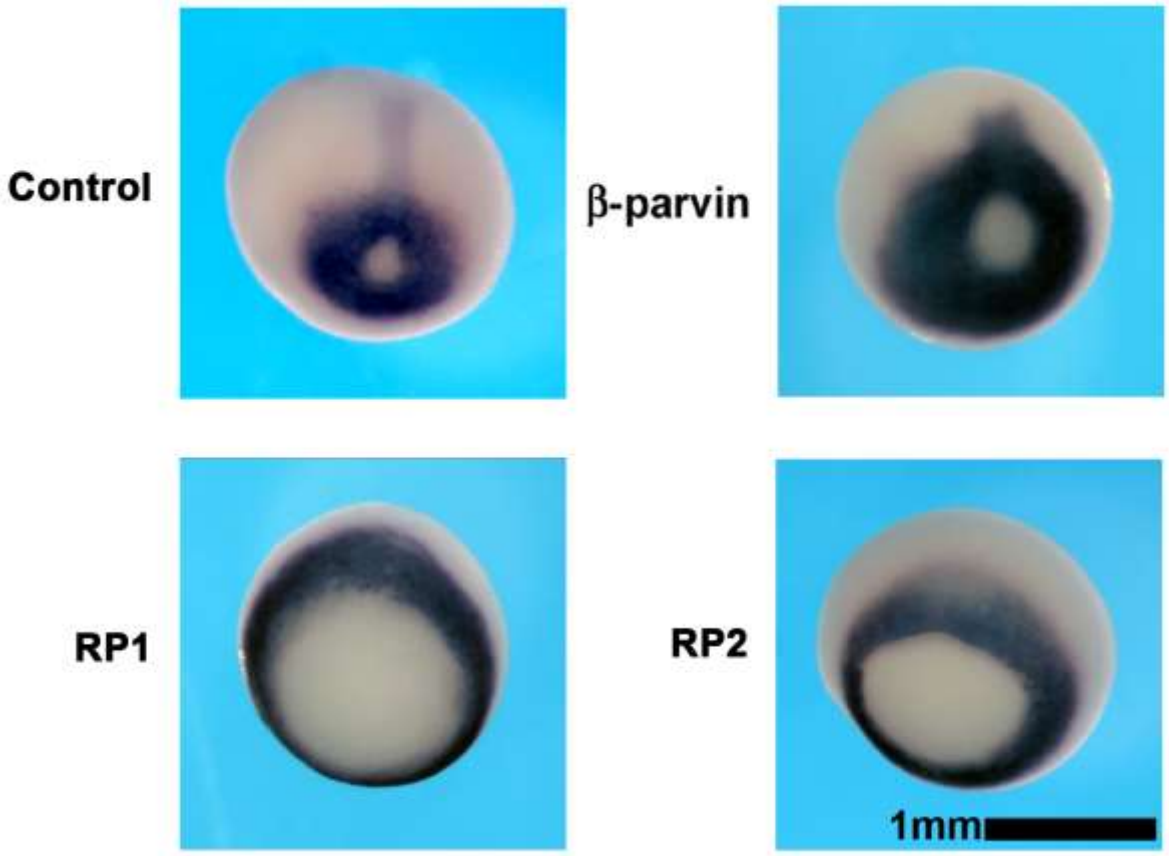

Figure 3.20 RP1 and RP2 inhibit morphogenesis. Stage two embryos were injected with GFP (control), or β-parvin GFP constructs in the animal pole, and cultured until stage 12.5. Whole-mount *in situ* hybridization was performed using an X*Bra* probe. Control and β-parvin over-expressing embryos exhibit normal X*Bra* expression pattern. RP1 and RP2 over-expressing embryos exhibit X*Bra* expression in pre-involution mesoderm, however, mesoderm involution around the blastopore lip was inhibited.

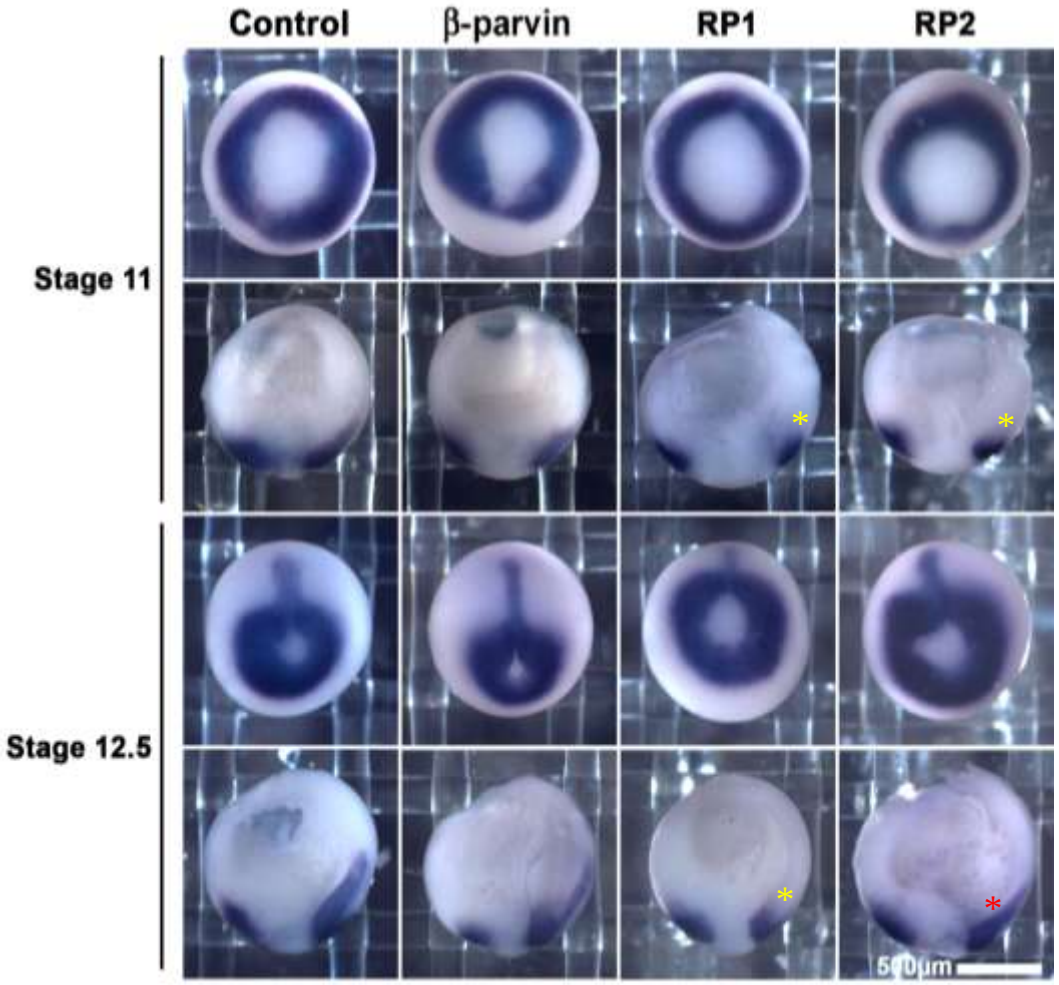

Figure 3.21 RP1 and RP2 inhibit morphogenesis independent of X*Bra* expression. Stage three embryos were injected with GFP (control) or β-parvin GFP constructs in the two dorsal blastomeres. Stage 11 and 12.5 embryos were subjected to *in situ* hybridization using an X*Bra* probe. The vegetal pole of whole stage 11 and 12.5 embryos (1st and 3rd rows) was visualized. Embryos were also dissected along the sagittal plane to visualize mesoderm involution in stage 11 and 12.5 embryos. Control and β-parvin over-expressing embryos exhibit similar X*Bra* expression patterns in both stage 11 and 12.5 embryos. RP1 over-expressing embryos show an inhibition of mesoderm involution in stage 11 and 12.5 embryos (yellow asterisk). RP2 over-expressing embryos show an inhibition of involution in stage 11 embryos (yellow asterisk), where mesoderm has involuted in stage 12.5 embryos, but is accumulating at the dorsal lip (red asterisk).

3.8 The RP2 Construct Inhibits Integrin Function

Cells isolated from the BCR can attach to FN, and upon exposure to activin-A spread and migrate (Smith et al., 1990; Ramos et al., 1996). Since integrin α5β1-FN interactions seem to be maintained in RP1, but inhibited in RP2 over-expressing cells, I asked whether a change in integrin α5β1 adhesion to FN could be detected. Stage two embryos were injected with GFP or β-parvin GFP constructs and dissociated BCR cells treated with activin-A and plated on FN. Cell adhesion was expressed as a percentage of original cells remaining after washing away non-adherent cells. Ninety-nine percent of control cells adhere, and similar to this 96% of RP1 over-expressing cells adhere (Figure 3.22). β-parvin over-expressing cells adhere slightly less at 83%, while 69% of RP2 over-expressing cells adhere (Figure 3.22). This suggests that RP2 over-expression decreases integrin α5β1 affinity for FN substrates.

Cell migration was monitored using dissociated BCR cells treated with activin-A. Cells were plated onto a FN matrix at the onset of gastrulation, and time-lapse imaging was used to track the cells over a 2.8 hour time period. Control, β-parvin, and RP1 over-expressing cells appear similar in their migration patterns (Figure 3.23). RP2 over-expressing cells moved in small circular pathways, remaining close to the original site of adhesion (Figure 3.23). Control, β-parvin, and RP1 over-expressing cells show similar total distances, while RP2 over-expressing cells migrate poorly (Figure 3.24). This suggests that RP2 inhibits integrin function.

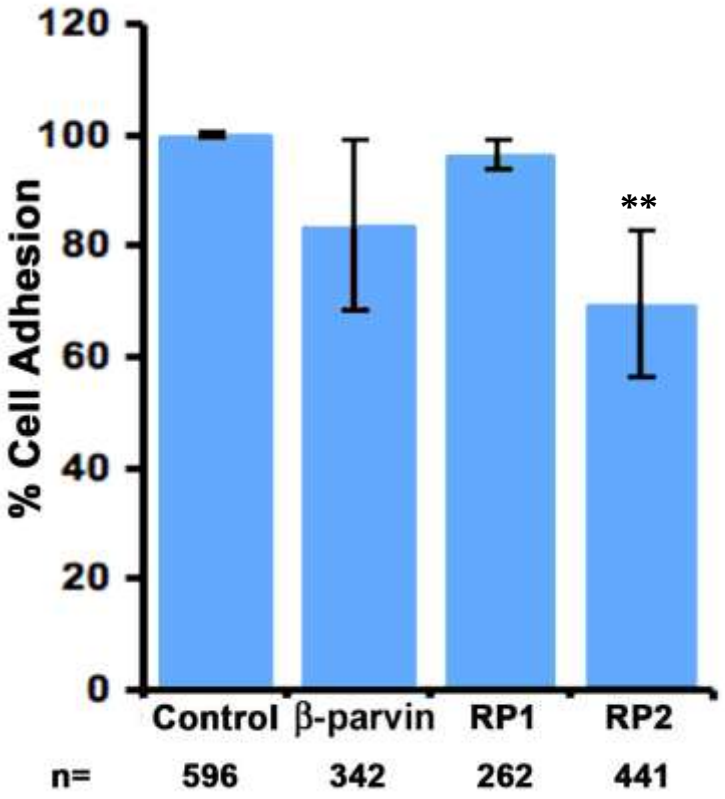

Figure 3.22 RP2 decreases integrin α5β1 adhesion to FN substrates. Stage two embryos were injected with GFP (control) or β-parvin GFP constructs and cultured until stage eight. BCR cells were dissociated, treated with Activin-A, and plated on a FN substrate. Percent cell adhesion is expressed as a % of original cells remaining after wash. Control cells are 99 ±0.5% adherent. β-parvin over-expressing cells are 83±15% adherent. RP1 over-expressing cells are 96±2.6% adherent. RP2 over-expressing cells decrease integrin α5β1 adhesion, as cells are 69±15% adherent. ** indicates $p<0.01$ compared to controls.

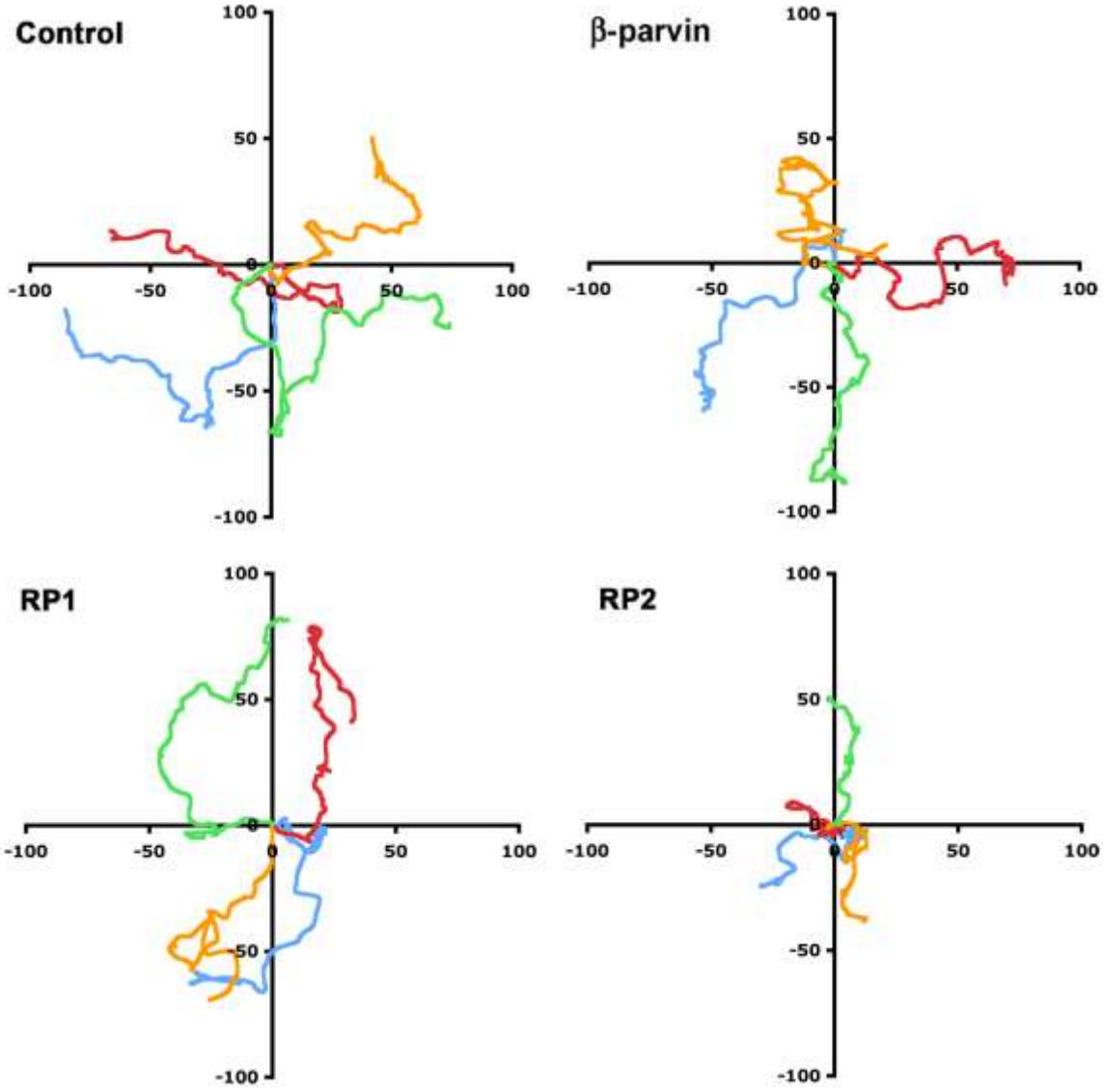

Figure 3.23 RP2 inhibits cell migration. Spider graphs represent migration tracks of individual BCR cells over-expressing GFP or β-parvin GFP constructs plated on FN substrates. Each graph contains four representative tracks with each cell in a different colour, and start point set at (0,0). The horizontal and vertical scales are in μm. RP2 over-expressing cells have decreased migration paths compared to control, β-parvin, or RP1 over-expressing cells.

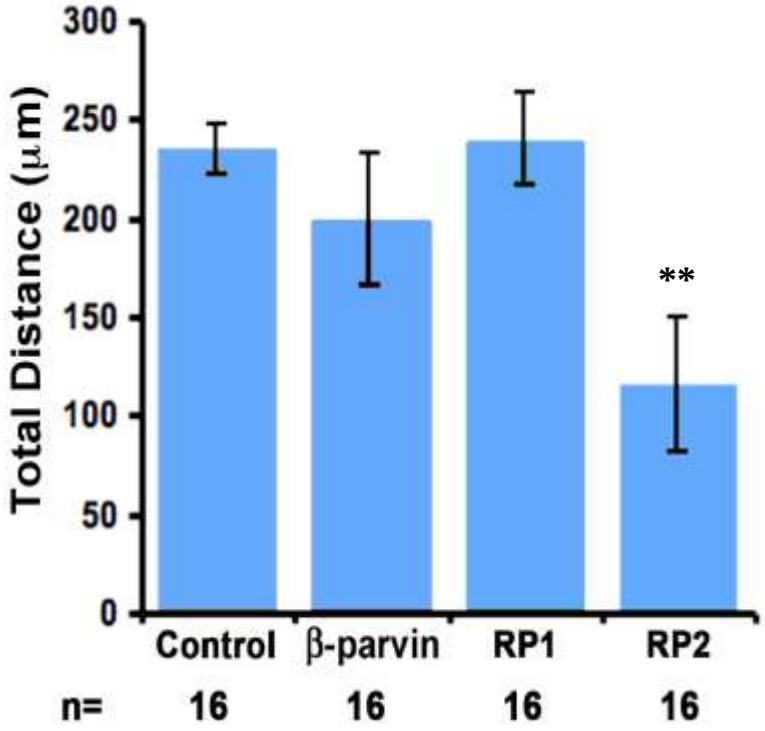

Figure 3.24 RP2 inhibits mesoderm induced cell migration. Dissociated BCR cells treated with activin-A were plated onto FN substrates, and cell migration paths tracked to obtain a total distance traveled. Control cells traveled 235±12μm. RP1 over-expressing cells exhibited cell migration similar to controls with total distance of 240 ±23μm. β-parvin over-expressing cells traveled slightly less with 199±34μm, while RP2 over-expressing cells traveled the least with 115±34μm. ** indicates $p<0.01$ compared to controls.

3.9 The IPP Complex Does Not Exist *in vivo*

The hypothesis to emerge from these experiments is that RP2 is inhibiting integrin α5β1 function, causing decreased integrin α5β1-FN adhesion. Since the IPP complex is known to exist in cultured cells (Wickstrom et al., 2010, Zhang et al., 2004) and ILK has been shown

to bind directly to β1 integrin tails (Hannigan et al., 1996) I asked whether RP2 is inhibiting integrin α5β1 function and if this inhibition is acting through the IPP complex *in vivo*. Lysates obtained from embryos over-expressing GFP or β-parvin GFP constructs were subjected to immunoprecipitation using anti-GFP antibody. A moderate amount of ILK was co-immunoprecipitated with β-parvin and RP2, while far less was co-immunoprecipitated with RP1 (Figure 3.25).

I performed another immunoprecipitation using anti-GFP antibody to determine whether PINCH was in complex with β-parvin constructs. PINCH failed to co-immunoprecipitate with GFP, β-parvin-GFP, GFP-RP1, or GFP-RP2, indicating that the IPP complex does not exist in the gastrula stage embryo (Figure 3.26).

IPP complex assembly and localization to focal adhesions *in vitro* has been shown to be dependent upon paxillin binding to ILK (Nikolopoulos and Turner, 2001; Nikolopoulos and Turner, 2002). Therefore, I performed another immunoprecipitation using anti-GFP antibody to determine if β-parvin was in complex with paxillin. There was no pull-down of paxillin in any of the samples, demonstrating that paxillin is not in complex with β-parvin *in vivo* (Figure 3.27).

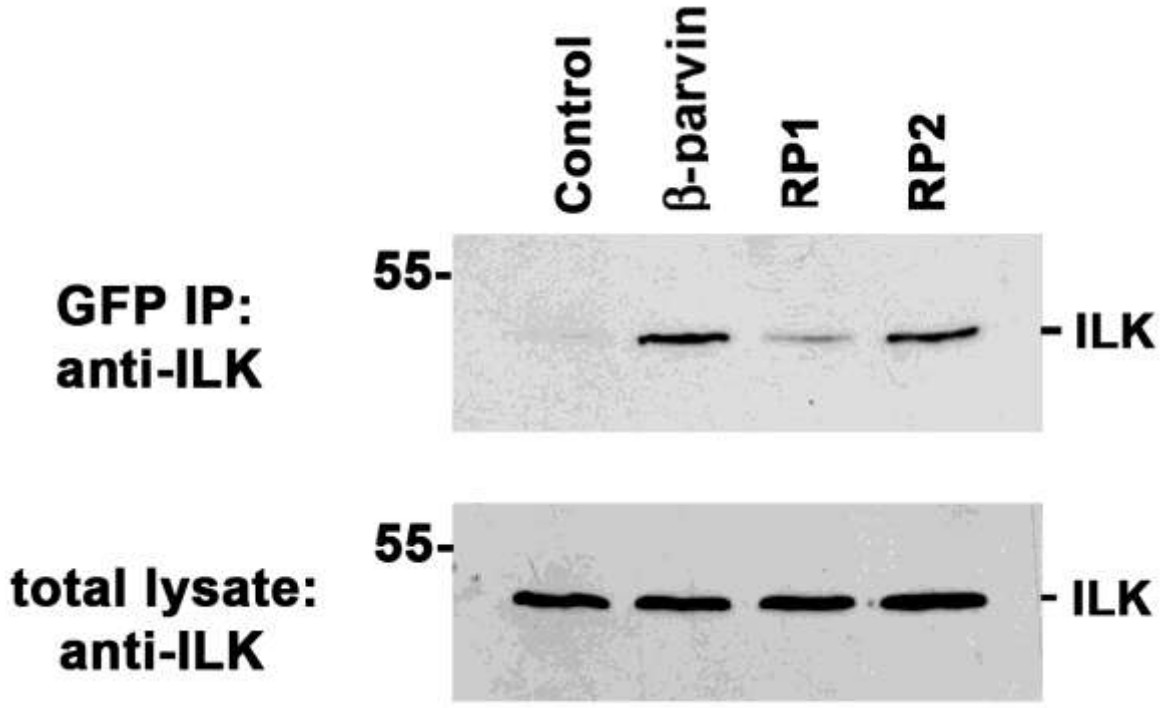

Figure 3.25 The CH2 domain of β-parvin interacts with ILK *in vivo*. Stage two embryos were injected in the animal pole with GFP or β-parvin GFP constructs and cultured until stage 12. Embryos were lysed in ESB and subjected to co-immunoprecipitation with anti-GFP antibody bound to protein G beads. The anti-GFP immunoprecipitates and protein G immunoprecipitates (total lysate) were subjected to SDS-PAGE followed by Western blotting with anti-ILK antibody. Lysate from β-parvin and RP2 over-expressing embryos exhibit co-immunoprecipitation with ILK. A small amount of ILK immunoprecipitates with RP1-GFP. A small fraction of ILK immunoprecipitates with control-GFP indicating some unspecific binding. ILK is equally expressed in whole embryos (total lysate) prior to immunoprecipitation.

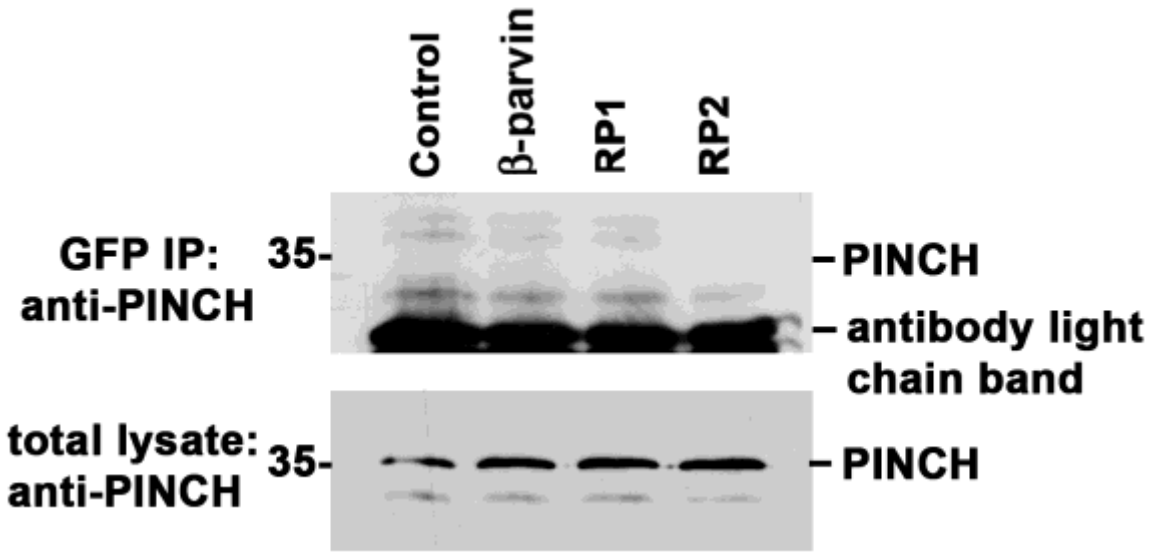

Figure 3.26 β-parvin does not interact with PINCH *in vivo*. Stage two embryos were injected in the animal pole with GFP or β-parvin GFP constructs and cultured until stage 12. Embryos were lysed in ESB and subjected to immunoprecipitation using anti-GFP antibody bound to protein G beads. Protein G (total lysate) and anti-GFP immunoprecipitates were subjected to SDS-PAGE followed by Western blotting with anti-PINCH antibody. PINCH is equally expressed in whole embryos (total lysate) prior to immunoprecipitation. PINCH was not detected in any of the lysates subjected to anti-GFP immunoprecipitation.

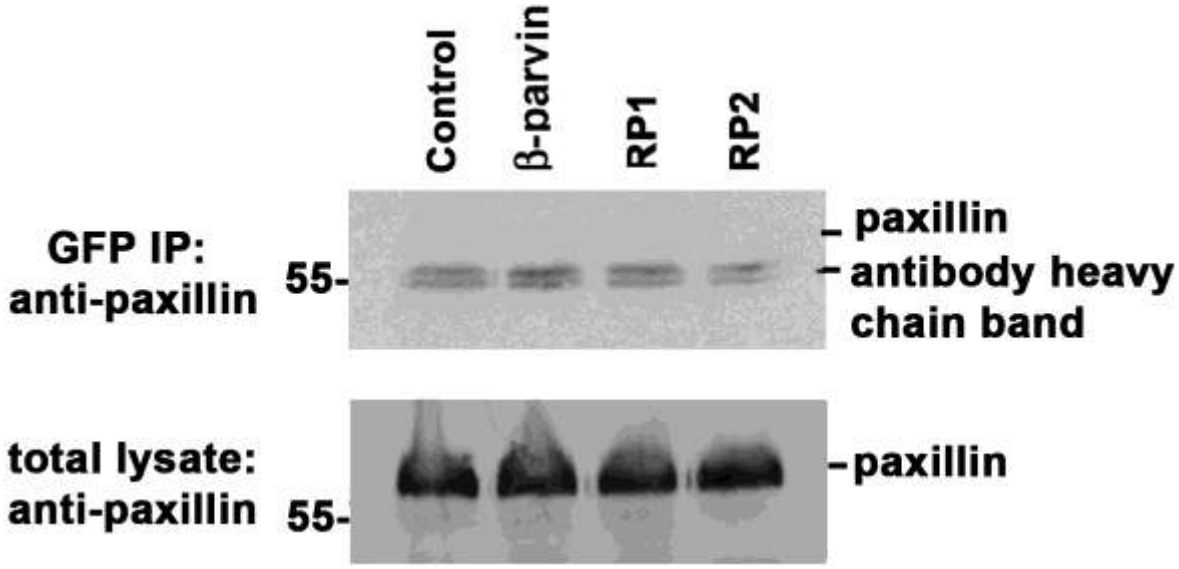

Figure 3.27 β-parvin does not interact with paxillin *in vivo*. Stage two embryos injected with GFP or β-parvin GFP constructs in the animal pole were cultured until stage 12 and lysed in ESB. Lysate was subjected to immunoprecipitation using anti-GFP antibody or protein G beads (total lysate) followed by SDS-PAGE and Western blotting using anti-paxillin antibody. No paxillin was detected in any of the immunoprecipitated lysate. Total lysate shows equal expression of paxillin in whole embryo lysate.

3.10 β-parvin Regulates Cadherin Adhesion

Integrin α5β1 function in RP1 over-expressing embryos is not impaired (Figure 3.22-3.24), but RP1 over-expression inhibits FN fibrillogenesis (Figure 3.13, 3.16) suggesting an alternative explanation for this observation. C-cadherin mediated adhesion is also required for FN matrix assembly (Dzamba et al., 2009), therefore I asked if C-cadherin adhesion is altered in RP1 over-expressing cells. To elucidate whether RP1 alters C-cadherin mediated

adhesion, I plated cells onto C-cadherin substrates and measured adhesion based on the percentage of original cells remaining after loose cells were rinsed away. Embryos were injected with GFP or β-parvin GFP constructs in the animal pole of stage two embryos and cultured until stage ten. Dissociated animal cap cells were plated onto C-cadherin substrates, and 96% of the control cells adhered (Figure 3.28). Similar to controls, 93% of β-parvin over-expressing cells and 95% of RP2 over-expressing cells adhered (Figure 3.28). RP1 over-expression decreased C-cadherin adhesion, as 79% of cells adhered (Figure 3.28).

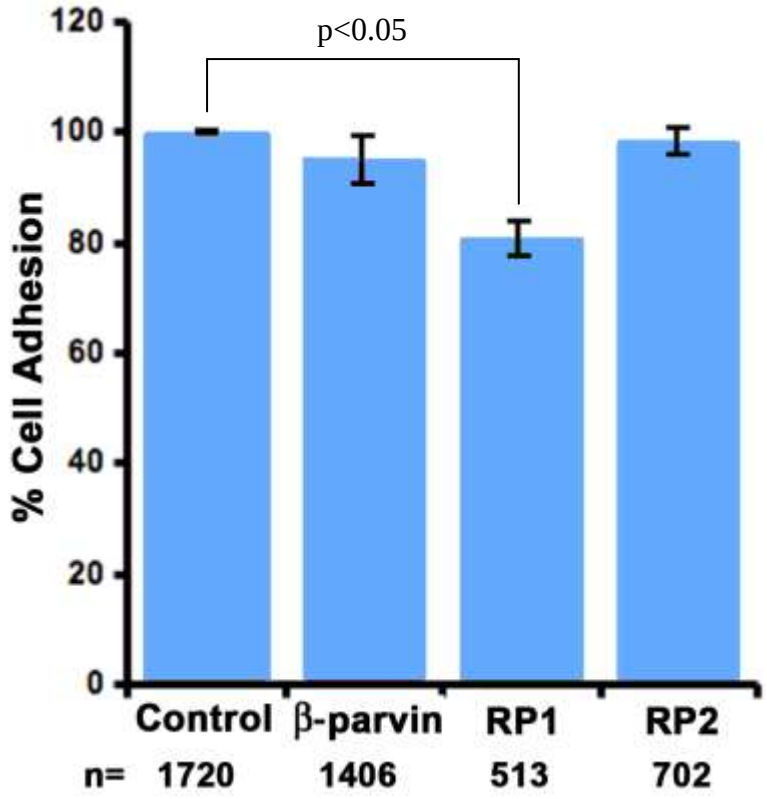

Figure 3.28 RP1 decreases cadherin adhesion. Stage two embryos were injected in the animal pole with GFP or β-parvin GFP constructs and cultured until stage ten. Animal caps were excised and cells dissociated. Cells were plated onto C-cadherin substrates, and cell adhesion was measured as a percentage of cells that remained attached after washing away loose cells. Average C-cadherin adhesion in control cells is 96±7.39%. Average C-cadherin adhesion in β-parvin over-expressing cells is 93±5.05%. RP2 over-expressing cells had an average C-cadherin adhesion of 95±5.07%. RP1 over-expressing cells had an average C-cadherin adhesion of 79±4.01%.

Since RP1 was able to decrease C-cadherin adhesion, I asked whether RP1 localized to sites of cell-cell adhesion. Dissociated cells over-expressing GFP or β-parvin GFP constructs were plated in low density onto FN substrates to observe protein localization upon formation of nascent cell-cell junctions. Control and RP2 showed no localization to nascent cell-cell junctions (Figure 3.29). Both β-parvin and RP1 translocated to sites of cell-cell adhesion (Figure 3.29).

Protein localization was also observed *in vivo* in BCRs. Animal caps were excised from embryos over-expressing GFP and β-parvin GFP constructs, and stained for actin to visualize cell boundaries. Both β-parvin and RP1 were able to co-localize with actin in distinct accumulations at cell boundaries (Figure 3.30, white arrowheads). In control and RP2 over-expressing BCRs, no co-localization with actin was observed, however, there is some overlap between control and actin proteins as control proteins are dispersed throughout the cesells (Figure 3.30, white arrowheads). This suggests that the CH1 domain of β-parvin has the ability to recruit β-parvin to sites of cell-cell adhesion.

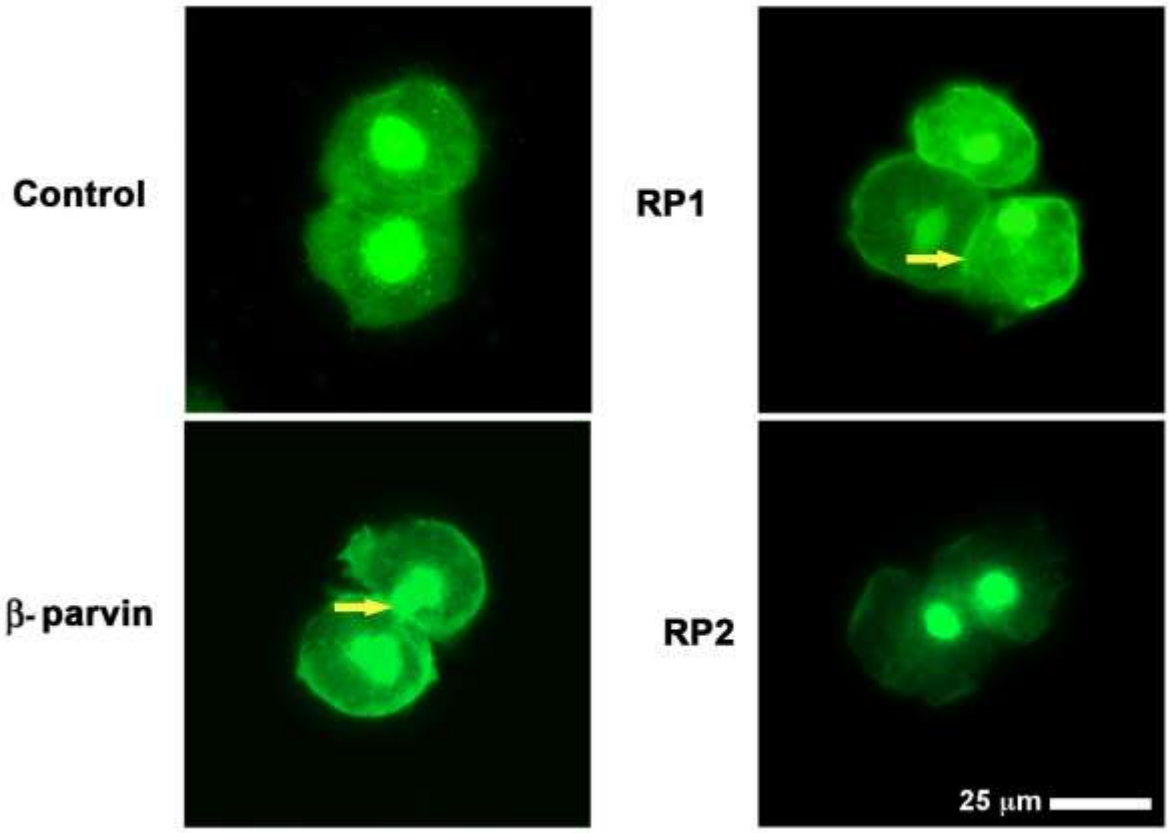

Figure 3.29 The CH1 domain of β-parvin mediates translocation to cell-cell contacts. Embryos were injected with GFP or β-parvin GFP constructs in the animal pole at stage two. Embryos were cultured until stage 11 and dissociated BCR cells over-expressing GFP constructs were plated onto exogenously supplied FN substrates. β-parvin and RP1 GFP proteins translocate to sites of cell-cell contact. Control and RP2 GFP proteins show no localization to sites of cell-cell contact.

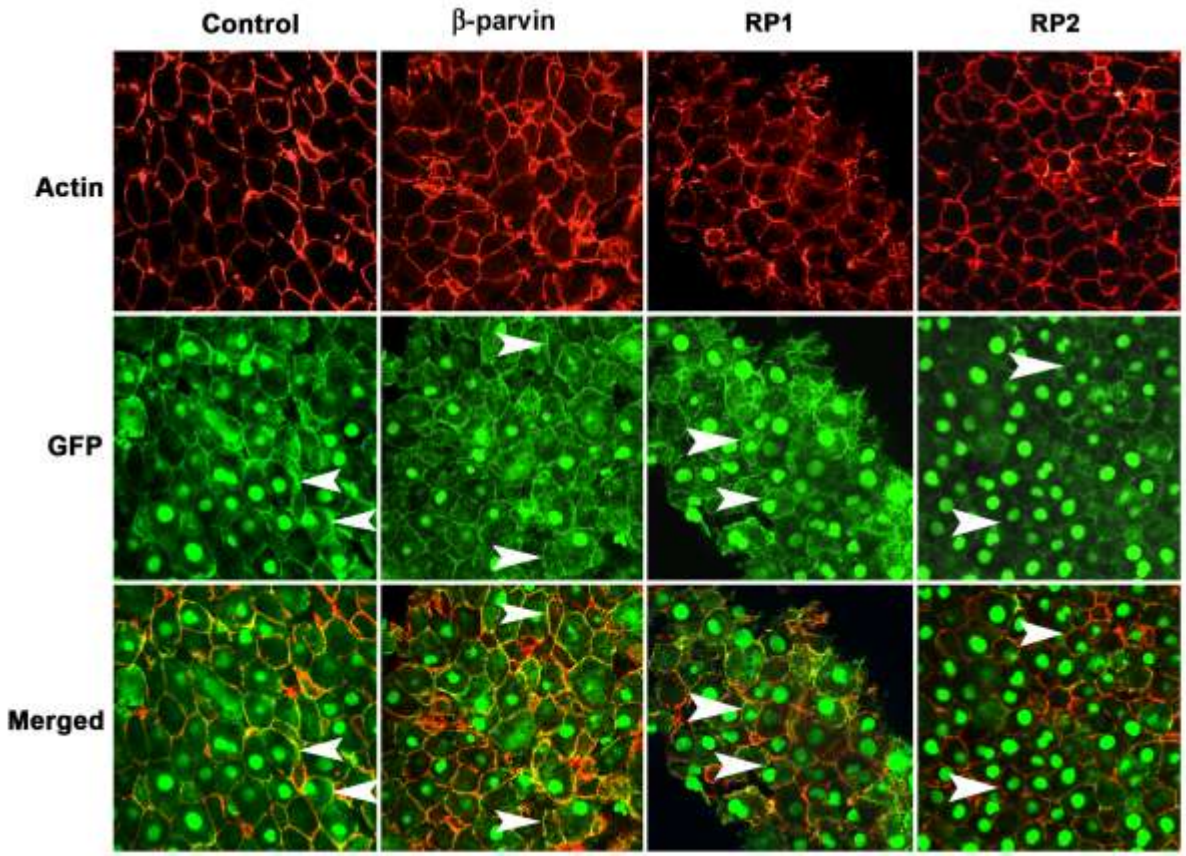

Figure 3.30 β-parvin and RP1 localize to cell-cell junctions *in vivo.* Embryos were injected with GFP or β-parvin GFP constructs in the animal pole, and cultured until stage 11. BCRs were excised and stained for actin to visualize cell boundaries. GFP has diffuse localization throughout the cells (white arrowheads in GFP panel), and does not localize preferentially to sites of actin accumulation (white arrowheads in merged panel). β-parvin and RP1 translocate to sites of cell-cell adhesion (white arrowheads in GFP panel) where actin accumulates (white arrowheads in merged panel). RP2 does not localize to sites of cell-cell adhesion (white arrowheads in GFP panel) where actin localization is seen (white arrowheads in merged panel).

Since inhibition of C-cadherin expression has been shown to reduce cell-cell adhesion (Brieber and Gumbiner, 1994; Lee and Gumbiner, 1995), I wanted to determine if RP1 decreased C-cadherin mediated adhesion via a decrease in C-cadherin expression *in vivo*. I performed a Western blot to visualize total C-cadherin expression levels in embryos over-expressing GFP or β-parvin GFP constructs. I compared β-tubulin expression levels to C-cadherin expression levels to determine if there were any differences in C-cadherin expression. C-cadherin expression was similar between all constructs (Figure 3.31) suggesting no inhibition in C-cadherin expression.

I next looked at C-cadherin surface expression. Cell surface proteins were biotinylated and I performed an immunoprecipitation using anti-C-cadherin. By comparing β-tubulin to C-cadherin expression I was able to determine that the β-parvin constructs had no effect on cadherin surface expression (Figure 3.32). This suggests that RP1 decreases C-cadherin adhesion via a mechanism independent of cadherin expression.

Overall, the results indicate that the CH1 domain of β-parvin has a role mediating cadherin signalling, while the CH2 domain of β-parvin is mediating integrin signalling.

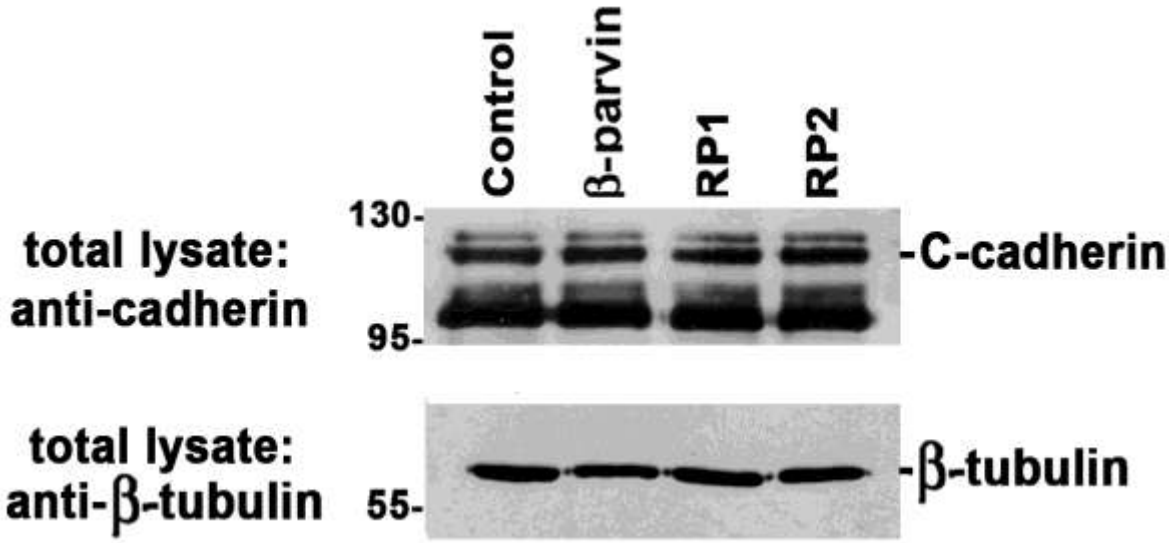

Figure 3.31 β-parvin does not regulate C-cadherin expression. Stage two embryos were injected with GFP or β-parvin GFP constructs and cultured until stage 12. Embryo lysate was subjected to SDS-PAGE and Western blotting using anti C-cadherin and anti β-tubulin antibodies. There was no difference in C-cadherin expression between control, β-parvin, RP1, or RP2 lysates. Anti-β-tubulin was used as a loading control.

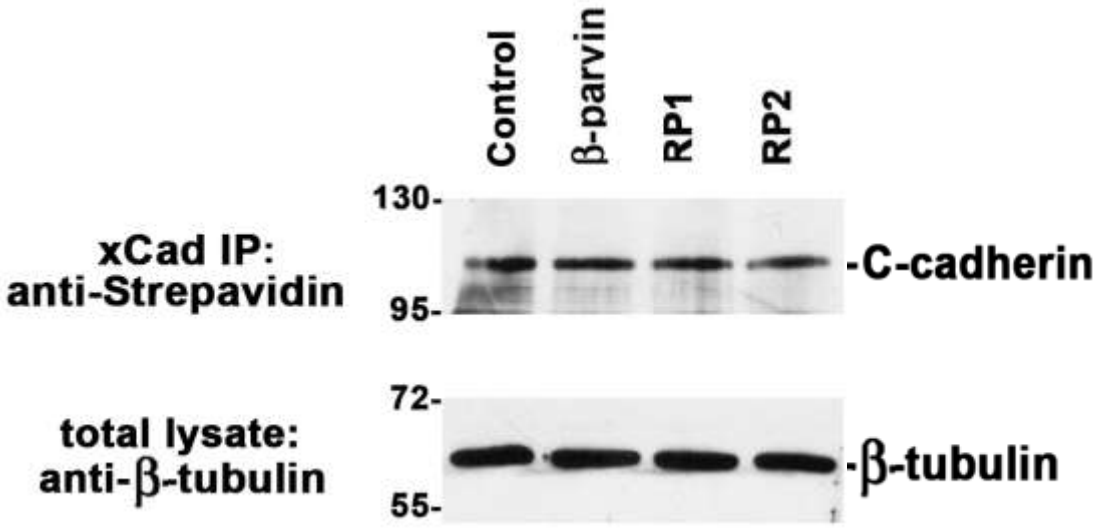

Figure 3.32 β-parvin does not regulate surface expression of C-cadherin. Animal caps were excised from embryos over-expressing GFP or β-parvin GFP constructs. Animal caps were biotinylated and subjected to immunoprecipitation with anti-C-cadherin antibody, followed by SDS-PAGE and Western blotting using strepavidin-HRP and anti-β-tubulin antibodies. C-cadherin surface expression was not affected by over-expression of β-parvin, RP1, or RP2 constructs. β-tubulin was used as a loading control.

3.11 β-parvin Regulates Tissue Separation

During *Xenopus* gastrulation, mesendoderm comes into contact with the cells of the BCR and the two tissues remain separate defining Brachet's cleft (Wacker et al., 2000). Brachet's cleft initially forms during vegetal rotation, and continues to extend as new tissue involutes around the dorsal blastopore lip. Maintenance of Brachet's cleft is necessary for the translocation of mesendoderm along the BCR (Winklbauer and Keller, 1996). Since RP1 and RP2 over-

expression inhibits attachment and translocation of the mesendoderm (Figure 3.15), I asked whether RP1 and RP2 over-expression inhibits tissue separation and formation of Brachet's cleft. Embryos over-expressing GFP or β-parvin GFP constructs in the DMZ were bisected along the sagittal plane to view Brachet's cleft. In control and β-parvin over-expressing embryos mesoderm involuted around the blastopore lip, and embryos exhibit normal Brachet's cleft formation (Figure 3.33). Mesoderm involution and Brachet's cleft formation was normal in 90% of control embryos (Figure 3.34). β-parvin over-expressing embryos are similar to controls as 88% have normal mesoderm involution and Brachet's cleft formation (Figure 3.34). RP1 over-expressing embryos show an inhibition of mesoderm involution (Figure 3.33). When location of the posterior end of Brachet's cleft was compared to blastopore lip location, there was an increase in the distance between these two structures in RP1 over-expressing embryos (Figure 3.33), suggesting an inhibition of posterior cleft formation. Only 22% of RP1 over-expressing embryos exhibited normal Brachet's cleft (Figure 3.34). Mesoderm involutes in RP2 over-expressing embryos, but fails to translocate across the BCR (Figure 3.33). In the area of RP2 over-expression pigmented cells are found in the deep layer of the ectoderm suggesting an abnormal mixing of the surface and deep cells at the dorsal lip (Figure 3.33). Only 5% of RP2 over-expressing embryos displayed normal Brachet's cleft formation (Figure 3.34). In RP2 over-expressing embryos, separation of pre- and post-involution tissue is expanded such that Brachet's cleft extends through the dorsal lip to the surface of the embryo (Figure 3.33). Tissue on the pre-involution side of Brachet's cleft in RP2 over-expressing embryos also displays a loose organization and seems

to lack polarity as the border of Brachet's cleft is irregular with several loose cells having invaded into the post-involution side of Brachet's cleft (Figure 3.33).

Figure 3.33 RP1 and RP2 inhibit normal Brachet's cleft formation. Embryos were injected with 2ng GFP, or β-parvin-GFP constructs in the two dorsal blastomeres of four-cell embryos, and incubated until stage 11.5. Embryos were dissected along the sagittal plane to view tissue involution around the dorsal blastopore lip. Control and β-parvin over-expressing embryos exhibit similar formation of Brachet's cleft, as the posterior end (black arrows) is in close proximity to the dorsal blastopore lip. RP1 over-expressing embryos exhibit an inhibition of the posterior end of Brachet's cleft (black arrow) as it is further from the dorsal blastopore lip than normal. RP2 over-expressing embryos exhibit Brachet's cleft formation extending to the surface of the embryo. Brachet's clefts are indicated by dashed red lines.

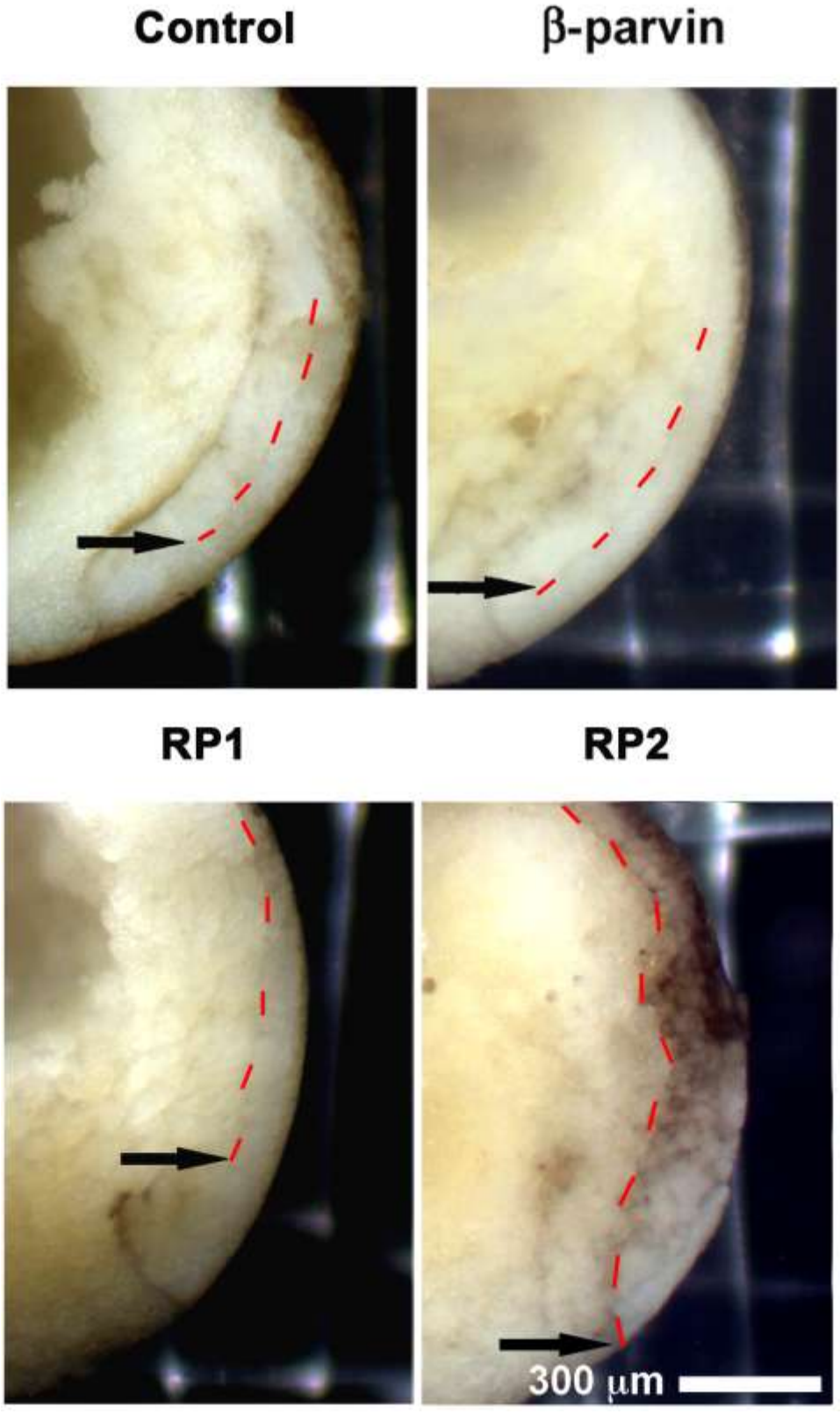
Control
β-parvin
RP1
RP2
300 μm

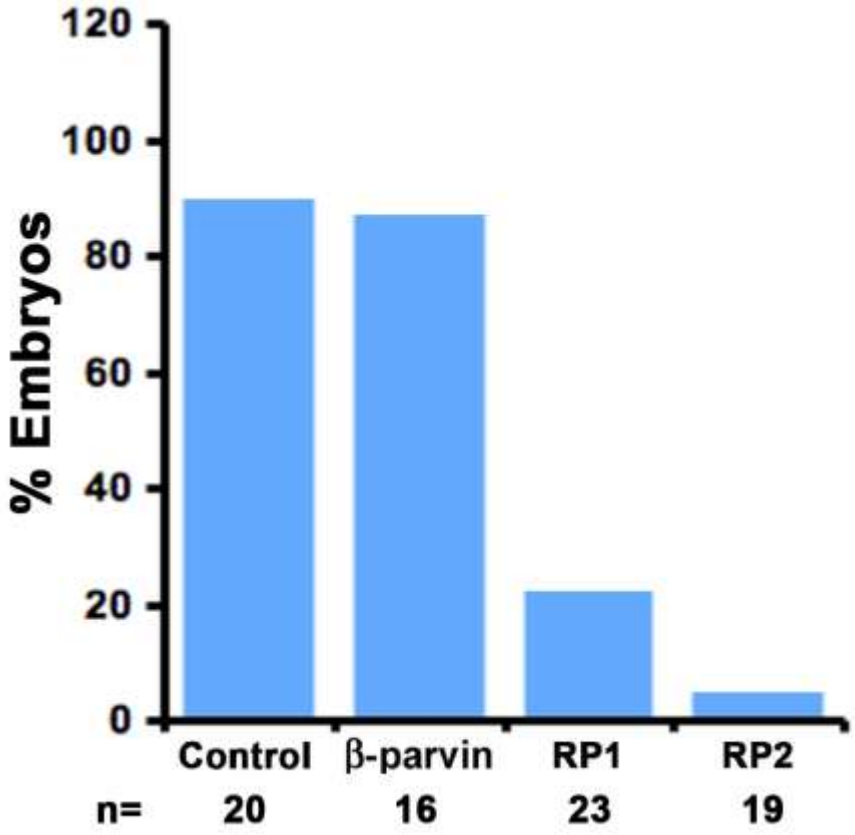

Figure 3.34 RP1 and RP2 inhibit normal formation of Brachet's cleft. Summary of Brachet's cleft formation in embryos injected with 2ng GFP or β-parvin GFP constructs in the two dorsal blastomeres of a four-cell embryo. Embryos over-expressing GFP (control) exhibit normal Brachet's cleft formation in 90% of embryos. Similar to controls, 88% of β-parvin over-expressing embryos exhibited normal Brachet's cleft formation. RP1 over-expression decreased normal Brachet's cleft formation to 22% and RP2 over-expression decreased normal Brachet's cleft to 5%.

Since RP1 and RP2 over-expression causes opposing phenotypes in the DMZ, I asked whether β-parvin constructs localized preferentially in cells of pre- versus post-involution tissue. Stage three embryos were injected with GFP or β-parvin GFP constructs in the two dorsal blastomeres and pre- and post-involution explants were removed at stage 11.5. Prior to involution, β-parvin localized to sites of cell-ECM adhesion (Figure 3.35, yellow arrows), whereas β-parvin translocated to sites of cell-cell adhesion in post-involution tissue (Figure 3.35, red arrows). Prior to involution RP1 is expressed throughout the cytoplasm (Figure 3.36, red arrow heads), whereas post-involution, RP1 translocates to sites of cell-cell adhesion (Figure 3.36, red arrows). RP2 remains consistently localized to sites of cell-ECM adhesion in both pre- and post-involution tissue (Figure 3.37). These results indicate that β-parvin is able to translocate from sites of integrin adhesion (mediated by the CH2 domain) to sites of cadherin adhesion (mediated by the CH1 domain) after involution around the blastopore lip. This suggests a dynamic regulation of β-parvin localization mediated by signalling in the dorsal marginal zone.

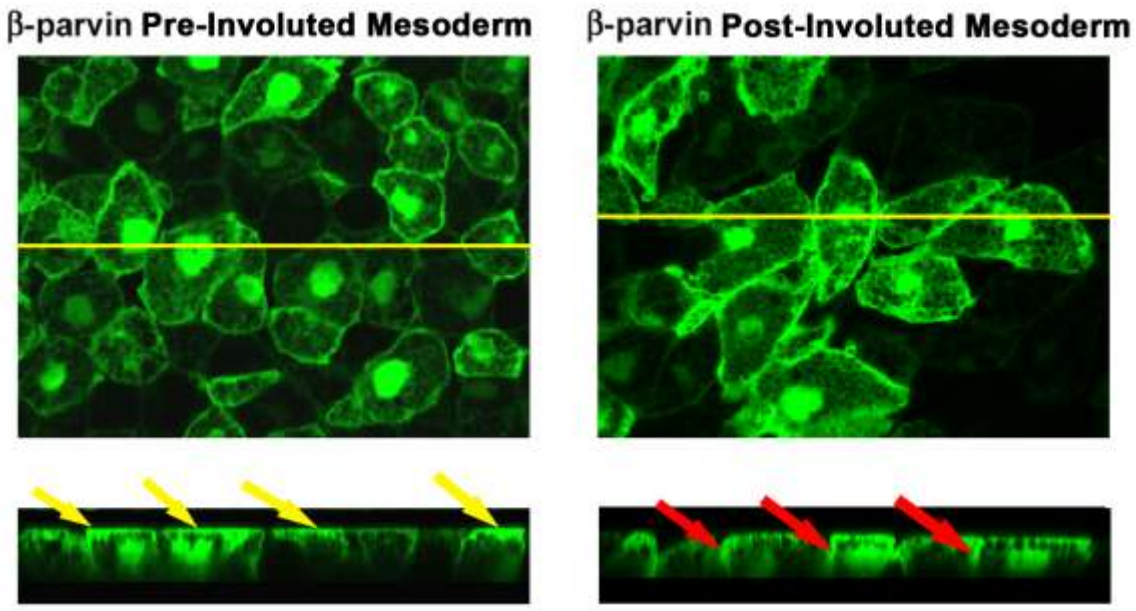

Figure 3.35 β-parvin translocates from sites of cell-ECM adhesion to sites of cell-cell adhesion in post-involution tissue. β-parvin-GFP mRNA was injected in the two dorsal blastomeres at the four-cell stage, and explants were removed at stage 11.5. β-parvin localizes to sites of cell-ECM adhesion in pre-involution tissue (yellow arrows). β-parvin localizes to sites of cell-cell adhesion in post-involution tissue (red arrows).

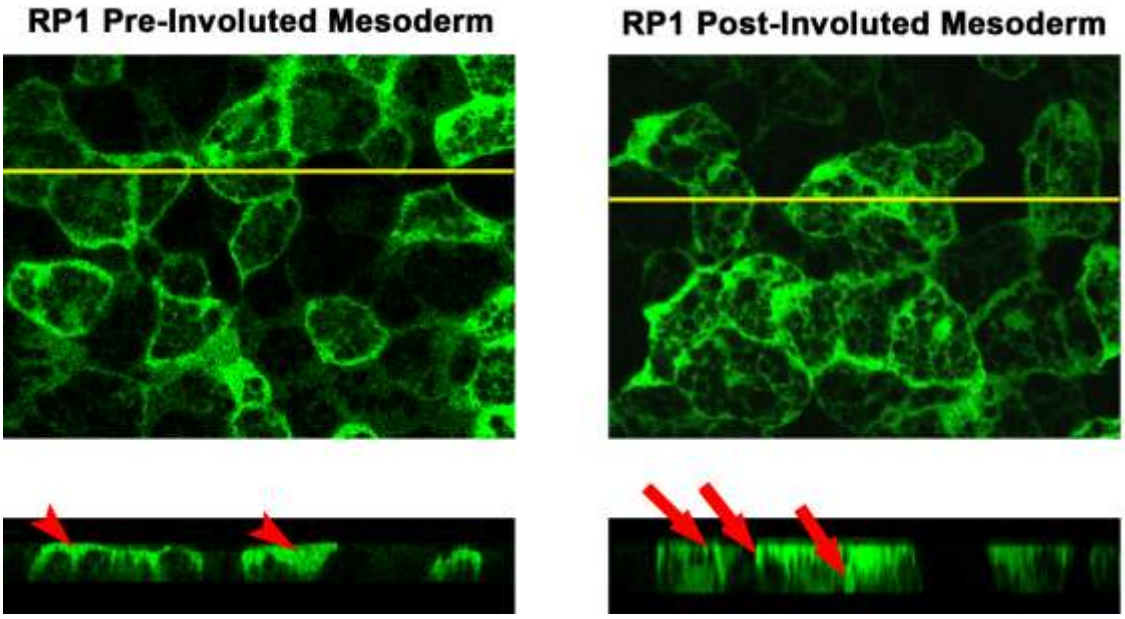

Figure 3.36 RP1 translocates to sites of cell-cell adhesion in post-involution tissue. Stage three embryos were injected in the two dorsal blastomeres with GFP-RP1 mRNA and explants were removed at stage 11.5. RP1 expression remained cytosolic in pre-involution tissue (red arrowheads). RP1 translocated to sites of cell-cell adhesion in post-involution tissue (red arrows).

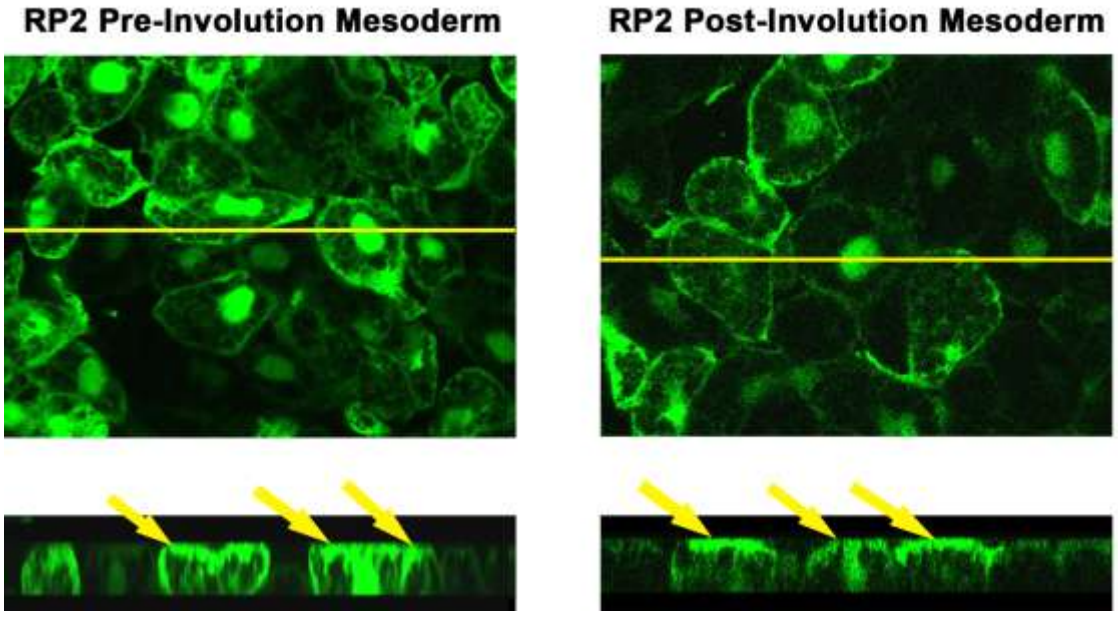

Figure 3.37 RP2 remains localized at sites of cell-ECM adhesion. Four-cell stage embryos were injected with GFP-RP2 mRNA into two dorsal blastomeres, and explants were removed at stage 11.5. RP2 localized to sites of cell-ECM adhesion in pre-involution tissue (yellow arrows). Involution around the dorsal blastopore lip had no effect on RP2 localization, as RP2 remained localized to sites of cell-ECM adhesion (yellow arrows).

To determine whether abnormal Brachet's cleft phenotypes observed in RP1 and RP2 over-expressing embryos were due to tissue separation (TS), I tested TS using an *in vitro* assay (Wacker et al., 2000). Marginal zone mesoderm cells exhibit TS behaviour after involution and will not reintegrate into an ectodermal explant, whereas pre-involution mesoderm cells that have not acquired TS behaviour will reintegrate into the BCR (Wacker et al., 2000). Therefore, pre-involution explants will reintegrate into the BCR, while post-involution explants acquire TS behaviour and remain distinctly separate.

Pre- and post-involution mesoderm explants were removed from embryos injected with GFP or β-parvin GFP constructs and placed on BCRs to score TS behaviour. The majority of control pre-involution explants reintegrated into the BCR (Figure 3.38 a, b, c, white arrows), as only 14% did not reintegrate (Figure 3.39), while 95% of control post-involution mesoderm explants did not reintegrate into the BCR demonstrating it retained TS behavior (Figure 3.38 a, b, c, white arrowheads; Figure 3.39). Pre-involution explants over-expressing β-parvin reintegrated into the BCR (Figure 3.38 a, yellow arrow), as reintegration was prevented in only 11% (Figure 3.39), while 100% of post-involution explants over-expressing β-parvin did not reintegrate demonstrating TS behavior was retained (Figure 3.38 a, yellow arrowhead). RP1 over-expression inhibits TS behavior as pre- and post- involution mesoderm explants reintegrated into the BCR (Figure 3.38 b, yellow arrows). None of the RP1 over-expressing pre-involution explants displayed TS behavior and only 35% of post-involution explants did not reintegrate and displayed TS behavior (Figure 3.39). RP2 over-expression promotes TS behavior, as 100% of both pre- and post- involution mesoderm did not reintegrate into the BCR (Figure 3.38 c, yellow arrowheads; Figure 3.39). These results indicate that RP1 and RP2 are acting in opposing fashion as over-expression of RP1 inhibits post-involution mesoderm cells from acquiring TS behavior, while RP2 over-expression in pre-involution mesoderm promotes acquirement of TS behavior.

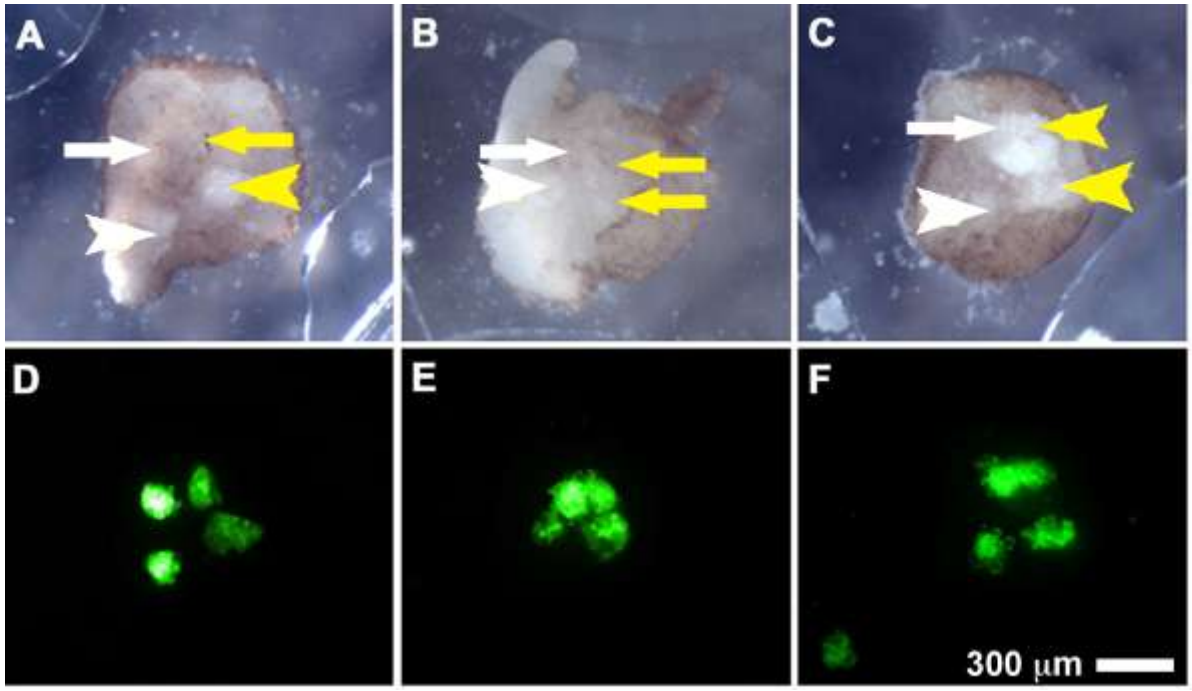

Figure 3.38 RP1 inhibits while RP2 promotes tissue separation during gastrulation. Stage two embryos were injected in the two dorsal blastomeres with GFP or β-parvin GFP constructs and cultured until stage 11. Pre- and post-involution mesoderm explants were placed on the surface of a BCR. Tissue separation was scored after 45-75 minutes. Control pre-involution explants reintegrated into the blastocoel roof (A, B, C, white arrows), while post-involution explants did not (A, B, C, white arrowheads). Pre-involution explants over-expressing β-parvin reintegrate into the BCR (A, yellow arrows), while post-involution explants exhibit TS behaviour and do not reintegrate (A, yellow arrowhead). RP1 over-expressing pre- and post-involution explants reintegrate into the BCR (B, yellow arrows). RP2 over-expressing pre- and post-involution explants do not reintegrate into the BCR (C, yellow arrowheads). GFP expression from A, B, and C are visualized in D, E, and F.

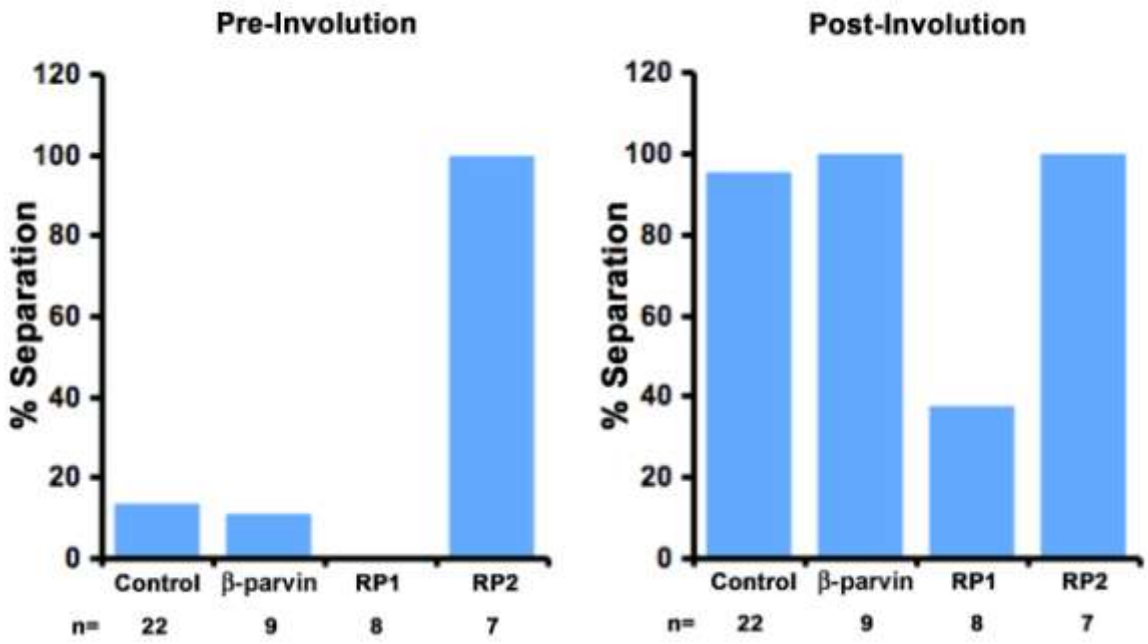

Figure 3.39 β-parvin regulates tissue separation. Compilation of the *in vitro* separation assays. Embryos were injected with GFP or β-parvin GFP constructs, and pre- and post-involution explants over-expressing each construct were plated onto the surface of a BCR. After 45-75 minutes, the percentage of explants that did not reintegrate was scored. Fourteen percent control, 11% β-parvin, 0% RP1, and 100% RP2 over-expressing pre-involution explants displayed TS behaviour. Ninety-five percent control, 100% β-parvin, 38% RP1, and 100% RP2 over-expressing post-involution explants displayed TS behaviour.

Regulation of Rac and Rho signalling is required for TS, as a decrease in active Rho or Rac inhibits TS, and an increase in active Rho or Rac can rescue TS downstream of PAPC and Ephrin/Eph (Park et al., 2011; Rohani et al., 2011; Medina et al., 2004). Since a balance of Rac and Rho is required for TS, I asked whether RP1 and RP2 could affect TS via regulation of Rac and Rho signalling. I performed *in vitro* TS assays using explants co-

expressing GFP or β-parvin GFP constructs along with dominant negative Rac (RacN) or Rho (RhoN), or constitutively active Rac (RacV) or Rho (RhoV).

GFP expression has no effect on TS in pre-involution mesoderm as 14% failed to reintegrate (Figure 3.39) and co-expression with either RacN (35% TS) or RacV (14% TS; Figure 3.43) in pre-involution mesoderm makes no difference, as pre-involution mesoderm reintegrated into the BCR (Figure 3.40, yellow arrows). Similarly co-expression of RhoN (17% TS) and RhoV (17% TS; Figure 3.43) with GFP in pre-involution tissue mesoderm had no effect on TS (Figure 3.40). In summary Rac and Rho have no effect on TS when over-expressed in pre-involution mesoderm.

In the post-involution mesoderm GFP expression had no effect on TS as 95% fail to reintegrate (Figure 3.43), and co-expression of GFP with RacV had no effect on tissue separation with 88% of explants displaying TS behaviour, whereas co-expression of GFP with RacN (58% TS; Figure 3.43) decreased TS behaviour (Figure 3.40 yellow arrowheads). A similar scenario was seen in tissues over-expressing the Rho constructs. RhoV had no effect on post-involution mesoderm with 100% displaying TS behaviour (Figure 3.40, yellow arrowheads; Figure 3.43). However, RhoN co-expressed with GFP resulted in a small decrease in TS behaviour (58% TS; Figure 3.43). This indicates that dominant active Rac and Rho have no effect on TS, whereas dominant negative constructs show a minor role in inhibition of TS behaviour in post-involution mesoderm. This decrease in TS was expected and is in agreement with previous over-expression of dominant negative Rac and Rho constructs (Rohani et al., 2011).

Similar to controls, β-parvin over-expression has no effect on TS in pre-involution mesoderm as 11% (Figure 3.44) failed to reintegrate into the BCR. Co-expression of β-parvin with either RacN (10% TS) or RacV (0% TS; Figure 3.44) in pre-involution mesoderm had no effect on TS as explants reintegrated into the BCR (Figure 3.41-3.42 yellow arrows). A similar scenario is seen in tissues over-expressing the Rho constructs as RhoN (17% TS) or RhoV (8% TS; Figure 3.44) explants failed to reintegrate into the blastocoel roof (Figure 3.41-3.42, yellow arrows).

Post-involution mesoderm constructs over-expressing β-parvin exhibit 100% TS (Figure 3.44), and co-expression with RacV (88% TS; Figure 3.44) had no effect on TS, whereas co-expression of β-parvin with RacN (40% TS; Figure 3.44) decreased TS behaviour similar to controls (Figure 3.41-3.42). Similarly, co-expression of RhoV (67% TS) results in a small decrease in TS, and co-expression of RhoN (55%; Figure 3.44) causes a decrease in TS behaviour (Figure 3.41-3.42). This indicates that dominant negative Rac and Rho decrease TS slightly when over-expressed in post-involution mesoderm.

TS in RP1 over-expressing pre-involution mesoderm was not affected as no explants exhibited TS behaviour (0% TS; Figure 3.45). Co-expression of RP1 with RacV, RacN, RhoV, or RhoN had no effect, as all pre-involution explants reintegrated into the BCR (0% TS; Figure 3.45; Figure 3.41-3.42, yellow arrows).

In post-involution mesoderm, expression of RP1 decreased TS to 38% (Figure 3.39). Co-expression of RP1 with RacV had an inhibitory effect on TS (0% TS), while co-expression with RacN (75% TS: Figure 3.45; Figure 3.41-3.42) rescues TS behaviour. Co-

expression of RP1 with RhoN in post-involution tissue did not rescue TS (25% TS), whereas co-expression with RhoV rescued TS completely (100% TS; Figure 3.45; Figure 3.41-3.42). This indicates that dominant negative Rho and constitutively active Rac had no effect on TS when co-expressed with RP1, however, when RP1 is co-expressed with constitutively active Rho and dominant negative Rac TS is rescued in post-involution mesoderm.

Interestingly RP2 co-expression with Rac and Rho constructs exhibit opposing effects on TS behaviour as RP1 expressing explants. RP2 over-expression promoted TS behaviour in pre-involution mesoderm (100% TS; Figure 3.46). Co-expression of RP2 with RacV (25% TS) rescued TS behaviour as pre-involution cells were able to reintegrate into the BCR, whereas co-expression with RacN (100% TS; Figure 3.46) was not able to rescue TS (Figure 3.41-3.42, yellow arrowheads). Co-expression of RP2 with RhoN (25% TS) was able to rescue TS, whereas co-expression with RhoV (75% TS; Figure 3.46) did not rescue TS behaviour (Figure 3.41-3.42).

In post-involution mesoderm RP2 over-expression had no effect on TS (100% TS; Figure 3.46), and co-expression of RP2 with RacV, RacN, RhoV, or RhoN had no effect on TS as 100% of the explants displayed TS behaviour (Figure 3.41-3.42, Figure 3.46). These results indicate that the effects of RP2 over-expression in pre-involution mesoderm can be rescued with co-expression of RacV or RhoN, promoting reintegration into the BCR.

Figure 3.40 Tissue separation in explants co-expressing GFP with RacV, RacN, RhoV, or RhoN. Stage two embryos were co-injected with GFP mRNA with 100pg RacN or RhoN, or 50pg RacV or RhoV DNA. Test explants were placed on BCRs and TS scored after 45-75 minutes. Over-expression of RacV and RhoV did not inhibit normal TS; as the majority of pre-involution mesoderm explants reintegrated into the BCR (yellow arrows) and post-involution mesoderm explants failed to reintegrate (yellow arrowheads). Over-expression of RacN increased TS in pre-involution explants (yellow arrowheads denote separation), and over-expression of RhoN decreased TS in post-involution explants (yellow arrow). GFP expression is visualized in the bottom panels of each group.

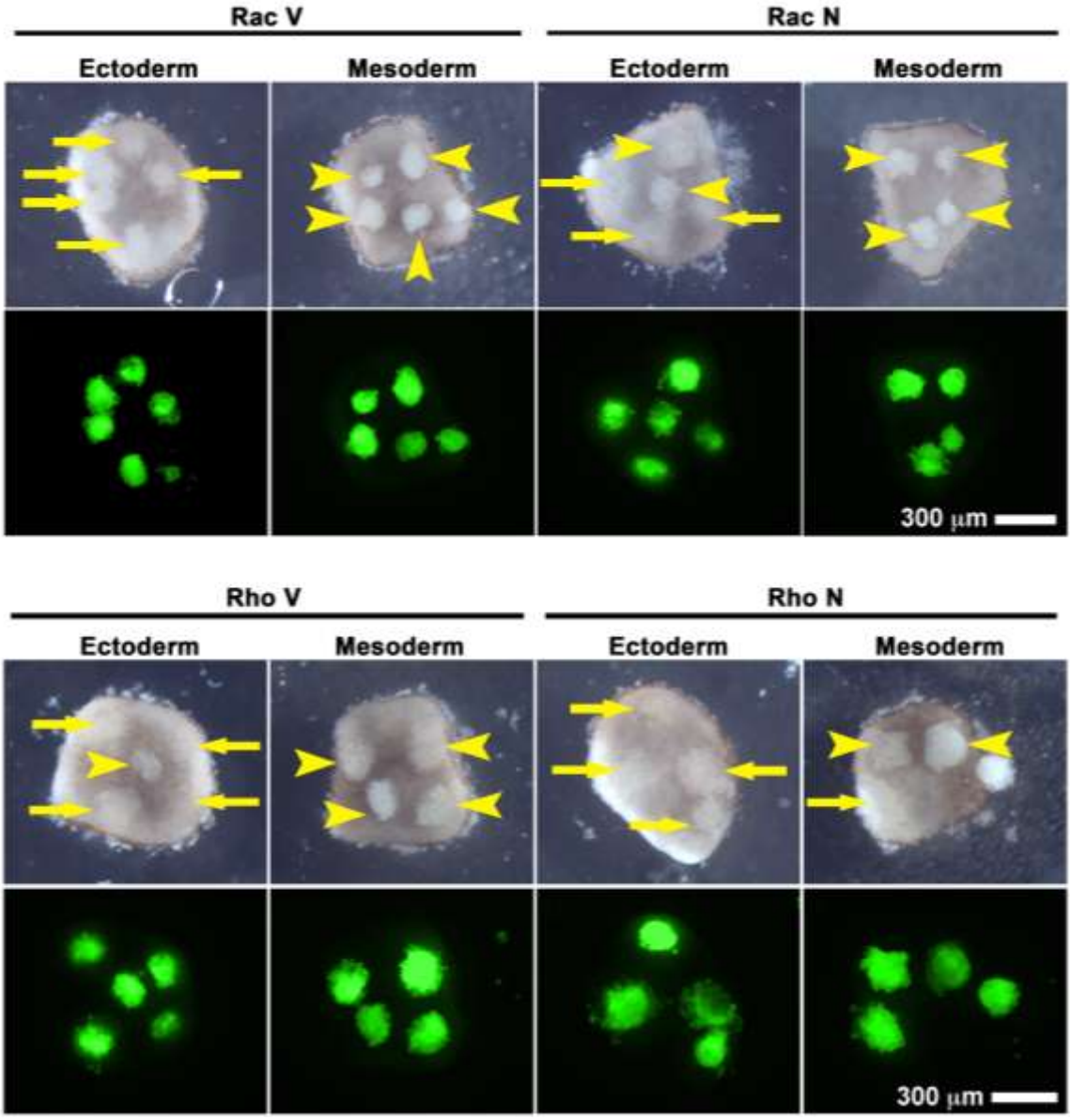
Rac V
Rac N
Ectoderm
Mesoderm
Ectoderm
Mesoderm
300 μm
Rho V
Rho N
Ectoderm
Mesoderm
Ectoderm
Mesoderm
300 μm

Figure 3.41 Co-expression of RacV with RP2 or RacN with RP1 rescues tissue separation. Two dorsal blastomeres of four-cell stage embryos were co-injected with β-parvin GFP constructs and 100pg RacN or 50pg RacV DNA. Explants were excised from stage 11 embryos and placed on the surface of a BCR. TS was scored after 45-75 minutes. White arrow and arrowheads denote explants injected with only β-parvin GFP constructs. Co-expression of RacV or RacN with β-parvin slightly decreases TS with most pre-involution explants reintegrating (yellow arrows) and post-involution explants exhibiting TS behaviour (yellow arrowheads). Co-expression of RacV with RP1 had no effect on TS, as both pre- and post- involution explants reintegrated into the BCR (yellow arrows). Co-expression of RacN with RP1 rescued TS in post-involution explants (yellow arrowhead). RacV co-expression with RP2 rescued TS as pre-involution explants reintegrated into the BCR (yellow arrow). RP2 co-expression with RacN had no effect on TS, as pre- and post-involution explants remained failed to reintegrate into the BCR (yellow arrowheads). GFP construct expression is shown in the bottoms panels for each group.

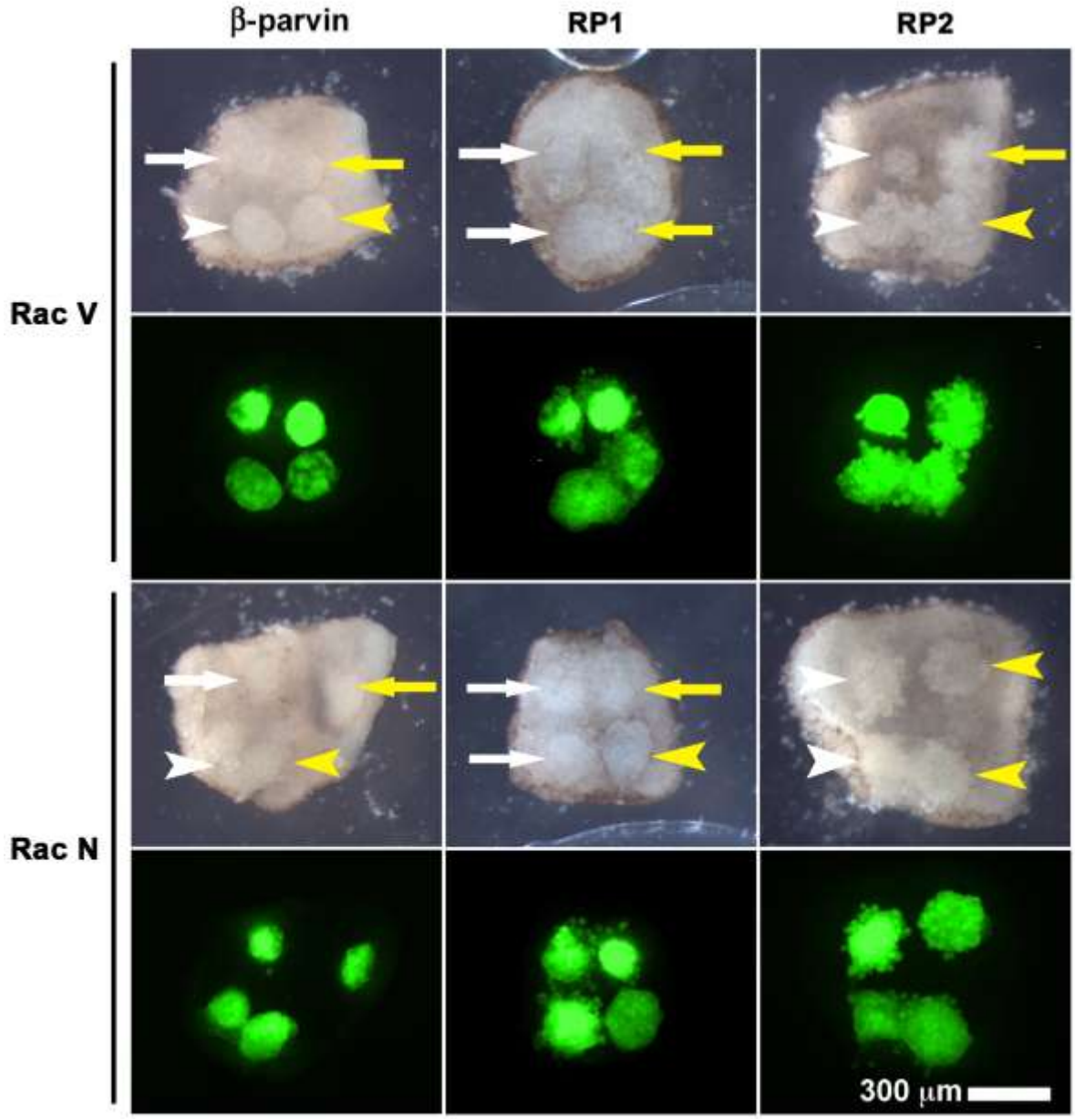
β-parvin
RP1
RP2
Rac V
Rac N
300 μm

Figure 3.42 Co-expression of RhoV with RP1 or RhoN with RP2 rescues tissue separation. Embryos were co-injected with β-parvin GFP constructs and 100pg RhoN or 50pg RhoV DNA, cultured until stage 11, explants placed on the BCR and TS scored after 45-75 minutes. White arrow and arrowheads denote explants injected with only β parvin-GFP constructs. Co-expression of RhoV or RhoN with β-parvin has a small effect on TS as the majority of pre-involution tissue reintegrates (yellow arrows) post-involution tissue exhibits TS behaviour (yellow arrowheads). TS was rescued in post-involution tissue with co-expression of RP1 with RhoV (yellow arrowhead), while pre- and post-involution explants co-expressing RP1 and RhoN reintegrated into the BCR (yellow arrows). TS was rescued in pre-involution tissue with co-expression of RP2 with RhoN (yellow arrow), while RP2 co-expression with RhoV did not promote reintegration (yellow arrowheads). GFP construct expression is shown in the bottoms panels for each group.

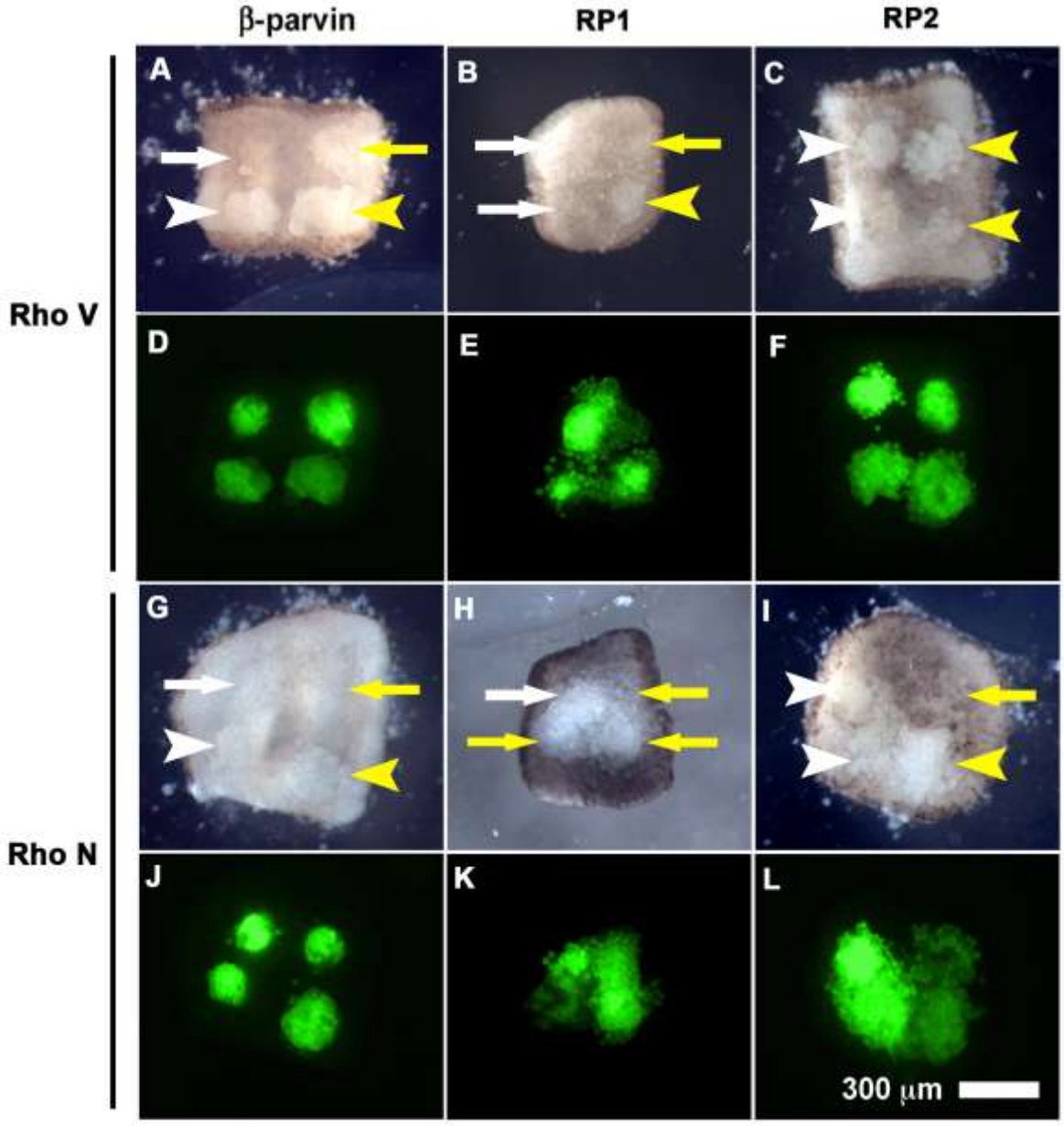
β-parvin
RP1
RP2
Rho V
Rho N
A
B
C
D
E
F
G
H
I
J
K
L
300 μm

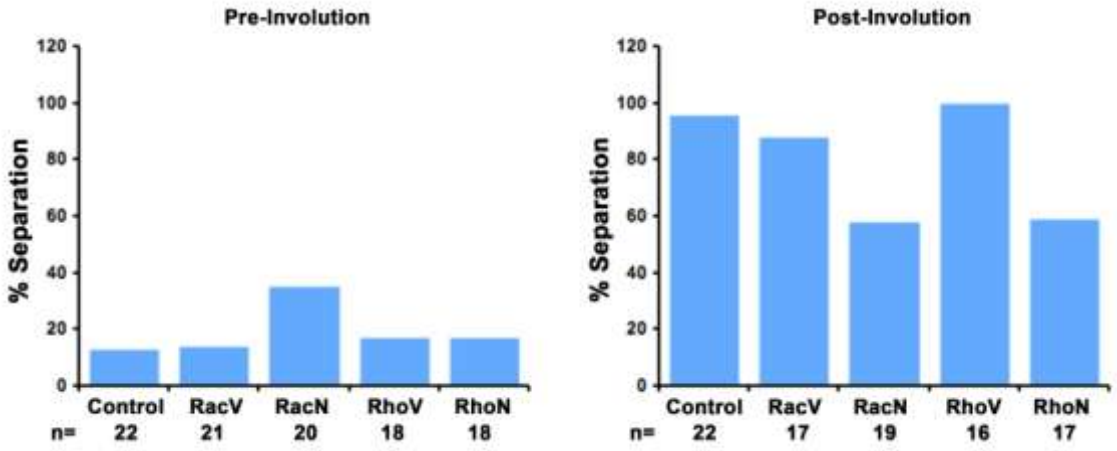

Figure 3.43 Co-expression of RhoN or RacN with GFP decreases tissue separation. Summary of tissue separation in explants over-expressing GFP (control), or co-expressing GFP with RacV, RacN, RhoV, or RhoN. Co-expression with Rac and Rho constructs does not affect TS in pre-involution mesoderm explants. Co-expression with RacN or RhoN decreases TS in post-involution mesoderm explants, while co-expression with RacV or RhoV has no effect on TS.

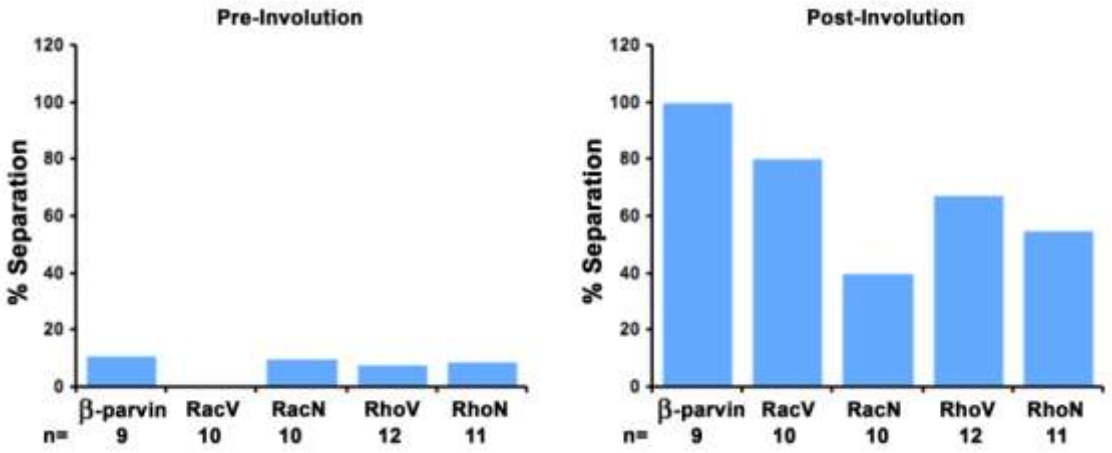

Figure 3.44 Co-expression of β-parvin with dominant negative Rac or Rho constructs decreases tissue separation. Summary of TS in explants over-expressing β-parvin-GFP, or co-expressing β-parvin-GFP with 50pg RacV or RhoV, or 100pg RacN or RhoN. Co-expression of β-parvin with Rac and Rho constructs in pre-involution mesoderm has no effect on TS. Co-expression of RacV, or RhoV with β-parvin slightly decreased TS in post-involution mesoderm. Co-expression of β-parvin with RacN or RhoN decreased TS in post-involution mesoderm.

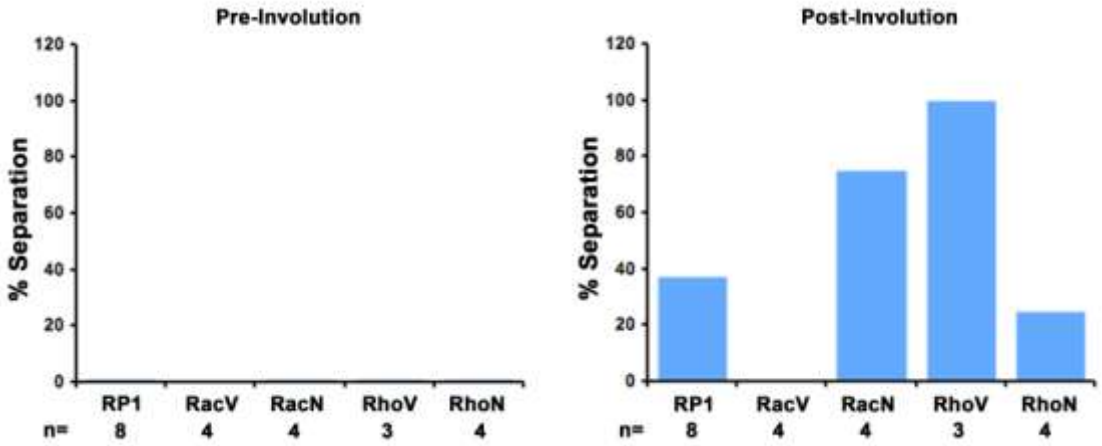

Figure 3.45 Co-expression of RP1 with RacN or RhoV rescues tissue separation. Summary of TS in explants injected with GFP-RP1, or co-injected with 50pg RacV or RhoV, or 100pg RacN or RhoN. Co-expression of RP1 with Rac and Rho constructs in pre-involution tissue had no effect on TS. Co-expression of RP1 with RacN or RhoV in post-involution tissue rescued TS. Co-expression of RP1 with RacV or RhoN with in post-involution tissue further inhibited TS.

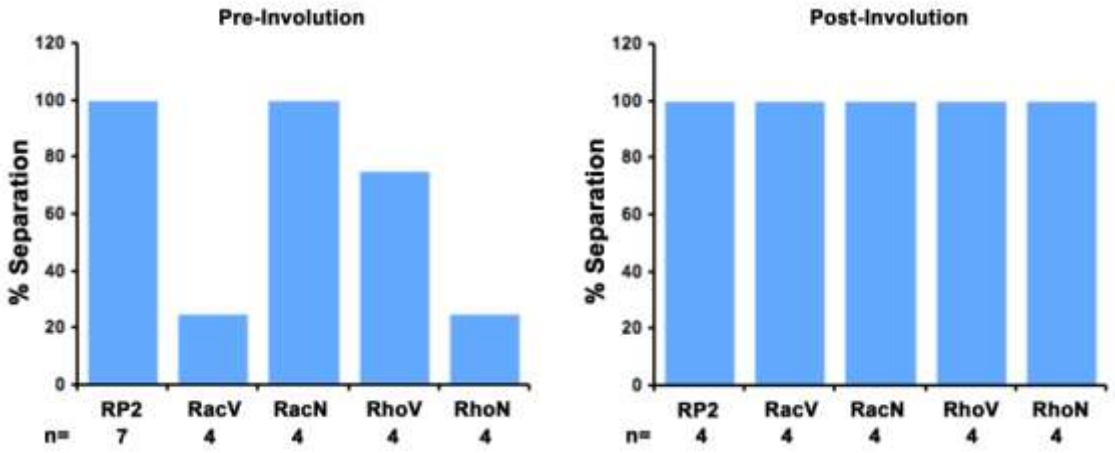

Figure 3.46 Co-expression of RP2 with RacV or RhoN rescues tissue separation. Summary of TS in explants injected with GFP-RP2 or co-injected with 50pg RacV or RhoV, or 100pg RacN or RhoN DNA. Explants were placed on BCRs and separation scored. Co-expression of RP2 with RacV or RhoN in pre-involution tissue rescued tissue separation. Co-expression of RP2 with RacN or RhoV in pre-involution had no effect on TS, and co-expression of RP2 with Rac or Rho constructs in post-involution tissue had no effect on TS as all explants remained separate from the blastocoel roof.

RP1 and RP2 over-expression exhibit opposite results on TS, and both can be rescued with alteration of Rac1 and RhoA signalling. Therefore, I asked whether the over-expression of RP1 and RP2 constructs are promoting an initial imbalance in levels of Rac1 and RhoA activity. I performed pull-downs of active Rac1 and RhoA from animal caps over-expressing GFP or β-parvin GFP constructs. Over-expression of β-parvin or RP1 increased Rac1 activity relative to controls (Figure 3.47). Over-expression of RP2 had no significant effect

on Rac1 activity (Figure 3.47). Over-expression of β-parvin or RP1 decreased RhoA activity compared to controls, whereas expression of RP2 increased RhoA activity (Figure 3.48).

The TS separation scores indicated that decreasing Rac1 activity in RP1 over-expressing explants, and decreasing RhoA activity in RP2 explants rescues TS. This is consistent with the pull-down data which suggest that RP1 increases Rac1 activity, and RP2 increases RhoA activity, indicating RP1 and RP2 act in opposing fashions through the small GTPases to regulate TS behaviour.

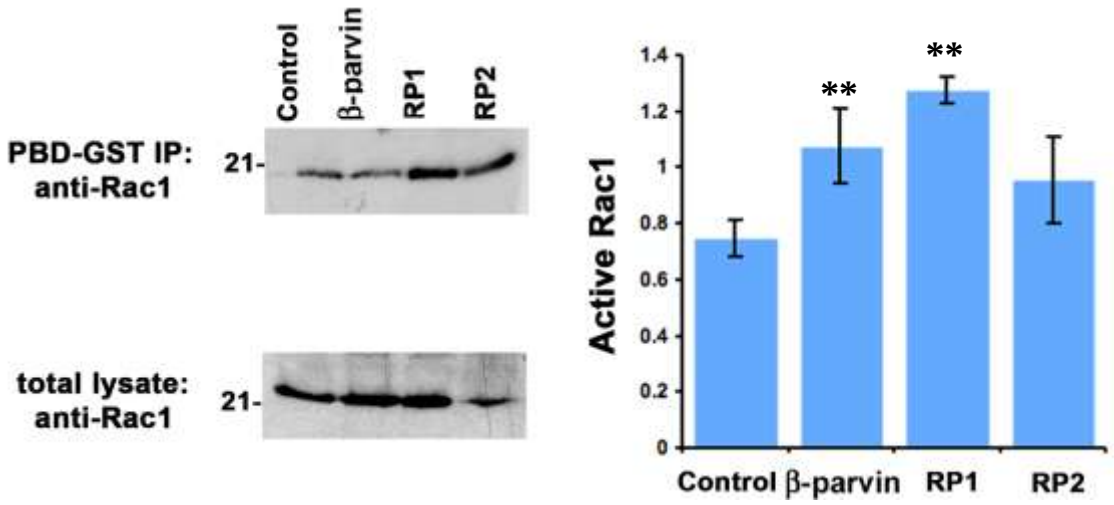

Figure 3.47 Expression of β-parvin or RP1 increases Rac1 activation. Stage two embryos were injected with GFP, or β-parvin-GFP constructs in the animal pole and animal caps were removed at stage 11 and lysed. Lysate was subjected to pull-downs using PBD-GST-conjugated beads followed by SDS-PAGE and Western blotting using anti-Rac1 antibody. Total cell lysate was used as a loading control. Quantification of Rac1 activation was performed using ImageJ, which revealed an increase in Rac1 activity in animal caps over-expressing the β-parvin or RP1 constructs. ** indicates $p<0.01$ compared to controls. n= 4 replicates.

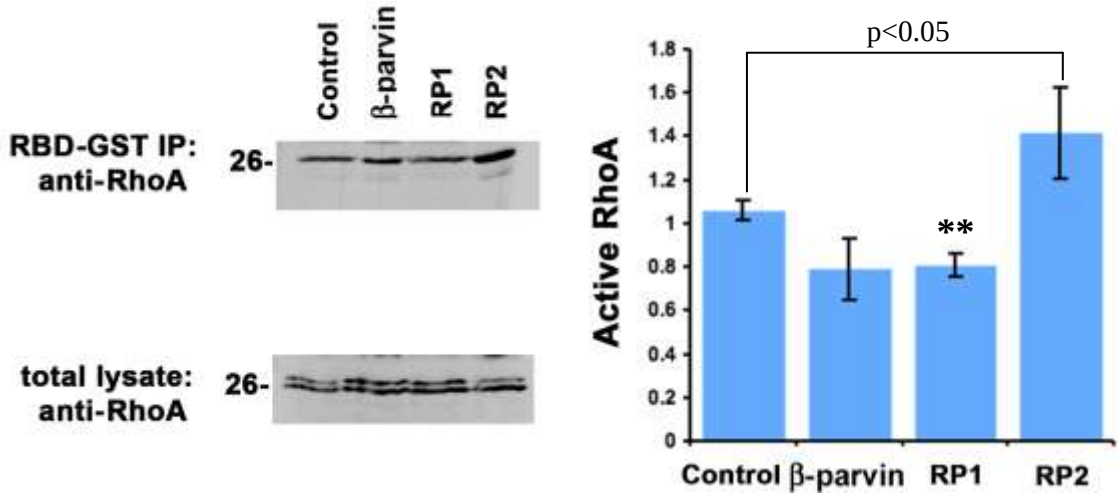

Figure 3.48 Expression of RP2 increases RhoA activation. Stage two embryos were injected with GFP or β-parvin-GFP constructs in the animal pole. Animal caps were removed from stage 11 embryos and lysed in RhoA lysis buffer. Lysate was subjected to pull-downs using RBD-GST-conjugated beads, which bind active RhoA. Lysate was subjected to SDS-PAGE and Western blotting using anti-RhoA antibody. Total cell lysate was used as a loading control. Quantification of RhoA activation was performed using ImageJ, which revealed an increase in RhoA activity in animal caps over-expressing the RP2 construct and a decrease in animal caps over-expressing the RP1 construct. ** indicates $p<0.01$ compare to controls. n= 4 replicates.

Chapter 4
Discussion

4.1 *Xenopus* β-parvin

I have characterized and made a preliminary study on the function of β-parvin in *Xenopus laevis*. A search of the EST database confirmed a full-length amino acid sequence of *Xenopus laevis* β-parvin (Accession NP_001089519.1), where β-parvin possesses conserved domain architecture when compared to cross species orthologs (Figure 3.1). β-parvin amino acid identity between *Xenopus* and bird or mammalian orthologs was 83.3-88.8%, with similarity ranging from 97-97.3% (Figure 3.2). This high level of conservation suggests the function of β-parvin including described binding partners may also be conserved among species.

β-parvin is a member of the parvin family, which contains α-, β-, and γ-parvin. In mammals these family members are encoded by distinct genes (Nikolopoulos and Turner, 2000; Tu et al., 2001; Olski et al., 2001; Yamaji et al., 2001). Interestingly, invertebrates possess only a single parvin ortholog, and in *Xenopus*, other amphibians and birds there are 2 parvins, α-parvin ortholog is missing. This led me to compare sequence alignments to gain an estimate of ancestral relatedness (Figure 4.1). Both β- and γ-parvin are conserved across vertebrates, however the sole parvin gene found in invertebrates such as *Drosophila* and *C. elegans* most closely resembles vertebrate β-parvin (Vakaloglou et al., 2012; Olski et al., 2001; Lin et al., 2003). The similarity of invertebrate parvin to vertebrate β-parvin suggests

that β-parvin is the ancestral gene, and that γ- parvin and α-parvin arose through separate duplication events, with α-parvin being the most recently derived member of the family. While α-parvin is not present in amphibians and birds, there are pieces of another parvin gene; perhaps representing what was once α-parvin. This parvin-like gene does not appear to be expressed as no ESTs are found and sequences upstream of the CH2 domain are missing. Due to the N-terminal truncation of the sequence it remains unclear whether α-parvin has been functionally deleted or if the complete sequence never arose in the genome through duplication. The presence of the truncated sequence suggests the former.

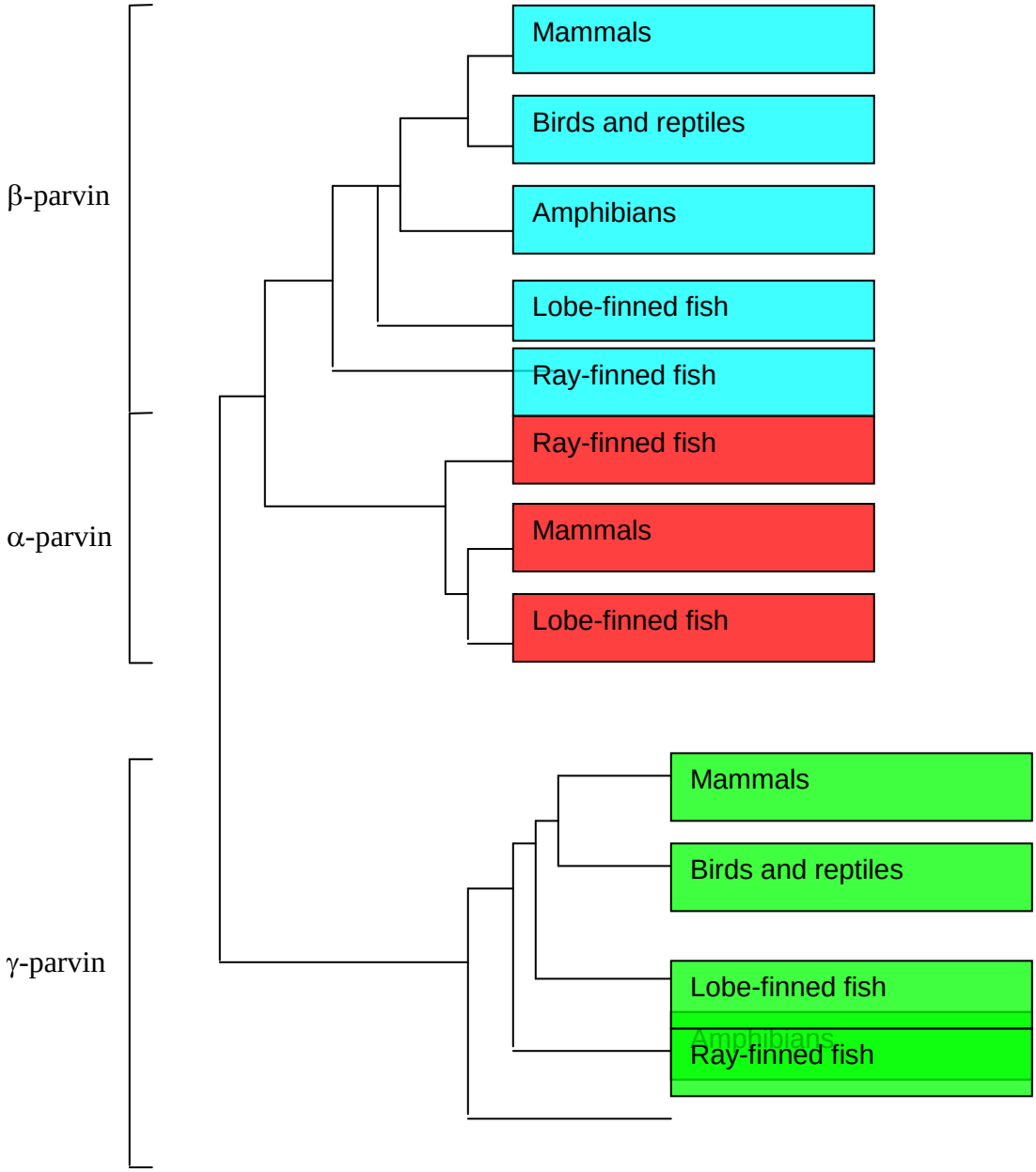

Figure 4.1 Dendrogram comparing α-, β-, and γ-parvin. Ensemble genome browser was used to create this tree. α- and β-parvin are more similar to each other, with γ-parvin being more divergent. Of the three proteins, only α-parvin is absent from birds, reptiles, and amphibians. β-parvin is indicated in blue, α-parvin in red, and γ-parvin in green.

Xenopus provides us with a simple model system to study the function of β-parvin. β-parvin is the sole parvin family member expressed in early *Xenopus* development and is known in mammalian tissue culture models to be intimately associated with integrin β1 and β3 subunits. During early *Xenopus* development integrins α5β1, α3β1, and αvβ? are expressed, however, integrins α3β1 and αvβ? are inactive (Hoffstrom, 2002). Integrin α5β1 binds to FN, the only ECM protein present in early gastrulation. Furthermore, integrin α5β1 function is dynamically regulated during gastrulation providing a simple integrin model amenable to the characterization of β-parvin *in vivo*.

β-parvin mRNA is expressed throughout *Xenopus laevis* embryogenesis (Figure 3.6) in tissues that undergo localized cell rearrangements that drive gastrulation (Figures 3.7-Figure 3.8). During gastrulation β-parvin is expressed in the BCR as DMZ (Figure 3.8) tissues that undergo movements regulated by integrin α5β1 function. Cell polarity is established in the BCR and DMZ via integrin α5β1-FN interactions (Marsden and DeSimone, 2001; Rozario et al., 2009), and this is required for intercalation behaviors that drive epiboly and CE and consequently the progression of tissue rearrangements that characterize gastrulation (Marsden and DeSimone, 2001, 2003; Davidson et al., 2006; Rozario et al., 2009). Due to the strong correlation between domains of β-parvin expression, integrin α5β1-FN ligation, and tissue rearrangements, I asked what role does β-parvin play during *Xenopus* gastrulation.

To elucidate the role of β-parvin in *Xenopus*, functional characterization of β-parvin and each of its domains were performed using over-expression of GFP-tagged β-parvin, RP1,

and RP2 constructs. Over-expression was used in these studies as attempts to knock down β-parvin expression using a morpholino (MO) failed. The 5' UTR sequences surrounding the translation start site of *Xenopus* β-parvin are extraordinarily AT-rich, and therefore are poor targets for antisense morpholino strategies. I attempted to knock down β-parvin expression using a start site directed MO (Appendix A). In my experiments the control MO had a stronger effect on development than the β-parvin directed MO. An alternative is to use a splice site MO to block pre-mRNA splicing creating a nonsense sequence (Draper et al., 2001), however the intron structure of β-parvin is such that any splice blocking MO would create a protein similar to the RP1 construct. Below I discuss the over-expression of RP1 and RP2 constructs to elucidate the role that the CH1 and CH2 domains play in *Xenopus* gastrulation.

4.2 Function of β-parvin CH1 Domain During *Xenopus* Gastrulation

Xenopus β-parvin has a highly conserved domain structure characterized by two CH domains. To examine the role CH1 and CH2 domains may play in *Xenopus* development, I utilized two deletion constructs that isolate the CH1 (RP1 construct) and CH2 (RP2 construct) domains (Mishima et al., 2004). Over-expression of the RP1 construct inhibits blastopore closure and axial extension (Figures 3.9-3.10, Figure 3.12), as well as epiboly (Figure 3.14) and mesoderm attachment to the BCR (Figure 3.15). Similar phenotypes are observed in embryos with inhibited integrin α5β1-FN interactions (Davidson et al., 2002,

2006; Marsden and DeSimone, 2001, 2003; Yang et al., 1999). While RP1 inhibits FN matrix assembly (Figure 3.13), it does not inhibit integrin α5β1-FN binding (Figure 3.16) or integrin function (Figures 3.22-Figure 3.24). Significantly, RP1 is unable to participate in integrin signaling as it does not bind ILK in *Xenopus* gastrulae (Figure 3.25), or localize to sites of integrin adhesion (Figure 3.4). This suggests that RP1 must be inhibiting FN matrix assembly through an alternative mechanism. FN fibrillogenesis on the BCR is a multistep process that first requires integrin α5β1-FN dimer binding at the cell surface and anchoring of integrin tails to the cytoskeleton (Mao and Schwarzbauer, 2005). Next, myosin II mediated tractoring of FN-bound integrins centripetally results in forces that unfold FN and mediates self-assembly (Pankov et al., 2000; Davidson et al., 2008). This process requires strong cell-cell adhesion, and an assembled actin cytoskeleton, a process mediated by C-cadherin, which results in increased tension across the BCR due to cytoskeleton assembly (Dzamba et al., 2009). RP1 is able to translocate to sites of cell-cell adhesion both in *ex vivo* dissociated cells forming nascent cell-cell junctions (Figure 2.39) and *in vivo* (Figure 3.30), and RP1 over-expression leads to a decrease in C-cadherin mediated adhesion (Figure 3.28) independent of expression (Figures 3.31-3.32). Previously, a decrease in C-cadherin adhesion of 20% was demonstrated to decrease tissue tension enough to inhibit FN matrix assembly (Dzamba et al., 2009). I saw similar decreases in C-cadherin adhesion when RP1 is over-expressed, suggesting that a subsequent decrease in tissue tension is the mechanism by which FN assembly fails. Upon performing certain experiments I also noticed that RP1 over-expression caused BCR and DMZ tissue surfaces to become uneven as cells were not maintaining tight cell-cell adhesion (DMZ in Figure 3.36) and the blastocoel retained a round shape in stage 11

embryos (Figure 3.21). In addition, RP1 over-expression in tissue explants increased the rate of dissociation as cells dissociated within a few minutes when placed in Modified Stearn's solution. Consistent with this, Rozario et al. (2009) discovered that the changed shape of the blastocoel from hemispheric to spherical increased bumpiness of the BCR, and this was due to decreased FN matrix assembly, which was suggested to be caused by a decrease in tissue tension.

Tadpoles over-expressing the RP1 construct have a shortened anterior-posterior axis (Figure 3.12), indicative of a failure in convergent extension (CE). However, CE movements in animal caps induced to become mesoderm are not inhibited by RP1 over-expression (Figure 3.17). This seemingly contradictory result can be explained through the role epiboly and integrin α5β1-FN ligation and matrix assembly plays in gastrulation. In *Xenopus* embryos, a thick FN matrix is localized to the boundaries of tissues that are rearranging during gastrulation (Lee et al., 1984; Davidson et al., 2004, 2006, Marsden and DeSimone, 2001, 2003). Blocking integrin α5β1-FN ligation with function blocking antibodies (Marsden and DeSimone, 2001, 2003; Davidson et al., 2002), FN MO (Davidson et al., 2006), or dominant negative integrin (Marsden and DeSimone, 2003) all result in a failure of matrix assembly. Inhibition of FN matrix assembly causes a loss of polarity in the BCR cells, leading to an inhibition of radial intercalation and epiboly (Marsden and DeSimone, 2001; Rozario et al., 2009). The inhibition of epiboly resulted in embryos with a shortened-anterior posterior axis (Marsden and DeSimone, 2001; Rozario et al., 2009); however, explanted DMZ tissue is able to undergo convergent extension movements (Rozario et al., 2009; Marsden and DeSimone, 2003), indicating that epiboly impinges on CE *in vivo*. These results

are similar to what is observed in RP1 over-expressing embryos, as over-expression of RP1 in the BCR inhibits FN matrix assembly (Figure 3.13) and epiboly (Figure 3.14); however, integrin-FN ligation was intact (Figure 3.16). Previous results by Rozario et al. (2009) have demonstrated that FN matrix assembly is not required for CE, however, the DMZ explants show some FN matrix assembly, suggesting that this is not a complete knock down of FN assembly observed in these explants. Interestingly RP1 over-expressing cells inhibit FN matrix assembly as only small punctae are visible (Figure 3.16) and explants are able to undergo CE movements, indicating that FN matrix assembly is either not necessary for CE movements, or that RP1 expression is able to rescue CE movements downstream of FN matrix assembly.

Tissue separation (TS) occurs during gastrulation when pre-involution DMZ mesodermal cells involute around the blastopore lip. This creates post-involution mesendoderm closely opposed to pre-involution mesoderm, and the interface between these two tissues is Brachet's cleft. While FN is found in Brachet's cleft, it does not form a physical barrier between the tissues (Nakatsuji and Jonhson, 1983), and while it has been demonstrated that integrin-FN interactions are necessary for the formation of the posterior portion of Brachet's cleft (Marsden and DeSimone, 2001), my results with RP1 over-expression indicate that regulation of integrin ligation is not the dominant mechanism involved in regulation of TS. It has been demonstrated that TS is regulated by multiple signaling pathways acting in parallel, including EphB-ephrinB interaction (Rohani et al., 2011; Park, 2011), Xfz7/PAPC signaling (Medina et al., 2004), and xGit2 and RhoGAP11A (Koster et al., 2011). Central to all of these signaling pathways is the downstream activation

of the small Rho GTPases to promote TS. TS and formation of the posterior portion of Brachet's cleft is dependent on the balance between Rac and Rho signaling in pre- and post-involution tissues (Medina et al., 2004; Koster et al., 2010; Rohani et al., 2011; Park et al., 2011). Inhibition of Rac and Rho in either pre- or post-involution tissue has been shown to decrease TS, whereas over-expression of constitutively active Rac or Rho constructs in either tissue rescues TS downstream of impaired EphB-ephrinB signaling (Rohani et al., 2011). RP1 over-expression inhibits TS (Figures 3.38-3.39) and the posterior portion of Brachet's cleft (Figures 3.33-3.34); however, TS can be rescued in RP1 over-expressing post-involution mesoderm through co-expression with constitutively active Rho (RhoV) or dominant negative Rac (RacN; Figures 3.41-3.42, Figure 3.45). There is previous evidence that Rac and Rho act in opposing fashion (Hall, 1998), and the complementary RacN and RhoV constructs may well be causing the same downstream effect. Given the antagonistic relationship between Rac and Rho and since RP1 over-expression leads to a large increase in Rac1 activity (Figure 3.47) and a smaller decrease in RhoA activity (Figure 3.48), it is likely that RP1 over-expression is directly impinging on the Rac1 pathway. RP1 over-expression results in a change in cellular behavior such that involuted cells are behaving as ectoderm, but are patterned as mesoderm as RP1 over-expressing cells do not inhibit xBra or xChd expression (Figures 3.19-3.21). Therefore RP1 over-expression is promoting ectoderm-like behavior in both pre- and post-involution mesoderm through activation of a Rac1 signaling pathway, independent of tissue patterning.

Finally, RP1 translocates to sites of cell-cell adhesion, both *ex vivo* and *in vivo*, and this translocation is enhanced in post-involution tissue (Figures 3.29-3.30, Figure 3.36). RP1

is specifically shuttling to sites of cell-cell adhesion, not to all sites of actin polymerization, as it does not translocate to sites of integrin adhesion. RP2 is not able to localize to sites of cell-cell adhesion, however, β-parvin shuttles to sites of cell-cell adhesion (Figures 3.28-3.29, Figure 3.35) similar to RP1, indicating that RP1 is the domain enabling shuttling of β-parvin. This shuttling may be allowing β-parvin to regulate cell-cell adhesion in cells forming nascent cell-cell junctions, and in tissues involved in morphogenetic movements during gastrulation. Since β-parvin shuttling to sites of cell-cell adhesion is enhanced in post-involution tissue, RP1 may be decreasing cell-cell adhesion in post-involution tissue. It is well established that post-involution mesoderm has decreased C-cadherin adhesion to promote cellular rearrangements that drive CE (Brieher and Gumbiner, 1994; Zhong et al., 1999). Therefore, β-parvin may play a key role in decreasing C-cadherin adhesion in post-involution mesoderm, but how β-parvin decreases cell-cell adhesion is not yet known.

4.3 Function of β-parvin CH2 Domain During *Xenopus* Gastrulation

The RP2 construct contains the CH2 domain of β-parvin. This domain is known to interact with ILK and mediate signals downstream of integrin ligation (Tu et al., 2001; Yamaji et al., 2001; Wickstrom et al., 2010; Legate et al., 2006). RP2 co-immunoprecipitates with ILK (Figure 3.25) and is recruited to sites of integrin adhesion in A6 cells (Figures 3.3-3.4) as well as the surface of pre- and post-involution mesoderm (Figure 3.37). Since cells over-expressing RP2 cannot attach to or migrate upon exogenously supplied FN (Figures 3.22-2.24) they have inhibited integrin function that likely stems from the RP2 interaction with

ILK. Consistent with this, RP2 over-expressing embryos exhibit a lack of FN matrix assembly on the BCR (Figure 3.13), and no FN accumulates on the surface of BCR cells (Figure 3.16), demonstrating that RP2 over-expression leads to the inhibition of integrin function and FN ligation. This is further demonstrated by an inhibition of mesoderm attachment to the blastocoel roof (Figure 3.15), since mesoderm attachment requires intact α5β1-FN binding. Inhibition of FN matrix assembly impinges on morphogenetic movements that drive gastrulation (see Section 4.2) including intercalation movements that are required for epiboly (Figure 3.14) and convergent extension (Figure 3.12, Figures 3.17-3.18). The inhibition of blastopore closure (Figures 3.9-3.10) in RP2 over-expressing embryos is likely due to defects in morphogenetic movements that define gastrulation. RP2 over-expression results in phenotypes reminiscent of studies using dominant negative integrin constructs (Marsden and DeSimone, 2001, 2003) or FN morpholino studies (Davidson et al., 2006) again promoting the conclusion that RP2 inhibits integrin function during *Xenopus* gastrulation. While RP1 and RP2 over-expressing embryos exhibit the same phenotypes, they arise by distinct mechanisms as RP2 directly impinges on integrin signaling, and has no affect on cadherin function (Figure 3.28) or expression (Figures 3.31-3.32) that is described in RP1 over-expression.

RP1 and RP2 over-expressing cells exhibit opposing functions in the regulation of tissue separation (TS). While RP1 inhibits tissue separation (TS) in post-involuted mesoderm via activation of Rac (discussed above), RP2 promotes TS behavior in pre-involution mesoderm (Figures 3.38-3.39) via activation of Rho (Figure 3.46). Since RP2 interacts with ILK during gastrulation, and ILK is a negative regulator of Rho activation (Kogata et al.,

2009) and positive regulator of Rac activation (Filipenko et al., 2005) in mammalian tissue culture cells, this suggests that not only is RP2 inhibiting integrin function, but also activation of Rac via ILK. Regular function of ILK is likely mediated by binding to the CH2 domain of β-parvin and transmitting signals through the CH1 domain to downstream effectors. As such, over-expression of RP2 would inhibit downstream signaling through the CH1 domain, effectively which could inhibit signaling cascades such as the activation of Rac via α-PIX (discussed in Section 4.4; Filipenko et al., 2005). Interestingly, RP2 over-expression promotes the extension of Brachet's cleft to the surface of the embryo (Figures 3.33-3.34), as well as mixing of surface and deep layers within the pre-involution mesoderm. This may also stem from an increase in Rho activity, as Rho is necessary for promotion and stability of cellular protrusions that drive mediolateral cell intercalations during CE in the DMZ (Tahinci and Symes, 2003). However, a balance between Rac and Rho activity in the DMZ is necessary for TS (Rohani et al., 2011). TS can be rescued in pre-involution mesoderm over-expressing RP2 through over-expression of a constitutively active Rac construct (RacV), or a dominant negative Rho construct (RhoN), allowing for tissue reintegration into the BCR (Figures 3.41-3.42, Figure 3.46). RP2 over-expression results in a change in cell behavior, as the pre-involution cells behave as mesoderm, but are patterned as ectoderm (Figures 3.19-21), indicating RP2 promotes mesoderm like behavior via activation of Rho, independent of tissue patterning. These results are the inverse of what is observed in RP1 over-expressing embryos, suggesting that RP1 and RP2 are involved in opposing signaling pathways in pre and post-involution mesoderm.

Finally, RP2 contains the domain that allows for shuttling of β-parvin to sites of integrin α5β1 adhesion (Figure 3.35, Figure 3.37), and β-parvin is preferentially localized to sites of integrin adhesion in pre-involution tissue (Figure 3.35). Since over-expression of the RP2 domain resulted in inhibition of integrin function, this suggests that β-parvin may be involved in regulating stable integrin α5β1-FN interactions required for FN matrix assembly on the BCR. Translocation of β-parvin away from sites of integrin adhesion in post-involution mesoderm (Figure 3.35) via the CH1 domain may result in decreased integrin α5β1 adhesion, promoting migration along the BCR. Such a scenario is supported by the observation that DMZ mesoderm cells have differing integrin behaviors pre and post-involution (see below; Ramos and DeSimone, 1996).

4.4 β-parvin Mediates Integrin and Cell-Cell Adhesion Receptor Cross-talk

One of the most intriguing observations is that while RP1 and RP2 constructs have deleterious effects on embryos, embryos expressing full-length β-parvin at similar levels (Appendix B) have no associated phenotype. β-parvin also has little or no effect on tissue patterning, similar to RP1 and RP2 over-expressed embryos (Figures 3.19-3.21). Although residual amounts of xBra and xChd expression were present in animal caps taken from embryos over-expressing GFP and β-parvin-GFP constructs, this can be attributed to animal cap explants being cut too large such that they may contain equatorial tissue (Figure 3.19). Full-length β-parvin also has little or no effect on embryo morphogenesis (Figures 3.9-3.10,

Figures 3.12-3.18) or TS (Figures 3.33-3.34, Figures 3.38-3.39). This cannot be ascribed to a balanced expression of the CH1 and CH2 domains, as co-expression of RP1 and RP2 constructs is more damaging than over-expression of either construct alone (Figure 3.11). This indicates that for proper function, the CH1 and CH2 domains need to be linked. A similar observation has recently been made in *Drosophila* where co-expression of CH1 and CH2 domains reveals different phenotypes than over-expression of full-length parvin (Chountala et al., 2012). In *Xenopus* it appears that having the CH1 and CH2 domains linked in full-length β-parvin results in a moderation of the effects mediated by the isolated domains. Indeed the over-expression of β-parvin results in decreased cadherin and integrin mediated adhesion (Figure 3.22, Figure 3.28); however, these decreases appear to be balanced such that normal embryogenesis occurs. This suggests that in the embryo it is not the absolute levels of adhesion that mediate morphogenesis, but the localized changes in relative levels of cadherin and integrin adhesion that are critical.

The observation that the CH1 domain can regulate cell-cell adhesion while the CH2 domain regulates cell-matrix adhesion coupled with the requirement for a full-length β-parvin suggests that β-parvin may act as a mediator of adhesion receptor cross-talk. At Brachet's cleft β-parvin is able to translocate from sites of integrin adhesion in pre-involution tissue, to sites of cell-cell adhesion in post-involution tissue (Figure 3.35). This movement is particularly interesting as the dorsal lip is the site where both integrin and cadherin mediated cell behaviors are altered (Ramos et al., 1996; Ramos and DeSimone, 1996; Fagotto and Gumbiner, 1994; Angres et al., 1991; Ogata et al., 2007). Pre-involution mesoderm can attach, but not migrate on FN, while post-involution cells migrate on FN (Ramos and

DeSimone, 1996), suggesting a temporal-spatial regulation of integrin function. Similarly, C-cadherin adhesion is lower in post-involution mesoderm compared to the pre-involution mesoderm, and increasing cadherin adhesion in the post-involution mesoderm results in a failure in gastrulation as CE movements are inhibited (Zhong et al., 1999). The localization of β-parvin is likely regulated through its CH domain interactions. β-parvin interacts with ILK through the CH2 domain (Tu et al., 2001), and localization of β-parvin to sites of integrin adhesion is likely mediated through binding of ILK, which binds directly to β1 and β3 integrin subunit tails (Hannigan et al., 1996). *Xenopus* ILK is necessary for gastrulation, as depletion of ILK results in inhibition of blastopore closure and CE independent of tissue patterning (Yasunaga et al., 2005). Inhibition of ILK in *Xenopus* also causes defects in integrin adhesion, as cells do not adhere to exogenously supplied FN substrates (Yasunaga et al., 2005), similar to RP2 over-expressing cells. Since these defects are similar to those in RP2 over-expressing embryos, this suggests that β-parvin signaling through integrin α5β1 is likely mediated by ILK. Inhibition of ILK function via RP2 over-expression leads to the indirect activation of Rho as Rac activation that is normally mediated by ILK signaling through the CH1 domain of β-parvin to αPIX is inhibited (see below; Filipenko et al., 2005).

The CH1 domain of β-parvin binds αPIX and β-PIX *in vitro* (Rosenberger et al., 2003; Mishima et al., 2004; Matsuda et al., 2008). αPIX forms a complex with PAK and GIT1, which translocates to sites of integrin adhesion (Rosenberger et al., 2003). αPIX and PAK are not exclusively associated with integrins and also localize to sites of cell-cell adhesion where this complex regulates E-cadherin localization and surface expression (Tay

et al., 2010). This suggests that β-parvin translocation to sites of cell-cell adhesion and regulation of C-cadherin mediated adhesion may be mediated by αPIX/PAK complex. This complex is also involved in Rac1 activation, suggesting that increased Rac1 activity observed in RP1 and β-parvin over-expressing embryos may be due to interactions with the αPIX/PAK complex (Feng et al., 2001).

4.5 Conclusions

During gastrulation tissues rearrange in a precisely choreographed manner. The regulation of these tissue movements occurs at the cellular level and is temporally and spatially regulated. It is well established that most cell movements occur independent of cell fate determination, as inhibition of morphogenetic movements can occur independently of inhibition in cell fates. While it is known that cell movement is precisely regulated, both the molecules and mechanisms behind this remain unknown. Here I present evidence that β-parvin, an integrin associated scaffolding protein, plays critical roles in the regulation of cell adhesion at the dorsal lip during *Xenopus* gastrulation. It has been known for several years that integrin α5β1 signaling can modulate C-cadherin activity during *Xenopus* gastrulation (Marsden and DeSimone, 2003); however, the molecular mechanisms by which integrins regulate cadherin activity remain unclear. β-parvin is able to regulate integrin α5β1 and C-cadherin function by shuttling between sites of cell-ECM and cell-cell adhesion. This shuttling of β-parvin is able to temporally and spatially regulate integrin α5β1 in pre-involution mesoderm and C-cadherin in post-involution mesoderm. β-parvin influences integrin signaling through the

CH2 domain interacting with ILK. How the CH1 domain influences C-cadherin remains elusive. The mechanism by which β-parvin acts downstream of cell adhesion is not clear, however, it would appear that it impinges on the small Rho GTPases and when over-expressed can influence both Rac and Rho activity. The spatial regulation of Rac and Rho are known to be critical in regulating the cell movements that drive *Xenopus* gastrulation (Tahinci and Symes, 2003; Habas et al., 2001, 2003; Koster et al., 2010).

The results presented here rely upon over-expression and must be interpreted with caution that comes with all over-expression studies. When over-expressed the isolated CH1 and CH2 domains could well be influencing pathways with which they are not normally involved. Interestingly, in my experiments CH1 and CH2 seem to act in a binary fashion with polar opposite effects on cell behavior and signaling. When both CH domains are in the same polypeptide as in full-length β-parvin, the effects of these two domains becomes balanced and cell behaviors as well as cell signaling is a moderated equilibrium of the two isolated domains. Not only do the effects become moderated, but full length β-parvin when over expressed has little effect on development, reinforcing the notion that it is the relative balanced levels of cell adhesion that are important, not the absolute levels of adhesion. The localization of the different β-parvin constructs matches the effects on cell adhesion, CH1 localizes to and appears to regulate cadherin mediated adhesion, while CH2 localizes to sites of integrin adhesion and disrupts interactions with FN. This indicates these domains are responsible for subcellular localization of β-parvin. When both CH domains are present in the same polypeptide as in full length β-parvin, there is spatial and temporal regulation of the

localization indicating that while β-parvin influences cell adhesion there is a higher level regulation of β-parvin localization. As such I am confident that the over-expression experiments presented here are providing insights into the normal function of *Xenopus* β-parvin.

4.6 Future Directions

My work has provided temporal, spatial, and preliminary functional characterization of β-parvin in *Xenopus* using over-expression assays. I was unable to determine temporal and spatial expression of endogenous β-parvin protein, therefore production of an antibody to β-parvin for use in *Xenopus* would be beneficial. Since the IPP complex does not form in *Xenopus* gastrulae, there must be a unique signaling complex, and a yeast two-hybrid screen could be performed to determine potential binding partners of *Xenopus* β-parvin. An initial yeast two-hybrid screen was performed for potential RP1 binding proteins, and proteasome subunit β type-1 (PSMB1) was discovered to be a potential binding partner (Kyle Novakowski, personal communication). Preliminary work with *Xenopus* PSMB1 demonstrated that when transfected into tissue culture cells no localization to sites of cell-cell or cell-ECM was seen. This suggests that although PSMB1 is able to bind RP1, it is not able to recruit or shuttle RP1 to sites of cell-cell adhesion. Therefore further yeast two-hybrid studies would be beneficial to aid in identifying how β-parvin is recruited to sites of cell-cell adhesion *in vivo*, and elucidate the mechanism behind an increase in Rac1 activation caused by RP1 over-expression and an increase in RhoA activation caused by RP2 over-expression.

Appendix A

Table A.1 Morpholino sequences

Construct	Sequence
β-parvin morpholino	5’ GTGCCCCTCAGCAGCACCCTGAGCT 3’
Control morpholino	5’ GTcCCgCTCAcCAGCACCgTGAcCT 3’

Appendix B

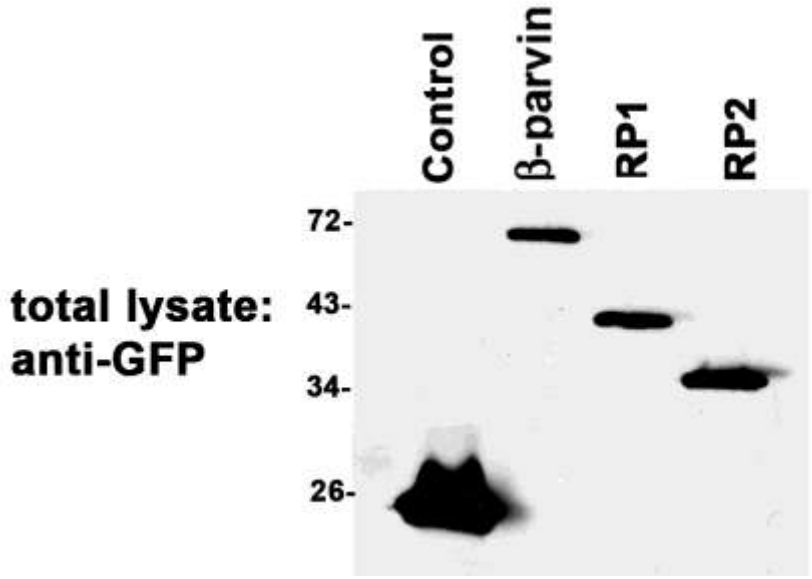

Figure B.1 Equal expression of GFP constructs. Embryos were injected with 2ng of GFP, β-parvin-GFP, GFP-RP1, and GFP-RP2 mRNA. Whole embryo lysate was subjected to Western blotting using anti-GFP primary antibody. β-parvin, RP1, and RP2 constructs were expressed at approximately equal levels. Each lane represents approximately 3 embryo equivalents.

Bibliography

Angres, B., Muller, A.H.J., Kellerman, J., and Hausen, P. (1991) Differential expression of two cadherins in *Xenopus laevis. Development* **111**, 80229-44.

Brieher, W.M. and Gumbiner, B.M. (1994) Regulation of cadherin function during Activin induced morphogenesis of *Xenopus* animal caps. *J. Cell. Biol.* **126**, 519-27.

Campbell, R.E., Tour, O., Palmer, A.E., Steinback, P.A., Baird, G.S., Zacharias, D.A., and Tsien, R.Y. (2002) A monomeric red fluorescent protein. *Proc. Natl. Acad. Sci. U.S.A.* **99**, 7877-82.

Chomczynski, P., and Sacchi, N. (1987) Single-Step Method of RNA Isolation by Acid Guanidinium Thiocyanate-Phenol-Chloroform Extraction. *Anal Biochem*. **162**, 156-159.

Chountala, M., Vakaloglou, K.M.,. and Zervas, C.G. (2012) Parvin overexpression uncovers tissue-specific genetic pathways and disrupts F-actin to induce apoptosis in the developing epithelia in *Drosophila*. *PLoS ONE* **7**, 47355.

Clarke, D.M., Brown, M.C, Lalonde, D.P., and Turner, C.E. (2004) Phosphorylation of actopaxin regulates cell spreading and migration. *J. Cell. Biol*.**166**, 901-12.

Cowan, C.A., and Henkemeyer, M. (2001) The SH2/SH3 adaptor Grb4 transduces B-ephrin reverse signals. *Nature* **413**, 174-79.

Davidson, L.A., Hoffstrom, B.G., Keller, R., and DeSimone, D.W. (2002) Mesendoderm extension and mantle closure in *Xenopus laevis* gastrulation: combined roles for integrin α5β1, fibronectin, and tissue geometry. *Dev. Biol*. **242**, 109-29.

Davidson, L.A., Marsden, M., Keller, R., and DeSimone, D.W. (2006) Integrin α5β1 and fibronectin regulate polarized cell protrusions required for *Xenopus* convergence and extension. *Curr. Biol*. **16**, 833-44.

Davidson, L.A., Dzamba, B.J., Keller, R., and DeSimone, D.W. (2008) Live imaging of cell protrusive activity, and extracellular matrix assembly and remodeling during morphogenesis in the frog, *Xenopus laevis*. *Dev. Dyn*. **237**, 2684-92.

Draper, B.W., Morcos, P.A., and Kimmel, C.B. (2001) Inhibition of Zebrafish fgf3 pre-mRNA splicing with morpholino oligos: a quantifiable method for gene knockdown. *Genesis* **30**,154-6.

Dzamba, B.J., Jakab, K.R., Marsden, M., Schwartz, M.A., and DeSimone, D.W. (2009) Cadherin adhesion, tissue tension, and noncanonical Wnt signaling regulate fibronectin matrix organization. *Dev Cell* **16**, 421-432.

Fagotto, F., Gumbiner, B.M. (1994) Beta-catenin localization during *Xenopus* embryogenesis: accumulation at tissue and somite boundaries. *Development* **120**, 3667-79.

Feng, Q., Albeck, J.G., Cerione, R.A., and Yang, W. (2001) Regulation of the Cool/PIX proteins key binding partners of the Cdc42/Rac targets, the p21-activated kinases. *J. Biol. Chem*. **277**, 5644-50.

Filipenko, N.R., Attwell, S., Roskelley, C., and Dedhar, S. (2005) Integrin-linked kinase activity regulates Rac- and Cdc42-mediated actin cytoskeleton reorganization via alpha-PIX. *Oncogene* **38**, 5837-49.

Fukuda, T., Chen, K., Shi, X. and Wu, C. (2003) PINCH-1 is an obligate partner of integrin-linked kinase (ILK) functioning in cell shape modulation, motility, and survival. *J. Biol. Chem.* **278**, 51324-33.

Gawantka, V., Joos, T.O., and Hausen, P. (1994) A beta 1-integrin associated alpha-chain is differentially expressed during *Xenopus* embryogenesis. *Mech. Dev*. **47**, 199-211.

Gumbiner, B.M. (2005) Regulation of cadherin-mediated adhesion in morphogenesis. *Nature reviews Mol. Cell Biol.* **6**, 622-34.

Habas, R., Kato, Y., and He, X. (2001) Wnt/Frizzled activation of Rho regulates vertebrate gastrulation and requires a novel Formin homology protein *Daam1*. **Cell** 107, 843-54.

Habas, R., Dawid, I.B., and He, X. (2003) Coactivation of Rac and Rho by Wnt/Frizzled signaling is required for vertebrate gastrulation. *Genes Dev*. **17**, 295-309.

Hall, A. (1998) Rho GTPases and the actin cytoskeleton. *Science* **279**, 509-14.

Hannigan, G.E., Leung-Hagesteijn, C., Fitz-Gibbon, L., Coppolino, M.G., Radeva, G., Filmus, J., Bell, J.C., and Dedhar, S. (1996) Regulation of cell adhesion and anchorage-dependent growth by a new beta 1-integrin-linked protein kinase. *Nature* **379**, 91-96.

Hardin, J., and Keller, R. (1988) The behavior and function of bottle cells during gastrulation of *Xenopus laevis. Development* **103**, 211-30.

Hoffstrom, B.G. (2002) Integrin function during *Xenopus laevis* gastrulation. Diss. University of Virginia, USA, *Dissertations and Thesis*.

Hynes, R.O. (2002) Integrins: Bidirectional Allosteric Signaling Machines. *Cell* **110**, 673-87.

Ibrahim, H., and Winklbauer, R. (2001) Mechanisms of mesendoderm internalization in the *Xenopus* gastrula: lessons from the ventral side. *Dev. Biol*. **240**, 108-22.

Joos, T.O., Whittaker, C.A., Meng, F., DeSimone, D.W., Gnau, V., and Hausen, P (1995) Integrin alpha 5 during early development of *Xenopus laevis. Mech. Dev*. **50**, 187-99.

Keller, R. (1978) Time-lapse cinemicrographic analysis of superficial cell behavior during and prior to gastrulation in *Xenopus laevis*. *J. Morphol*. **157**, 223-48.

Keller, R.E. (1980) The cellular basis of epiboly: an SEM study of deep-cell rearrangement during gastrulation in *Xenopus laevis. J. Embryol. Exp. Morphol*. **60**, 201-34.

Keller, R., and Jansa, S. (1992) *Xenopus* gastrulation without a blastocoel roof. *Dev. Dyn*. **195**, 162-76.

Keller, R., Shih, J., and Domingo, C. (1992) The patterning and functioning of protrusive activity during convergence and extension of the *Xenopus* organizer. *Dev. Suppl*. 81-91.

Keller, R., Davidson, L., Edlund, A., Elul, T., Ezin, M., Shook, D., and Skoglund, P. (2000) Mechanisms of convergence and extension by cell intercalation. *Phil. Trans. R. Soc. Lond. B*. **355**, 897-922.

Keller, R., Davidson, D.A., and Shook, D.R. (2003) How we are shaped: The biomechanics of gastrulation. *Differentiation* **71**, 171-205.

Kogata, N., Tribe, R.M., Fassler, R., Way, M., and Adams, R.H. (2009) Integrin-linked kinase controls vascular wall formation by negatively regulating Rho/ROCK-mediated vascular smooth muscle contraction. *Genes Dev*. **23**, 2278-83.

Koster, I., Jungwirth, M.S., and Steinbeisser, H. (2010) xGit2 and xRhoGAP 11A regulate convergent extension and tissue separation in *Xenopus* gastrulation. *Dev. Biol*. **344**, 26-35.

Koster, I. (2010) Transcriptional regulation of tissue separation during gastrulation of *Xenopus laevis. PhD thesis, University of Heidelberg.*

Kovalevich, J., Tracy, B., and Langford, D. (2011) PINCH: More than just an adaptor protein in cellular response. *J. Cell. Physiol.* **226**, 940-47

Kraft, B., Berger, C.D., Wallkamm, V., Steinbeisser, H., and Wedlich, D. (2012) Wnt-11 and Fz7 reduce cell adhesion in convergent extension by sequestration of PAPC and C-cadherin. *J. Cell Biol*. **198**, 695-709.

Kuhl, M., and Wedlich, D. (1996) *Xenopus* cadherins: sorting out types and functions in embryogenesis. *Dev. Dyn*. **207**, 121-34.

Lee, G., Hynes, R., and Kirschner, M. (1984) Temporal and spatial regulation of fibronectin in early *Xenopus* development. *Cell* **36**, 729-40.

Lee, C.H., and Gumbiner, B.M. (1995) Disruption of gastrulation movements in *Xenopus* by a dominant negative mutant for C-cadherin. *Dev. Biol*. **171**, 363-73.

Legate, K.R., Montanez, E., Kudlacek, O., Fassler, R. (2006) ILK, PINCH, and parvin: the tIPP of integrin signaling. *Nat. Rev. Mol. Cell. Biol.* **1**, 20-31.

Mao, Y., and Schwarzbauer, J.E. (2005) Fibronectin fibrillogenesis, a cell-mediated matrix assembly process. *Matrix Biol*. **6**, 389-99.

Marsden, M., and DeSimone, D.W (2001) Regulation of cell polarity, radial intercalation and epiboly in *Xenopus*: novel roles for integrin and fibronectin. *Development* **128**, 3635-47.

Marsden, M., and DeSimone, D.W. (2003) Integrin-ECM interactions regulate cadherin-dependent cell adhesion and are required for convergent extension in *Xenopus. Curr. Biol.* **13**, 1182-91.

Matsuda, C., Kameyama, K., Suzuki, A., Mishima, W., Yamaji, S., Okamoto, H., Nishino, I., and Hayashi, Y.K. (2008) Affixin activates Rac1 via betaPIX in C2C12 myoblast. *FEBS Lett*. **582**, 1189-96.

Medina, A., Swain, R.K., Kuerner, K.M., and Steinbeisser, H. (2004) *Xenopus* paraxial protocadherin has signaling functions and is involved in tissue separation. *Embo. J*. **16**, 3249-58.

Mishima, W., Suzuki, A., Yamaji, S., Yoshimi, R., Ueda, A., Kaneko, T., Tanaka, J., Miwa, Y., Ohno, S., and Ishigatsubo, Y. (2004) The first CH domain of affixin activates Cdc42 and Rac1 through alphaPIX, a Cdc42/Rac1-specific guanine nucleotide exchange factor. *Genes Cells* **9**, 193-204.

Nakatsuji, N., and Johnson, K. (1983) Conditioning of a culture substratum by the ectodermal layer promotes attachment and oriented locomotion by amphibian gastrula mesodermal cells. *J. Cell Sci*. **59**, 43-50.

Nieuwkoop, P.D. and Faber, J. (1994) "Normal Table of *Xenopus laevis*," Garland Publishing, New York.

Nikolopoulos, S.N., and Turner, C.E. (2000) Actopaxin, a new focal adhesion protein that binds paxillin LD motifs and actin and regulates cell adhesion. *J. Cell Biol*. **151**, 1435-48.

Nikolopoulos, S. N. and Turner, C.E. (2002) Molecular dissection of actopaxin-integrin-linked kinase-paxillin interactions and their role in subcellular localization. *J. Biol. Chem*. **277**, 1568-75.

Nishida, E. (2005) *Xenopus* ILK (integrin-linked kinase) is required for morphogenetic movements during gastrulation. *Genes Cells* **4**, 369-79.

Ogata, S., Morokuma, J., Hayata, T., Kolle, G., Niehrs, C., Ueno, N., and Cho, KWY. (2007) TGF-beta signaling-mediated morphogenesis: modulation of cell adhesion via cadherin endocytosis. *Genes Dev*. **21**, 1817-31.

Olsli,, T.M., Noegel, A.A., and Korenbaum, E. (2001) Parvin, a 42 kDa focal adhesion protein, related to the alpha-actinin superfamily. *J. Cell. Sci*. **114**, 525-38.

Pankov, R., Cukierman, E., Katz, B.Z., Matsumoto, K., Lin, D.C., Lin, S., Hahn, C., and Yamada, K.M. (2000) Integrin dynamics and matrix assembly: tensin-dependent translocation of alpha(5)beta(1) integrins promotes early fibronectin fibrillogenesis. *J. Cell Biol.* **6**, 1075-90.

Park, E.C., Cho, G.S., Kim, G.H., Choi, S.C., and Han, J.K. (2011) The involvement of Eph-Ephrin signaling in tissue separation and convergence during *Xenopus* gastrulation movements. *Dev. Biol*. **350**, 441-50.

Pilli, B. (2012) Role of PINCH during early *Xenopus* embryogenesis. *MSc Thesis. University of Waterloo.*

Ramos, J.W., Whittaker, C.A., and DeSimone, D.W. (1996). Integrin-dependent adhesive activity is spatially controlled by inductive signals at gastrulation. *Dev* **122**, 2873-2883.

Ramos, J.W., and DeSimone, D.W. (1996) *Xenopus* embryonic cell adhesion to fibronectin: position-specific activation of RGD/synergy site-dependent migratory behavior at gastrulation. *J. Cell Biol*. **134**, 227-40.

Reintsch, W.E., and Hausen, P. (2001) Dorsoventral differences in cell-cell interactions modulate the motile behavior of cells from the *Xenopus* gastrula. *Dev. Biol*. **240**, 387-403.

Ren, X.D., Klosses, W.B., and Schwartz, M.A. (1999) Regulation of the small GTP-binding protein Rho by cell adhesion and the cytoskeleton. *EMBO J*. **3**, 578-85.

Rohani, N., Canty, L., Luu, O., Fagotto, F., and Winklbauer, R. (2011). EphrinB/EphB Signaling Controls Embryonic Germ Layer Separation by Contact-Induced Cell Detachment. *PLoS Biol* **9**, e1000597. Doi:10.1371/journal.pbio.1000597.

Rosenberger, G., Jantke, I., Gal, A., and Kutsche, K. (2003) Interaction of αPIX (ARHGEF6) with β-parvin (PARVB) suggests an involvement of αPIX in integrin-mediated signaling. *Hum. Mol. Genet*. **12**, 155-67.

Rozario, T., Dzamba, B., Weber, G.F., Davidson, L.A., and DeSimone, D.W. (2009) The physical state of fibronectin matrix differentially regulates morphogenetic movements *in vivo*. *Dev. Biol.* **15**, 386-98.

Sambrook, J., and Russel, D.W. (2001) Molecular cloning: a laboratory manual. 3rd ed. New York: Cold Spring Harbor Laboratory Press.

Sander, E.E., van Delft, S., ten Klooster, J.P., Reid, T., van der Krammen, R.A., Michiels, F., and Collard, J.G. (1998) Matrix-dependent Tiam1/Rac signaling in epithelial cells promotes either cell-cell adhesion or cell migration and is regulated by phosphatidylinositol 3-kinase. *J. Cell Biol*. **143**, 1385-98.

Sepulveda, J.L., and Wu, C. (2006) The parvins. *Cell. Mol. Life* 63, 25-35.

Shih, J., and Keller, R. (1992) Cell motility driving mediolateral intercalation in explants of *Xenopus*. *Development*. **116**, 901-14.

Sive, H. L., Grainger, R. M., and Harland, R. M. (1996). "Early Development of *Xenopus laevis*; Course Manual," Cold Spring Harbor Laboratory Press, New York.

Sive, H. L., Grainger, R. M., and Harland, R. M. (2000). "Early Development of *Xenopus Laevis:* A Laboratory Manual," Cold Spring Harbor Laboratory Press, New York pp: 249-97.

Smith, J.C., Symes, K., Hynes, R.O., DeSimone, D. (1990) Mesoderm induction and the control of gastrulation in *Xenopus laevis*: the roles of fibronectin and integrins. *Development* **108**, 229-38.

Stanchi, F., Grashoff, C., Nguemeni Yonga, C.F., Grall, D., Fassler, R., Van Obberghen-Schilling E. (2009) Molecular dissection of the ILK-PINCH-parvin triad reveals a fundamental role for the ILK kinase domain in the late stages of focal-adhesion maturation. *J. Cell Sci*. **22**, 1800-11.

Symes, K. and Smith, J.C. (1987) Gastrulation movements provide an early marker of mesoderm induction in *Xenopus laevis*. *Development* **101**, 339-49.

Tahinci, E., and Symes, K. (2003) Distinct functions of Rho and Rac are required for convergent extension during *Xenopus* gastrulation. *Dev. Biol*. **259**, 318-35.

Tay,, H.G., Ng, Y.W., and Manser, E. (2010) A vertebrate-specific Chp-PAK-PIX pathway maintains E-cadherin at adherens junctions during zebrafish epiboly. *PLoS One* **4**:e10125. doi: 10.1371/journal.pone.0010125

Tsuiji, H., Xu, L., Schwartz, K., and Gumbiner, B.M. (2007) Cadherin conformations associated with dimerization and adhesion. *J. Biol. Chem*. **282**, 12871-882.

Tu, Y., Li, F., and Wu, C. (1998) Nck-2, and novel Src homology 2/3-containing adaptor protein that interacts with the LIM-only protein PINCH and components of growth factor receptor kinase-signaling pathways. *Mol. Biol. Cell* **9**, 3367-82.

Tu, Y., Huang Y,. Zhang, Y., Hua, Y., and Wu, C. (2001). A new focal adhesion protein that interacts with integrin-linked kinase and regulates cell adhesion and spreading. *J Cell Biol* **153**, 585-98.

Vakaloglou, K.M., Chountala, M., and Zervas, C.G. (2012) Functional analysis of parvin and different modes of IPP-complex assembly at integrin sites during *Drosophila* development. *J. Cell Sci*. **125**, 3221-32.

Wacker, S., Grimm, K., Joos, T., and Winklbauer, R. (2000) Development and control of tissue separation at gastrulation in *Xenopus. Developmental Biology* **224**, 428-39.

Wickstrom, S.A., Lange, A., Montanex, E., and Fassler, R. (2010) The ILK/PINCH/parvin complex: the kinase is dead, long live the pseudokinase! *Embo. J.* **29**, 281-91.

Winklbauer, R., and Keller, R. (1996) Fibronectin, mesoderm migration, and gastrulation in *Xenopus. Dev. Biol*. **177**, 413-26.

Winklbauer, R. (1998) Conditions for fibronectin fibril formation in the early *Xenopus* embryo. *Dev. Dyn*. **212**, 335-45.

Winklbauer, R., and Schurfeld, M. (1999) Vegetal rotation, and new gastrulation movement involved in the internalization of the mesoderm and endoderm in *Xenopus*. *Development* **126**, 3703-13.

Wolpert, L., and Tickle, C. (2011) Principles of Development Fourth Edition. *Oxford University Press.*

Yamaji, S., Suzuki, A., and Sugiyama, Y. (2001) A novel integrin-linked kinase-binding protein, affixin, is involved in the early stage of cell-substrate interaction. *J. Cell. Biol*. **153**,

1251-65.
Yang, J.T., Bader, B.I., Kreidberg, J.A., Ullman-Cullere, M., Trevithick, J.E., and Hynes, R.O. (1999) Overlapping and independent functions of fibronectin receptor integrins in early mesendodermal development. *Dev. Biol*. **215**, 264-77.

Yasunaga, T., Kusakabe, M., Yamanaka, H., Hanafusa, H., Masuyama, N., and Nishida, E. (2005) *Xenopus* ILK (integrin-linked kinase) is required for morphogenetic movements during gastrulation. *Genes Cells* **10**, 1369-79.

Zaidel-Bar, R., and Geiger, B. (2010) The switchable integrin adhesome. *J. Cell Sci*. **123**, 1385-88.

Zervas, C.G., Gergory, S.L., and Brown, N.H. (2001) *Drosophila* integrin-linked kinase is required at sites of integrin adhesion to link the cytoskeleton with the plasma membrane. *J. Cell Biol.* **152**, 1007-18.

Zervas, C.G., Psarra, E., Williams, V., Solomon, E., Vakaloglou, K.M., and Brown, N.H. (2011) A central multifunctional role of integrin-linked kinase at muscle attachment sites. *J. Cell. Sci*. **124**, 1316-27.

Zhang, Y., Chen, K., Guo, L., and Wu, C. (2002a) Characterization of PINCH-2, a new focal adhesion protein that regulates the PINCH-1-ILK interaction, cell spreading, and migration. *J. Biol. Chem*. **277**, 38328-38.

Zhang, Y., Chen, K., Tu, Y., Velyvis, A., Yang, Y., Qin, J., and Wu, C. (2002b) Assembly of the PINCH-ILK-CH-ILKBP complex precedes and is essential for localization of each component to cell-matrix adhesion sites. *J. Cell Sci*. **115**, 4777-86.

Zhang, Y.J., Chen, K., Tu, Y.Z., and Wu, C.Y. (2004) Distinct roles of two structurally closely related focal adhesion proteins, α-parvins and β-parvins, in regulation of cell morphology and survival. *J. Biol. Chem*. **279**, 41695-705.

Zhong, Y., Brieher, W.M., and Gumbiner, B.M. (1999) Analysis of C-cadherin regulation during tissue morphogenesis with an activating antibody. *J. Cell Biol*. **144**, 351-359.